Determination of Dielectric Constant and Loss Factor by Free Wave Method. I. Theoretical Part

By Masasi YASUMI[1]

(Received August 31, 1950)

Introduction

Recently microwave technique has been developed rapidly, and the determination of dielectric constant and loss factor in microwave region has become important. Great variety of methods has been deviced for this purpose among which the wave guide method is used generally. However earlier experiments were made by means of free wave method. The reason why the free wave method is not used generally lies partly in the incompleteness of the method of calculation to determine dielectric constant and loss factor from the values of reflection or transmission coefficient experimentally obtained.

To find a precise and convenient method for this purpose, it seems desirable to determine theoretically the reflection and transmission coefficient of electromagnetic waves by multiple layer.

In this paper a theoretical formula will be derived for the reflection and transmission coefficient by multiple layer by solving Maxwell's equation in an orthodox way.

At the same time a convenient method will be reported for the determination of dielectric constant and loss factor from the values of reflection or transmission coefficient obtained by experiment.

Reflection and Transmission of Electromagnetic Wave by Multiple Layer. Behavior of Electromagnetic Wave in the Layer.

1. Fundamental Equations and Solutions. —If an electromagnetic wave is propagated in an isotropic ahd uniform medium, the electric field and magnetic field vectors will satisfy the following Maxwell's equations,[2]

$$\frac{\varepsilon'}{c}\frac{\partial \mathfrak{E}}{\partial t} + \frac{4\pi\sigma}{c}\mathfrak{E} = \operatorname{rot}\mathfrak{H} \tag{1a}$$

$$-\frac{1}{c}\frac{\partial \mathfrak{H}}{\partial t} = \operatorname{rot}\mathfrak{E} \tag{1b}$$

$$\operatorname{div}\mathfrak{E} = 0 \tag{1c}$$

$$\operatorname{div}\mathfrak{H} = 0 \tag{1d}$$

where ε' denotes dielectric constant, σ conductivity, c the velocity of light and $\mathfrak{E}$ and $\mathfrak{H}$ are electric and magnetic field vectors, respectively.

The electromagnetic wave is assumed to be propagated along x-axis (from minus to plus) and to be linearly polarized. Electric and magnetic field vectors are assumed to lie on y-axis and z-axis, respectively. Then the solution of Eq. (1) is expressed as:[3]

$$\mathfrak{E}_y = ae^{i\omega\left(t-\frac{px}{c}\right)} \tag{2a}$$

$$\mathfrak{H}_z = apE^{i\omega\left(t-\frac{px}{c}\right)} \tag{2b}$$

where

$$p^2 = \varepsilon' - i\frac{4\pi\sigma}{\omega}. \tag{3}$$

Here ω denotes circular frequency and a, a constant.

We rewrite Eq. (3) as follows:

$$p^2 = \varepsilon' - i\varepsilon'' \tag{3'}$$

where

$$\varepsilon'' = \frac{4\pi\sigma}{\omega}. \tag{4}$$

If we write

$$p = n - ik \tag{5}$$

then n and k are expressed as

$$n^2 = \frac{1}{2}\{\sqrt{\varepsilon'^2 + \varepsilon''^2} + \varepsilon'\} \tag{6a}$$

$$k^2 = \frac{1}{2}\{\sqrt{\varepsilon'^2 + \varepsilon''^2} - \varepsilon'\}. \tag{6b}$$

As stated above the electromagnetic wave is assumed to be propagated from $x = -\infty$ to $x =$

(1) Present address: Institute of Science and Technology, the University of Tokyo, Tokyo.

(2) The magnetic permeability of the medium μ is assumed to be 1.

(3) R. Becker "Theorie der Elektrizität" I, Leipzig and Berlin, 1933, p. 186.

CHEMISTRY HALL LIBRARY

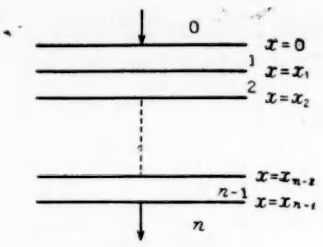

Fig. 1.

$+\infty$ A multiple layer consisting of $(n-1)$ sheets is placed with their boundary surfaces on $y-z$ planes as shown in Fig. 1. The origin of x-coordinate lies on the first boundary surface and the x-coordinate of the boundary surface between r th and $(r-1)$ th layers is noted x_r. Between $x=-\infty$ and $x=0$, there exists a semi-infinite medium, and another between $x=x_{n-1}$ and $x=+\infty$. They are numbered as 0 and n, respectively.

The electric and magnetic field vectors in $0, 1, \ldots, r, \ldots, (n-1), n$ media will be expressed by the following equations.

$$\mathfrak{E}_y^{(0)}=a\{e^{i\omega\left(t-\frac{p_0 x}{c}\right)}+\Re_0 e^{i\omega\left(t+\frac{p_0 x}{c}\right)}\} \quad (7a)$$

$$\mathfrak{H}_z^{(0)}=ap_0\{e^{i\omega\left(t-\frac{p_0 x}{c}\right)}-\Re_0 e^{i\omega\left(t+\frac{p_0 x}{c}\right)}\} \quad (7b)$$

$$\cdots\cdots\cdots\cdots$$

$$\cdots\cdots\cdots\cdots$$

$$\mathfrak{E}_y^{(r)}=a[\vartheta_r e^{i\omega\left\{t-p_r\frac{(x-x_r)}{c}\right\}}+\Re_r e^{i\omega\left\{t+p_r\frac{(x-x_r)}{c}\right\}}] \quad (8a)$$

$$\mathfrak{H}_z^{(r)}=ap_r[\vartheta_r e^{i\omega\left\{t-p_r\frac{(x-x_r)}{c}\right\}}-\Re_r e^{i\omega\left\{t+p_r\frac{(x-x_r)}{c}\right\}}] \quad (8b)$$

$$r=1, 2, \ldots, r, \ldots, (n-2), (n-1).$$

$$\mathfrak{E}_y^{(n)}=a\vartheta_n e^{i\omega\left\{t-p_n\frac{(x-x_{n-1})}{c}\right\}} \quad (9a)$$

$$\mathfrak{H}_z^{(n)}=ap_r\vartheta_n e^{i\omega\left\{t-p_n\frac{(x-x_{n-1})}{c}\right\}} \quad (9b)$$

$a\Re_r$ and $a\vartheta_r$ denote the complex amplitude of the elecric vector of reflected and penetrating waves at $x=x_r$, respectively.

2. Boundary Conditions.—The boundary conditions require that the electric and magnetic field vectors are continuous on the $x=x_r$ surfaces.

From the continuity of $\mathfrak{E}_y$ on the surface $=0$, we have

$$1+\Re_0=\vartheta_1 e^{i\omega p_1\frac{x_1}{c}}+\Re_1 e^{-i\omega p_1\frac{x_1}{c}} \quad (10_1)$$

and from the continuity of $\mathfrak{H}_z$ on the surface $x=0$, we have

$$p_0(1-\Re_0)=p_1\{\vartheta_1 e^{i\omega p_1\frac{x_1}{c}}-\Re_1 e^{-i\omega p_1\frac{x_1}{c}}\}. \quad (10_2)$$

Similarly on the surface $x=x_1$, the bonndary conditions require

$$\vartheta_1+\Re_1=\vartheta_2 e^{i\omega p_2\frac{(x_2-x_1)}{c}}+\Re_2 e^{-i\omega p_2\frac{(x_2-x_1)}{c}} \quad (10_3)$$

$$p_1(\vartheta_1-\Re_1)=p_2\{\vartheta_2 e^{i\omega p_2\frac{(x_2-x_1)}{c}}-\Re_2 e^{-i\omega p_2\frac{(x_2-x_1)}{c}}\}. \quad (10_4)$$

In general, on the surface $x=x_r$, we have

$$\vartheta_r+\Re_r=\vartheta_{r+1}e^{i\omega p_{r+1}\frac{(x_{r+1}-x_r)}{c}}+\Re_{r+1}e^{-i\omega p_{r+1}\frac{(x_{r+1}-x_r)}{c}} \quad (10_{2r+1})$$

$$p_r(\vartheta_r-\Re_r)=p_{r+1}\{\vartheta_{r+1}e^{i\omega p_{r+1}\frac{(x_{r+1}-x_r)}{c}}-\Re_{r+1}e^{-i\omega p_{r+1}\frac{(x_{r+1}-x_r)}{c}}\} \quad (10_{2r+2})$$

Finally from the boundary condition at $x=x_{n-1}$, the following equations are obtained.

$$\vartheta_{n-1}+\Re_{n-1}=\vartheta_n \quad (10_{2n-1})$$

$$p_{n-1}(\vartheta_{n-1}-\Re_{n-1})=p_n\vartheta_n \quad (10_{2n})$$

We put $i\omega p_{r+1}(x_{r+1}-x_r)/c=a_{r+1}$, and rewrite above equations as follows:

$$\begin{aligned}
\Re_0-\vartheta_1e^{+a_1}-\Re_1e^{-a_1}&=-1\\
-p_0\Re_0-p_1\vartheta_1e^{+a_1}+p_1\Re_1e^{-a_1}&=-p_0\\
\vartheta_1+\Re_1-\vartheta_2e^{+a_2}-\Re_2e^{-a_2}&=0\\
p_1\vartheta_1-p_1\Re_1-p_2\vartheta_2e^{+a_2}+p_2\Re_2e^{-a_2}&=0\\
&\cdots\cdots\cdots\\
&\cdots\cdots\cdots\\
\vartheta_{n-1}+\Re_{n-1}-\vartheta_n&=0\\
p_{n-1}\vartheta_{n-1}-p_{n-1}\Re_{n-1}-p_n\vartheta_n&=0.
\end{aligned} \quad (11)$$

We regard the equations (11) as a system of linear simultaneous equations of $2n$ unknown variables $\Re_0, \vartheta_1, \Re_1, \ldots, \vartheta_{n+1}, \Re_{n+1}$, and ϑ_n. For the existence of non-trivial solution of Eqs. (11) it is necessary that the following determinant does not vanish:

$$D = \begin{vmatrix} 1 & -e^{+a_1} & -e^{-a_1} & 0 & 0 & 0 & \cdots \\ -p_0 & -p_1e^{+a_1} & p_1e^{-a_1} & 0 & 0 & 0 & \cdots \\ 0 & 1 & 1 & -e^{+a_2} & -e^{-a_2} & 0 & \cdots \\ 0 & p_1 & -p_1 & -p_2e^{+a_2} & p_2e^{-a_2} & 0 & \cdots \\ \cdots & \cdots & \cdots & \cdots & \cdots & \cdots & \cdots \\ \cdots & \cdots & \cdots & \cdots & \cdots & \cdots & \cdots \\ \cdots & \cdots & \cdots & \cdots & \cdots & \cdots & \cdots \\ \cdots & \cdots & \cdots & \cdots & 1 & 1 & -1 \\ \cdots & \cdots & \cdots & \cdots & p_{n-1} & -p_{n-1} & -p_n \end{vmatrix} \tag{12}$$

We denote the determinant whose m th column is replaced by $(-1, -p_0, 0, \ldots, 0)$, D_m. $\Re_r$ and ϑ_r are expressed as follows:

$$\Re_r = \frac{D_{2r+1}}{D} \tag{13}$$

$$\vartheta_r = \frac{D_{2r}}{D} . \tag{14}$$

From Eqs. (7) (8) (9) and (14), the behavior of electromagnetic wave in the media is completely determined. (Except the arbitrary constant a.)

We may define $\Re_0$ and ϑ_n as complex reflection coefficient and complex transmission coefficient by multiple layer, respectively. These quantities are expressed as follows:

$$\Re_0 = \frac{D_1}{D} \tag{15}$$

$$\vartheta_n = \frac{D_{2n}}{D} \tag{15'}$$

For a single layer we have

$$\Re_0 = \frac{D_1}{D} , \tag{16}$$

where

$$D = \begin{vmatrix} 1 & -e^{a} & -e^{-a} & 0 \\ -p_0 & -p_1e^{a} & p_1e^{-a} & 0 \\ 0 & 1 & 1 & -1 \\ 0 & p_1 & -p_1 & -p_2 \end{vmatrix} \tag{17}$$

$$D_1 = \begin{vmatrix} -1 & -e^{a} & -e^{-a} & 0 \\ -p_0 & -p_1e^{a} & p_1e^{-a} & 0 \\ 0 & 1 & 1 & -1 \\ 0 & p_1 & -p_1 & -p_2 \end{vmatrix} \tag{18}$$

$$a = \frac{i\omega p_1 d}{c} \tag{19}$$

and d denotes the thickness of layer 1.

We define $\Re_{01}$ and $\Re_{12}$ by the following equations:

$$\frac{p_1-p_0}{p_1+p_0} = -\Re_{01} \tag{20}$$

$$\frac{p_2-p_1}{p_2+p_1} = -\Re_{12} . \tag{21}$$

$\Re_{01}$ is the complex reflection coefficient of semi-infinite medium 1, with respect to semi-infinite medium 0, when the linearly polarized plane wave penetrate from medium 0 into medium 1 at normal incidence. $\Re_{12}$ is the corresponding quantity with respect to media 1 and 2. Then D_1 and D are expressed as follows:

$$D_1 = e^{+a}(p_0+p_1)(p_1+p_2)\{\Re_{01}+\Re_{12}e^{-2a}\}$$

$$D = e^{+a}(p_0+p_1)(p_1+p_2)\{1+\Re_{01}\Re_{12}e^{-2a}\}$$

and from Eq. (15) we have

$$\Re_0 = \frac{\Re_{01}+\Re_{12}e^{-\frac{2i\omega p_1 d}{c}}}{1+\Re_{01}\Re_{12}e^{-\frac{2i\omega p_1 d}{c}}} . \tag{22}$$

Similarly,

$$\vartheta_1 = \vartheta_{01}e^{-\frac{i\omega p_1 d}{c}} / (1+\Re_{01}\Re_{12}e^{-\frac{2i\omega p_1 d}{c}}) \tag{23}$$

$$\Re_1 = \vartheta_{01}\Re_{12}e^{-\frac{i\omega p_1 d}{c}} / (1+\Re_{01}\Re_{12}e^{-\frac{2i\omega p_1 d}{c}}) \tag{24}$$

$$\vartheta_2 = \vartheta_{01}\vartheta_{12}e^{-\frac{i\omega p_1 d}{c}} / (1+\Re_{01}\Re_{12}e^{-\frac{2i\omega p_1 d}{c}}) \tag{25}$$

where

$$\vartheta_{01} = 1 + \Re_{01} \tag{26}$$

$$\vartheta_{12} = 1 + \Re_{12} . \tag{27}$$

The formulae (22) and (25) are in agreement with the results already obtained.[4]

Reflection Method

As stated above, the difficulties of the determination of dielectric constant and loss factor

(4) J. A. Stratton, "Electromagnetic Theory", 1st Ed., 1941, p. 510.

by free wave method lie partly in the calculation of their values from the reflection or transmission coefficient experimentally obtained. In the following we shall report a convenient method for the determination of dielectric constant and loss factor from the reflection coefficient of a dielectric sheet placed on a metal plate. In the case where the refractive index is much greater than absorption coefficient, we can derive approximate formulae which enable us to compute these quantities from the experimental values of the reflection coefficient. In other cases when these approximate formulae do not hold, we may make tables which are convenient for the evaluation of these values.

1. Reflection of Electromagnetic Wave by a Dielectric Layer on a Metal.—The plane electromagnetic wave is considered to be linearly polarized and to be propagated from the air into a dielectric sheet on a metal at normal incidence as shown in Fig. 2. The complex reflection coefficient is to be expressed as follows:

$$\Re = \frac{\Re_{12}+\Re_{23}e^{-\frac{2i\omega pd}{c}}}{1+\Re_{12}\Re_{23}e^{-\frac{2i\omega pd}{c}}}. \qquad (28)$$

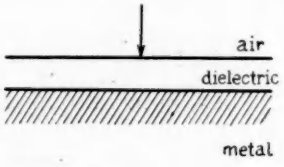

Fig. 2.

The equation (28) is essentially the same as the Eq. (22), but we have changed the subscripts in accordance with the convention adopted in other literatures.

Let ε', and ε'' respectively be the dielectric constant and loss factor of the dielectric and p^2 be $\varepsilon'-i\varepsilon''$. We have then

$$\Re_{12} = -\frac{(p-1)}{(p+1)}; \quad \Re_{23} = -1$$

and therefore,

$$\Re = -\left[\frac{-\Re_{12}+e^{-\frac{i2\omega pd}{c}}}{1+\Re_{12}e^{-\frac{i2\omega pd}{c}}}\right]. \qquad (29)$$

If we put

$$\Re_{12} = -R_{12}e^{-i\gamma}, \qquad (30)$$

then

$$R_{12} = \sqrt{\frac{(n-1)^2+k^2}{(n+1)^2+k^2}} \qquad (31)$$

and

$$\tan\gamma = \frac{2k}{(n^2-1)+k^2}. \qquad (32)$$

The square of the absolute value of $\Re$ is expressed as follows:

$$R^2 = \frac{\sinh^2\left(\frac{2\pi kd}{\lambda}+\frac{1}{2}\ln R_{12}\right)+\cos^2\left(\frac{2\pi nd}{\lambda}-\frac{\gamma}{2}\right)}{\sinh^2\left(\frac{2\pi kd}{\lambda}-\frac{1}{2}\ln R_{12}\right)+\cos^2\left(\frac{2\pi nd}{\lambda}+\frac{\gamma}{2}\right)} = \frac{R^2_{12}+e^{-\frac{8\pi kd}{\lambda}}+2R_{12}e^{-\frac{4\pi kd}{\lambda}}\cos\left(\frac{4\pi nd}{\lambda}-\gamma\right)}{1+R^2_{12}e^{-\frac{8\pi kd}{\lambda}}+2R_{12}e^{-\frac{4\pi kd}{\lambda}}\cos\left(\frac{4\pi nd}{\lambda}+\gamma\right)} \qquad (33)$$

where λ denotes the wave length of the electromagnetic wave in the air. R^2 may be called reflection coefficient, and represents the ratio of the intensity of the reflected wave to that of the incident wave.

n is the refractive index and k is the absorption coefficeient of the material composing the dielectric sheet of the thickness d. They are related to p, ε', and ε'' through the Eqs. (5) (6a) and (6b).

If we determine the value of R^2 for various values of d, we can calculate n and k by Eq. (33). However, as R^2 is a transcendental function of n and k, it is difficult to obtain their values directly from the experimental values of R^2. Therefore, we must either find approximate formulae appropriate to the calculation, or make tables useful to the computation.

2. The Case of $n \gg k$.—If $n \gg k$, approximate formulae can be obtained rather easily. In this case we have

$$\gamma \fallingdotseq 0 \qquad (34)$$

$$R_{12} \fallingdotseq \frac{n-1}{n+1}. \qquad (35)$$

In Eq. (33), variable d appears in the form of nd or kd. Moreover nd appears only in the trigonometric functions and kd in the exponential functions.

According to the assumption $n \gg k$, the exponential functions in Eq. (33) change so slowly when compared to the trignometric

functions that the former may be considered as constant in the small region of the variable d. Hence Eq. (33) may be rewritten as follows:

$$R^2 = \frac{a+b\cos\left(\frac{4\pi nd}{\lambda}\right)}{c+b\cos\left(\frac{4\pi nd}{\lambda}\right)} \tag{36}$$

where

$$a = R^2_{12}+e^{-\frac{8\pi kd}{\lambda}}$$
$$b = 2R_{12}e^{-\frac{4\pi kd}{\lambda}}$$
$$c = 1+R_{12}^2e^{-\frac{8\pi kd}{\lambda}}.$$

a, b, c may be regarded as constant in the small region of variable d.

We denote the maximum and minimum values of R^2 as R^2_M and R^2_m, and the corresponding values of d as d_M and d_m, respectively. They may be obtained by ordinal method of differentiation, and we find

$$R^2_M = \left(\frac{R_{12}+e^{-\frac{4\pi kd_M}{\lambda}}}{1+R_{12}e^{-\frac{4\pi kd_M}{\lambda}}}\right)^2 \tag{37}$$

$$R^2_m = \left(\frac{R_{12}-e^{-\frac{4\pi kd_m}{\lambda}}}{1-R_{12}e^{-\frac{4\pi kd_m}{\lambda}}}\right)^2 \tag{38}$$

$$d_M = \frac{2N\lambda}{4n} \tag{39}$$

$$d_m = \frac{(2N+1)\lambda}{4n} \tag{40}$$

where $N=0, 1, 2, \ldots$.

As stated above, our problem is to determine n and k (or ε' and ε'') from the experimental curve of R^2 *vs.* d. For this purpose we first determine n from the value of d_M or d_m experimentally obtained by Eq. (39) or (40). Next we calculate R_{12} by Eq. (35) using the value of n thus obtained. Then we determine k from the values of R_M or R_m by Eq. (37) or (38), the values of n, R_{12} and d_M (or d_m). Eq. (37) or (38) is a linear equation of exp $(-4\pi kd_M/\lambda)$ or exp $(-4\pi kd_m/\lambda)$, so we can obtain these values easily, from which we can determine the value k, using the tables of exponential function.[5] For higher approximation, we substitute the value of k into Eq. (31), and obtain the value of R_{12}. Using the value of R_{12} thus obtained, we can determine the value of k from Eq. (37) or (38) more exactly.

In the case when we can find many values of extrema though the value of k is very small we can determine the value of k from the decreasing rate of the extrema. Eq. (37) or (38) may be expanded with respect to $y = 4\pi kd/\lambda$, putting $e^{-y} = 1-y+1/2\,y^2\ldots$, and as first order expansion, we have

$$R_M \fallingdotseq 1-\frac{1-R_{12}}{1+R_{12}}y \tag{41}$$

$$R_m \fallingdotseq 1-\frac{1+R_{12}}{1-R_{12}}y. \tag{42}$$

Differentiating with respect to $d/\lambda = z$, we have

$$\frac{dR_M}{dz} = -\frac{(1-R_{12})}{(1+R_{12})}4\pi k \tag{43}$$

$$\frac{dR_m}{dz} = -\frac{(1+R_{12})}{(1-R_{12})}4\pi k. \tag{44}$$

Thus from the curve R_M *vs.* d_M, or R_m *vs.* d_m, we can obtain the value of k.

3. The Case when the Assumption $n \gg k$ does not Hold.—In the case when $n \gg k$ does not hold, we can obtain the values of ε' and ε'' (or n and k) from the experimental values of R^2 according to the following method. We draw a curve which represents R^2 *versus* d/λ according to Eq. (33) for fixed values of ε' and ε'' (or n and k).

We draw another curve (which represents R^2 *vs.* d/λ according to Eq. (33)), for another fixed value of ε'' and the same value of ε' (or another fixed value of k and the same value of n). Thus we can obtain many curves representing R^2 *vs.* d/λ, a part of which is related to constant values of ε' and ε'', and the other to the same value of ε' and the different values of ε''. Then we have many curves of similar type which correspond to other fixed values of ε'. Thus we have many curves R^2 *vs.* d/λ corresponding to ε' and ε'' (or n and k) in the required region.

A curve R^2 *vs.* d/λ is characterized by two parameters ε' and ε''. Maximum value of R^2, R^2_M or minimum value R^2, R^2_m are determined principally by ε'', and the corresponding value of d, d_M and d_m by ε'.

From a curve, R^2 *vs.* d/λ, thus obtained, we mark R^2_M, R^2_m, d_M and d_m, and for a fixed value of ε' we draw curves R^2_M *vs.* ε'' and

(5) K. Hayashi, "Koto Kansu Hyo" (Tables of higher functions), 1st Ed., 1945; "En oyobi Sokyokusen Kansu Hyo" (Tables of circular and hyperbolic functions), 1st Ed., 1945.

R^2_m *vs.* ε''. Similarly, for a fixed value of ε'', we draw curves d_M *vs.* ε' and d_m *vs.* ε'.

To obtain the values of ε' and ε'' from the experimental values of reflection coefficients, we draw a curve R^2 *vs.* d/λ, and compare it with the curves calculated by the afore-described procedure. Thus we can obtain rough values of ε' and ε''. Using the value of ε'' thus obtained, we can obtain ε' from the curve d_M/λ *vs.* ε' or d_m/λ *vs.* ε' by interpolation. (The value ε' thus obtained is almost a true value, for the curves d_M/λ *vs.* ε' or d_m/λ *vs.* ε' are insensitive to the value ε''.) Similarly we can determine ε'' from the curve R^2_M *vs.* ε'' or R^2_m *vs.* ε'', using rough value of ε'. (The curves R^2_M *vs.* ε'' or R^2_m *vs.* ε'' are insensitive to the value ε'.) The above procedure is essentially the same when we use n and k instead of ε' and ε''.

Transmission Method

In the following a method will be reported, which consists in determining dielectric constant ε' and loss factor ε'' of a material from the relation of the transmission coefficient and thickness of dielectric sheet concerned.

1. The Formula of Transmission Coefficient.—The plane electromagnetic wave of unit amplitude is considered to be linearly polarized and to be propagated in the air. A dielectric sheet with plane boundary surface is placed as shown in Fig. 3.

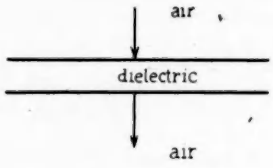

Fig. 3.

The direction of the propagation of incident wave is considered to be normal to the boundary surface. A part of the wave will be transmitted through the sheet characterized by dielectric constant ε', loss factor ε'' and thickness d. The complex amplitude of the electric field vector of the transmitted wave is given by Eq. (25). If we change the notation ϑ_2, and p_1, to ϑ, and p, and considering

$$\vartheta_{01}\vartheta_{12}=\frac{4p}{(1+p)^2}, \qquad \Re_{01}\Re_{12}=\left(\frac{p-1}{p+1}\right)^2$$

then we have

$$\vartheta=\frac{e^{-\frac{i2\pi pd}{\lambda}}\times\frac{4p}{(1+p)^2}}{1+\left(\frac{p-1}{p+1}\right)^2 e^{-\frac{i4\pi pd}{\lambda}}}. \tag{45}$$

If we write

$$\frac{p-1}{p+1}=-R_{12}e^{-i\gamma}$$

then ϑ is expressed as follows, considering $p=n-ik$.

$$\vartheta=e^{-\frac{2\pi kd}{\lambda}}\times\frac{e^{-\frac{i2\pi nd}{\lambda}}(1-R_{12}^2e^{-i2\gamma})}{1-R_{12}^2e^{-i2\left(\frac{2\pi nd}{\lambda}+\gamma\right)}}\cdot e^{-\frac{4\pi kd}{\lambda}}$$

The transmission coefficeint of the sheet D^2 may be defined as $D^2=|\vartheta|^2$, and expressed as:

$$D^2=e^{-\frac{4\pi kd}{\lambda}}\times\frac{(1+R_{12}^4)-2R_{12}^2\cos 2\gamma}{1+R_{12}^4e^{-\frac{8\pi kd}{\lambda}}-2R_{12}^2e^{-\frac{4\pi kd}{\lambda}}\cos\left(\frac{4\pi nd}{\lambda}+2\gamma\right)}$$

$$=\frac{\sinh^2(-\ln R_{12})+\sin^2\gamma}{\sinh^2\left(\frac{2\pi kd}{\lambda}-\ln R_{12}\right)+\sin^2\left(\frac{2\pi nd}{\lambda}+\gamma\right)} \tag{46}$$

2. Approximate Formulae.—(i) If $R_{12}^2\ll 1$, we have

$$D^2\fallingdotseq e^{-\frac{4\pi kd}{\lambda}} \tag{47}$$

In this case, the value of k can be obtained easily from the curve D^2 *vs.* d/λ experimentally obtained.

(ii) If $n\gg\kappa$, we have the relations expressed with Eqs. (34) and (35). Eq. (46) is rewritten as

$$D^2\fallingdotseq e^{-4\pi kx}\times\frac{(1-R_{12}^2)^2}{1+R_{12}^4e^{-8\pi kx}-2R_{12}^2e^{-4\pi kx}\times\cos 4\pi nx} \tag{48}$$

where $x=d/\lambda$.

As stated in the case of reflection method, exponential function in Eq. (48) change very slowly when compared to trigonometric function according to the assumption that $n\gg k$, so that the former can be considered as a constant in a small region of variable x. Eq. (48). can be rewritten as follows, considering $\exp(-4\pi kx)=a$, a constant, in this region.

$$D^2=\frac{a(1-R_{12}{}^2)^2}{1-2aR_{12}{}^2\cos 4\pi nx+R_{12}{}^4a^2} \quad (49)$$

The maximum and minimum value of D^2 and corresponding values of d, can at once be obtained. If we denote these values $D_M{}^2$, $D_m{}^2$, and the corresponding values of d, d_M and d_m, then we have

$$D_M=e^{-\frac{2\pi kd_M}{\lambda}}\times\frac{(1-R_{12}{}^2)}{(1-e^{-\frac{4\pi kd_M}{\lambda}}R_{12}{}^2)} \quad (50)$$

$$D_m=e^{-\frac{2\pi kd_m}{\lambda}}\times\frac{(1-R_{12}{}^2)}{(1+e^{-\frac{4\pi kd_m}{\lambda}}R_{12}{}^2)} \quad (51)$$

$$d_M=\frac{2N}{4n} \quad (52)$$

$$d_m=\frac{(2N+1)}{4n} \quad (53)$$

$N=0,1,2,\cdots$

To obtain the values of n and k (accordingly ε' and ε'') from the curve D^2 *vs.* d/λ which was experimentally obtained, we find at first the value of n from Eq. (52) or (53), then the value of k from Eq. (50) or (51), calculating the value of R_{12} from Eq. (35). Using these value of n and k thus obtained, more accurate value of k can be obtained from Eq. (50) or (51), calculating the value of R_{12} from Eq. (31).

(iii) If $k\ll 1$, the value of k may be obtained from the curves of extrema *vs.* x. Omitting the detailed calculations, we can finally express the derivatives of D_M and D_m with respect to x as follows:

$$\frac{dD_M}{dx}\fallingdotseq-\left(1+\frac{2R_{12}{}^2}{1-R_{12}{}^2}\right)\cdot 2\pi k \quad (54)$$

$$\frac{dD_m}{dx}\fallingdotseq-\left(\frac{1-R_{12}{}^2}{1+R_{12}{}^2}\right)\frac{(1-R_{12})^2}{(1+R_{12}{}^2)}\cdot 2\pi k \quad (55)$$

3. The Case when the Assumption $n\gg k$ is not valid.—In this case the values of ε' and ε'' can be obtained from the curve of D^2 *vs.* d/λ which was experimentally obtained by a similar method as described in the case of reflection method. That is, we draw many curves of D^2 *vs.* d/λ for the values of ε' and ε'' in the suitable region, and obtain the values of ε' and ε'' by interpolation.

Summary

The reflection and transmission coefficient of electromagnetic waves by multiple layer has been obtained theoretically.

A convenient method has been deviced to determine dielectric constant and loss factor of a material in a form of a sheet placed on a metal, from the reflection coefficeint.

A convenient method has also been developed to determine the dielectric constant and loss factor from experimental curve of transmission coefficient versus thickness of dielectric sheet concerned.

The author is grateful to Prof. San-ichiro Mizushima for his guidance, to Mr. Kenji Kuratani and to Mr. Kenji Nukazawa for their kind advices. His thanks are also due to the Ministry of Education for a grant in aid of this research.

Radiation Chemistry Research Institute, the University of Tokyo, Tokyo.

Determination of Dielectric Constant and Loss Factor by Free Wave Method. II. Measurement on Water and Some Insulators at $\lambda = 9.8$ cm.

By Masasi YASUMI, Kenji NUKAZAWA[1] and San-ichiro MIZUSHIMA

(Received September 26, 1950)

I. Measurement on Water by Reflection Method

Several attempts have been made to determine the dielectric constant and loss factor of a substance by the measurement of the reflection coefficient of a dielectric sheet placed on a metallic plate.[2] The experimental results cannot, however, be considered as sufficiently accurate, because of the incomplete method of calculating dielectric constant and loss factor from reflection coefficient and of the considerable experimental error which seems to arise mainly from the imperfect and unsteady source and the uneven metallic plate used as a reflector.

The former difficulty was already removed by one of us, as reported in the previous paper.[3] As to the latter, we have tried to remove it by constructing a steady and powerful source of wave and by using a mercury sheet as the reflector.

With an apparatus constructed in this way we have measured the dielectric constant and loss factor of water at the wave length of 9.8 cm. As will be reported in the following, water shows anomalous dispersion and absorption at this wave length.

The apparatus is shown schematically in Fig. 1. The 9.8 cm. wave generated with split-anode magnetron A was emitted vertically into the free space from a horn B through a wave guide G. A wooden vessel V with a rectangular surface of 60×60 cm.^{2} was placed horizontally under B. This area was just sufficient to remove the edge effect. A crystal detector C consisting of silicon crystal and nickel wire was so adjusted that the deflection of microammeter attached to it was proportional to the energy of the wave. C was moved vertically between B and V, and the energy distribution of the standing wave was determined.

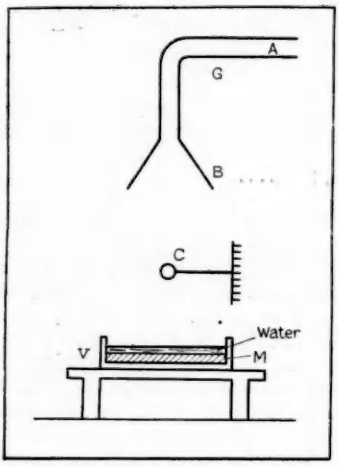

Fig. 1.

The measurement was carried out as follows. The vessel V is first filled with mercury M only. The incident wave with an amplitude E_0 is reflected by M to form a standing wave between B and M. The maximum and minimum values of the energy of the standing wave would be proportional to $4E_0^2$ and zero, respectively, when there would be no reflection other than that from the surface of the mercury. We could show that this was actually the case in our experiment.

Next, we place on the mercury a water layer whose thickness can be calculated accurately from the volume of water and the area of the vessel. The reflected and incident waves now form an imperfect standing wave, and the maximum and minimum values of its intensity will become proportional to $E_0^2(1+R)^2$ and $E_0^2(1-R)^2$, respectively. In other words, the ratio of the extreme values will be $(1-R)^2/(1+R)^2$. This ratio can be determined experimentally by moving C vertically and reading the microammeter deflections. The value of R can at once be calculated from this ratio.

(1) Now at Research Institute of Applied Electricity (the University of Hokkaidō).
(2) See *e.g.* G. Bäz, *Physik. Z.*, **40**, 394 (1939).
(3) M. Yasumi, this Bulletin, **24**, 53 (1951).

Such a measurement is made at different thickness d of the water layer and finally a curve of R^2 *vs.* d is obtained.

We can also determine the wave length in air from the positions of C corresponding to the extreme values of microammeter reading. The wave length thus determined was 9.8 cm. in agreement with the value obtained by the Lecher wire method.

The procedure of calculating dielectric constant ε' and loss factor ε'' (or refractive index n and absorption coefficient k) was reported in a previous paper.[3] The part necessary for the following discussion will be briefly repeated here.

The reflection coefficient of water layer of thickness d placed on mercury is expressed as

$$R^2=\frac{\sinh^2\left(\frac{2\pi kd}{\lambda}+\frac{1}{2}\ln R_{12}\right)+\cos^2\left(\frac{2\pi nd}{\lambda}-\frac{\gamma}{2}\right)}{\sinh^2\left(\frac{2\pi kd}{\lambda}-\frac{1}{2}\ln R_{12}\right)+\cos^2\left(\frac{2\pi nd}{\lambda}+\frac{\gamma}{2}\right)} \tag{1}$$

where

$$R_{12}^2=\frac{(n-1)^2+k^2}{(n+1)^2+k^2} \tag{2}$$

$$\tan\gamma=\frac{2k}{(n^2-1)+k^2}. \tag{3}$$

For $n \gg k$, the maximum and minimum values R_M^2, R_m^2 of R^2 are calculated approximately as follows:

$$R_M \doteqdot \frac{R_{12}+e^{-\frac{4\pi kd_M}{\lambda}}}{1+R_{12}e^{-\frac{4\pi kd_M}{\lambda}}} \tag{4}$$

$$R_m \doteqdot \frac{R_{12}-e^{-\frac{4\pi kd_m}{\lambda}}}{1-R_{12}e^{-\frac{4\pi kd_m}{\lambda}}} \tag{5}$$

$$R_{12} \doteqdot \frac{n-1}{n+1} \tag{6}$$

$$d_M = \frac{2N\lambda}{4n} \tag{7}$$

$$d_m = \frac{(2N+1)\lambda}{4n} \tag{8}$$

$$(N=0,1,2,\ldots.)$$

where d_M and d_m are the values of d corresponding to R_M^2 and R_m^2, respectively.

In the present experiment, n and k were obtained from the curve R^2 *vs.* d in the following way. We found first an approximate value of n, using Eq. (7) or (8), and calculated approximate value of R_{12}, substituting the value of n into Eq. (6). An approximate value of k could be obtained from Eq. (4) or (5), using the said value of R_{12}, and d_M or d_m. We drew a curve of R^2 *vs.* d, putting the values of n and k obtained above into Eq. (1) and compared it with the experimental curve. The calculated curve was slightly different from the experimental one, and we changed the values of n and k slightly until the former curve became almost identical with the latter. Thus the more exact values of n and k could be obtained.

The values of reflection coefficient R^2 of water at 5.5°C. obtained at various thicknesses d of the layers are shown in Table 1. The values of n and k which are obtained by above-described procedure are shown in Table 2 which includes also those of the absorption index $\kappa(=k/n)$ and the real (ε') and imaginary (ε'') parts of the complex dielectric constant.

Table 1

The Reflection Coefficient R^2 of the Water Layer of the Thickness d (mm.) Measured at 5.5°C.

d, mm.	R^2	d, mm.	R^2
0.00	1.00	9.61	0.638
2.20	0.776	10.96	0.762
2.74	0.090	12.31	0.678
3.02	0.242	13.66	0.540
3.83	0.727	14.01	0.554
5.18	0.873	14.28	0.568
6.53	0.789	14.57	0.650
7.88	0.429	15.39	0.678
8.80	0.471		

Table 2

Dielectric Data for Water

t, °C.	5.5	$\kappa=(k/n)$	0.120
λ, cm.	9.8	ε'	73.8
n	8.65	ε''	18.1
k	1.04		

The value of static dielectric constant of water at this temperature amounts to 86.1[4], which is much greater than the value of $\varepsilon'=73.8$ found in this experiment. Therefore water shows anomalous dispersion at this wave length. This is in conformity with the value of absorption index ($\kappa=0.120$) found by us. The detailed discussions on relaxation time, etc. will, however, be postponed until we obtain more data at different wave lengths.

(4) Calculated from the equation given by Drake, Pierce and Dow (*Phys. Rev.*, **35**, 613 (1930)).
$\varepsilon_t=78.59[1-0.00461(t-25)+0.0000155(t-25)^2]$
See also, Wymann, *Phys. Rev.*, **35**, 623 (1930).

Measurement on Some Insulators by Transmission Method

The previous paper described the procedure of obtaining the dielectric constant and the loss factor of an insulating material from the transmission coefficient and the thickness of the sheet.[3] In the following we shall report some experimental data of transmission coefficient and the values of dielectric constant and loss factor obtained therefrom.

The apparatus is shown schematically in Fig. 2. As in the reflection experiment a linearly polarized wave of the wave-length of 9.8 cm. was generated from a split-anode magnetron A and was emitted vertical into the free space from a horn B through a wave guide G. A large aluminium plate P was placed at an angle of 45° to the floor to avoid the reflection of the wave from it. The fact that the reading of the microammeter connected to the crystal detector C remained constant in the middle part of the space between the horn and the aluminium plate showed that there was actually no reflection from the floor. As in the reflection experiment the detector system was so adjusted as to make the microammeter reading proportional to the intensity of the wave.

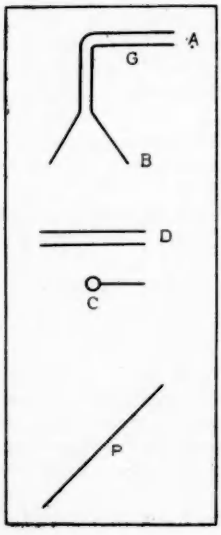

Fig. 2.

We now place a dielectric sheet D to be measured between the horn and the detector, and record the microammeter reading Id proportional to the energy of the transmitted wave. Then we remove the sheet and again record the microammeter reading I_0 proportional to the energy of the incident wave. The transmission coefficient of the sheet is simply given by

$$D^2 = I_d/I_0. \qquad (9)$$

In this measurement we have, however, to show that in the former case the microammeter reading indicates only the energy of the transmitted wave. This was shown by the fact that the microammeter showed no deflection when an aluminium plate of the same size as the sample (70×70 cm.^{2}) was placed upon the sample.

The transmission experiment was made on the sheets of ebonite, bakelite, methacryl resin, and polystyrene of various thicknesses d. The results are shown in Table 3.

Table 3

The Transmission Coefficient D^2 of Several Substances of the Thickness d (mm.) Measured at the Wave-length of 9.8 cm.

Ebonite 15°C.		Bakelite 15°C.		Methacryl resin 15°C.		Polystyrene 5°C.	
d	D^2	d	D^2	d	D^2	d	D^2
5	0.92	3	0.87	6	0.79	2	1.00
12	0.79	8	0.62	12	0.68	3.5	0.99
15	0.80	13	0.59	25	0.90	5	0.98
20	0.85	15	0.60	31	0.94	7	0.93
25	0.92	18	0.72			8.5	0.88
32	0.98	23	0.83				
35	0.96	28	0.82				

From these values of the transmission coefficient obtained at different thicknesses we can calculate refractive indices n, absorption coefficients k, dielectric constants ε', and loss angles δ according to the procedure reported in the previous paper.[3] In Table 4 are shown the results of the calculation except that for polystyrene for which we have too few data to calculate these quantities.

Table 4

Dielectric Data for Ebonite, Bakelite and Methacryl Resin (15°C.)

	Ebonite	Bakelite	Methacryl resin
n	1.60	1.92	1.65
$\kappa=k/n$	0.005	0.035	0.015
ε'	2.6	3.7	2.7
$\tan\delta$	0.01	0.07	0.05

For these samples the condition $n \gg k$ holds and we can also use the approximate formulae derived by one of us.[3] Repeating them briefly,

$$D_M^2 = \frac{e^{-\frac{4\pi k d_M}{\lambda}}(1-R_{12}^2)^2}{(1-R_{12}^2 e^{-\frac{4\pi k d_M}{\lambda}})^2} \quad (10)$$

$$D_m^2 = \frac{e^{-\frac{4\pi k d_m}{\lambda}}(1-R_{12}^2)^2}{(1+R_{12}^2 e^{-\frac{4\pi k d_m}{\lambda}})^2} \quad (11)$$

$$R_{12} = \frac{n-1}{n+1} \quad (6)$$

$$d_M = \frac{2N\lambda}{4n} \quad (7)$$

$$d_m = \frac{(2N+1)\lambda}{4n} \quad (8)$$

$$N = 0, 1, 2, 3, \ldots.$$

we have D_M^2 and D_m^2 are the maximum and the minimum values of D^2, d_M and d_m the corresponding values of thickness d, and λ is wave length. Using Eq. (7) or Eq. (8), we first obtain the value of n which we put into Eq. (6) and then calculate the value of k from Eq. (10) for Eq. (11).

Summary

The reflection coefficient of water layer placed on mercury has been measured at a wave length 9.8 cm. and at 5.5°C. From the curve of reflection coefficient *vs.* thickness of the water layer, dielectric constant and loss factor (or refractive index and absorption coefficient) have been calculated according to the procedure described previously.

Water has shown anomalous dispersion and absorption at this wave length.

The dielectric constant and loss factor have been measured for ebonite, bakelite and methacryl resin at the same wave length, by the transmission method.

In conclusion we wish to thank Mr. Isao Ichishima and Mr. Kenji Kuratani for their kind advices, and to Mr. Yoichiro Mashiko who prepared the samples used in this experiment. We are indebted to the Ministry of Education for a research grant.

Radiation Chemistry Research Institute and Faculty of Science, the University of Tokyo, Tokyo

Energy of Hydrogen Bond in Tetragonal Pentaerythritol

By Isamu NITTA, Syûzô SEKI and Keisuke SUZUKI

(Received September 12, 1950)

Introduction

There appeared already numerous papers dealing with the energy of hydrogen bond. In most of these papers, it is estimated from experimental data of substances in pure liquid or solution state. Generally, in the pure liquid or solution state, the molecular arrangement is not known so accurately that the net contribution of the hydrogen bond cannot be sorted out exactly. On the other hand, the energy of association of some carboxylic acids determined from the temperature variation of equilibrium constant for the hydrogen bond dimerization in the gaseous state[1] would be of unambiguous significance for the derivation of the hydrogen bond energy, since the molecular structure of these dimers have already been determined by the electron diffraction method.[2] In the same sense, the energy data of a crystalline substance, of which the structure is known by the x-ray analysis, will be also useful for this purpose. The only one example of such investigation hitherto carried out is the case of the hydrogen bond energy for ice.[3],[4] Now that the crystal structure of pentaerythritol is completely determined independently by one of the present authors and

(1) (a) Davies, *Ann. Report Chem. Soc.*, (1947); (b) F. W. Johnson and L. U. Nash; *J. Am. Chem. Soc.*, **72**, 547 (1950).

(2) (a) J. Karle, L. O. Brockway, *J. Am. Chem. Soc.*, **66**, 574 (1944); (b) V. Schomaker, J. U. O'Gorman, *J. Am. Chem. Soc.*, **69**, 2338 (1947).

(3) Unfortunately, the unit cell of ice is not determined uniquely.

(4) (a) Bernal and Fowler, *J. Chem. Phys.*, **1**, 515 (1933); (b) T. Ogura, *Busseiron* (in Japanese), No. 12, 1. (1948); (c) A. W. Searcy, *J. Chem. Phys.*, **17**, 210 (1949).

by Cox and his co-workers,[5] this substance may be suitable for the determination of strength of hydrogen bond in the crystalline state. Thus, we attempted to determine the heat of sublimation of this material and compare the results with the calculated values of the lattice energy.

Experimental

The sample used in the present investigation is the product of Kahlbaum Company. It was recrystallized from distilled water and was purified by fractional sublimation under high vacuum (below 1×10^{-5} mm. Hg) at about 130°. By the method of differential thermal analysis, the melting point of the extremely purified sample finally employed for the experiment was determined to be 265.5°C[6]. The vapor pressures were measured by the effusion method, of which we have already described in a previous paper.[7] The obtained numerical values are summarized in Table 1 and the vapor pressure equation derived from these experimental data is given at the bottom. Some thermodynamical data calculated from it are shown in Table 2.

Table 1

Vapor Pressures of Pentaerythritol

t°C	$P_{\text{mm. Hg}}\times10^3$	$(\log P_{\text{mm. Hg}}+3)_{obs.}$	$(\log P_{\text{mm. Hg}}+3)_{calc.}$
123.8	1.70	0.230	0.235
126.1	2.25	0.350	0.345
129.8	3.15	0.498	0.496
132.2	3.93	0.594	0.599
134.5	4.96	0.696	0.697
136.9	6.19	0.792	0.791

$$\log P_{\text{mm. Hg}} = 14.525 - 6861.1/T$$

Table 2

$\Delta H_s = 31.4 \pm 0.2$ kcal./mole
$\Delta S_s = 53.3 \pm 0.6$ e. u./mole
$\Delta G_{298.1} = 15.5 \pm 0.4$ kcal./mole
ΔH_s : Heat of sublimation
ΔS_s : Entropy of sublimation
ΔG : Free energy of sublimation

Calculation of Lattice Energy

(a) van der Waals Energy. — In a series of papers,[8] we have calculated the lattice energies of more or less complicated crystals and showed empirically that the application of the Slater-Kirkwood formula for the van der Waals interaction may be used within the error of about 10% of the observed values. In these calculations, the contributions of the atoms or atomic groups, into which the molecule is splitted, are summed up. The general agreement between the calculated and the observed values to about 10% may be looked upon as suggesting that the higher order interactions such as Margenau's force are roughly compensated by the repulsive forces.[8a]

In the present case of pentaerythritol, the molecule is splitted into three kinds of force centers; that is, the central C atom, CH_2 and OH groups. According to the Slater-Kirkwood theory the interaction energy between two molecules is given in the form of the following equation:

$$V=-\frac{3}{2}\frac{e\hbar}{m^{1/2}}\sum_{ij}\frac{\alpha_i\alpha_j}{(\alpha_i/n_i)^{1/2}+(\alpha_j/n_j)^{1/2}}\frac{1}{R_{ij}^6} \qquad (1)$$

where e is the elementary charge, m mass of electron, $\hbar=h/2\pi$, n the number of electrons in the outermost electronic shell, α polarizability of an atom or an atomic group, R_{ij} distance between the centers of force, suffix i or j denotes one or the other of the considered pair of the centers.

The molecular arrangement in the crystal with numbers assigned to molecules for convenience is illustrated in Fig. 1. The lattice constants adopted in the calculation are respectively $a=6.074$ Å. and $c=8.877$Å. at 130°.[9] The polarizabilities of atomic groups are estimated as follows. To obtain the polarizability of CH_2 group, we could make use of either the difference of molecular refractions corresponding to the increase of a CH_2 group in the homologous series of normal hydrocarbons and of normal alcohols or the similar quantities deduced from the symmetrically branched hydrocarbon series.[10]

For the former two series, there are sufficient data of refractive indices for wave lengths of H_α, H_β, H_γ, and D-line, while the data for the latter exist only for the wave length of D-line. Using these values, it is possible to calculate the mean molecular refraction of CH_2 group at infinite wave length, $(M_{\lambda=\infty})$ by application

(5) (a) F. J. Llewllyn, E. G. Cox, T. H. Goodwin. *J. Chem. Soc.*, 883, **1937**; (b) I. Nitta, T. Watanabé, *Nature*, **140**, 365 (1937); *Sci. Papers. Inst. Phys. Chem. Research*, **34**, 1669 (1938).

(6) Ebert, 260.5°; Mark, 252.5°; Seifert, 252°; Schleede, 257°.

(7) J. Nitta, S. Seki, M. Momotani and K. Sato, *J. Chem. Soc. Japan*, **71**, 378 (1950).

(8) (a) I. Nitta, S. Seki, *J. Chem. Soc. Japan*, **64**, 475 (1945); (b) S. Seki, H. Chihara, *Sci. Papers. Osaka Univ.* **1**, 1 (1949); (c) I. Nitta, S. Seki, M. Momotani, *J. Chem. Soc. Japan*, **71**, 430 (1950).

(9) These lattice constants are calculated from the experimental data of thermal expansion coefficient determined by x-ray method in this laboratory (unpublished).

(10) We have utilized the refractive indices of $C(CH_3)_4$, $(CH_3)_3C(C_2H_5)$, $(CH_3)_2C(C_2H_5)_2$, $(CH_3)C(C_2H_5)_3$ and of $C(C_2H_5)_4$.

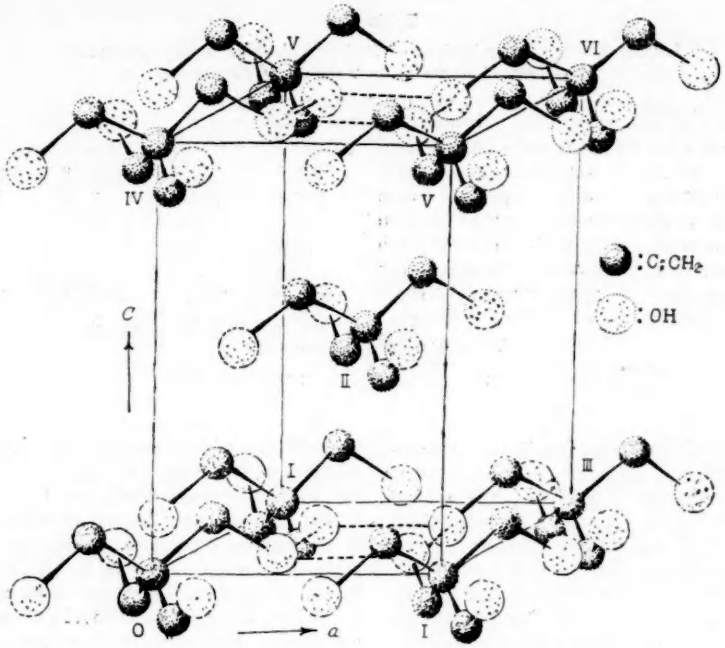

Fig. 1.—Crystal structure of tetragonal pentaerythritol (dotted lines show the hydrogen bonds).

of the Cauchy dispersion formula. In Table 3, there are given mean molecular refraction of a CH_2 group from these three sources.

Table 3

Mean Molecular Refraction of CH_2 Group

	M_γ	M_β	M_D	M_a	$M_{\lambda=\infty}$
From normal alcohols	4.72	4.68	4.64	4.61	4.51
From normal paraffines	4.76	4.68	4.64	4.61	4.51
From branched(*) paraffines	—	—	4.45	—	4.32

* Egloff, "Physical Constants of Hydrocarbon", (1939).

In Table 3 it can be seen that the values derived from the upper two series are in very good agreement with each other, while those from the third is considerably smaller. The $M_{\lambda=\infty}$ value for the last one is estimated by assuming the same relative decrement with wave length as the former. We used the value of 4.32 for calculation, since the situation of CH_2 group in pentaerythritol may rather be approximated to that of the branched chain hydrocarbon series. The molecular refractions of a OH group and the central carbon atom are deduced from the data of normal alcohols and of branched paraffines. From these values of molecular refraction at infinite wave length, we obtain the polarizabilities of the three atomic groups, which are tabulated in Table 4.[11]

Table 4

Molecular Refraction[11] and Polarizabilities

	M_D	$M_{\lambda=\infty}$	$\alpha \times 10^{24}$ cc.
CH_2 group	4.45	4.32	1.709
OH group	2.61	2.48	0.981
Central carbon	3.04	2.98	0.928

Inserting these polarizabilities and atomic parameters into the formula (1) and multipling by $N_A/2$ (N_A; the Avogadro number), we obtain the results shown in Table 5.

(11) The refractive index of this crystal measured by Dr. Kiriyama in this laboratory are $\omega=1.553$ and $\varepsilon=1.515$ for ordinary and extra-ordinary rays, respectively (D-line). Inserting these values in the Lorentz-Lorenz formula, we can obtain the values of $M_\omega=31.27$ and $M_\varepsilon=29.27$. On the other hand, assuming the additivity of atomic refraction, we have obtained from the data listed in Table 4 the value of molecular refraction; $M_D=31.28$ which is in better agreement with the M_ω value given above.

Table 5

Lattice Energy Contributions of Different Atomic Groups and the Numbers of Summation Taken in Calculation

Molecule	Distances from molecule 0	van der Waals interactions between different atomic groups						Total
		C~C	C~CH_2	C~OH	CH_2~CH_2	CH_2~OH	OH~OH	
I	6.073 Å.	4.5	70.0	94.4	269.9	702.2	1332.7	2473.7
II	6.178 Å.	4.0	58.4	48.6	254.3	352.1	71.2	788.6
III	8.590 Å.	0.5	7.8	10.0	24.5	65.8	85.4	194.0
IV	8.881 Å.	0.9	6.3	3.0	20.8	14.2	3.3	48.5
V	10.770 Å.	—	0.8	0.5	3.3	3.4	0.9	8.9
(part of summation)		53.8	797.4	816.4	3280.0	5944.4	6252.8	17144.8
(part of integration)		6	35	23	205	115	95	477
		Total van der Waals energy						17.622 kcal./mole
Numbers of pairs taken for summation		26	94	94	376	376	376	1334

In this calculation, van der Waals interactions between the molecule 0 and the first neighbors (molecules I and II), the second neighbors (molecules III and IV) and the third one (molecule V) are summed up one by one, and for the remaining part of these interactions, summation is replaced by integration, assuming the uniform distribution of the centers of attractive forces. As shown evidently in Table 5, the contribution of OH groups to the van der Waals energy is most predominant. It is also shown that the part due to integration does not exceed more than 3 %, indicating the approximation by integration is sufficient for the present purpose.

(b) Electrostatic Energy. — In the calculation of electrostatic interaction between free molecules, the dipole model is usually employed. However, for the molecular interaction in the crystalline state, the point charge model would be more adequate than the dipole model, for the intermolecular distance is much smaller here. In the present work, we used the point charge model, putting an effective charge $+\varepsilon$ on the nuclear position of the carbon atom in CH_2 group, $-(\varepsilon+\varepsilon')$ on the oxygen atom and $-\varepsilon'$ on the hydrogen atom in OH group. Exact estimation of such formal charges is of course difficult. In the present case, following the usual method, the charge ε is deduced from the bond moment 0.8 D for C—O by dividing this value by the corresponding bond distance 1.46 Å. This comes out to be 0.551×10^{-10} e.s.u., which corresponds to 11.5 % ionic character of this bond. The value of ε' can be estimated in the same way. However, the cyclic formation of hydrogen bonds will cause further elongation of the bond length as well as the increase of charge distribution of O—H bond. Taking this circumstances into account, we may use for trial three bond moments of 1.66 D, (bond moment of the free OH group in aliphatic alcohols), 1.79 D and 1.93 D, on the assumption of the normal bond length of 0.96 Å. These three values correspond respectively to the ionic character of 36 %, 39 % and 42 %. The formal charges derived from these values are $\varepsilon'=1.726$, 1.870 and 2.015×10^{-19} e.s.u. respectively. However, for the reason mentioned above, the latter two values will be preferable. The electrostatic potential V_{el} is expressed by the following equation:

$$V_{el}=\sum_{ij}\frac{\varepsilon_i\varepsilon_j}{R_{ij}} \tag{2}$$

where ε_i is the formal charge of the i-th atom, ε_j that of the j-th atom and R_{ji} is the distance between these point charges. We have used this equation only for the first and the second neighbors and the remaining part has been calculated approximately in the following manner.

We can rewrite equation (2) as follows:

$$V_{el}=\sum_{R}\sum_{ij}\frac{\varepsilon_i\varepsilon_j}{|\vec{R}-\vec{r}_i+\vec{p}_j|}=\sum_{R}\sum_{ij}\frac{\varepsilon_i\varepsilon_j}{|\vec{R}+\vec{\sigma}_{ij}|},\qquad \vec{\sigma}_{ij}=\vec{p}_j-\vec{r}_i \tag{3}$$

where $\vec{r}_i$ is the radius vector of the i-th point charge from the center of the molecule 0 (see Fig. 1) and p_j is that of the j-th point charge from the molecular center which is situated at $\vec{R}$ from the center of the molecule 0. For the contribution of the molecules of the third neighbors and of the molecules lying farther than these, the interation energies become

$$\Delta E=\sum_{R}{}'\sum_{ij}\frac{\varepsilon_i\varepsilon_j}{|\vec{R}+\vec{\sigma}_{ij}|} \tag{4}$$

where $\sum_k'$ implies the summations excluding the first and the second neighbors. Using the relation $R \gg \sigma$ this can be expanded by the Taylor theorem. In terms of components of these vectors ΔE becomes,

$$\Delta E \doteqdot \sum_1' \sum_1' \sum_2' \sum_{ij} \frac{1}{4!}\left(x_{ij}\frac{\partial}{\partial X}+y_{ij}\frac{\partial}{\partial Y}+z_{ij}\frac{\partial}{\partial Z}\right)^4 \frac{\varepsilon_i\varepsilon_j}{(X^2+Y^2+Z^2)^{1/2}}$$

$$=\sum_1' \sum_1' \sum_2' \{3(X^4+Y^4)+8Z^4+6X^2Y^2 -24Z^2(X^2+Y^2)\}/(X^2+Y^2+Z^2)^{9/2} \times \frac{3}{16}\sum_{ij}(r^2_{xi}+r^2_{yi}-2r^2_{zi})(p^2_{xj}+p^2_{yj}+p^2_{zj})\varepsilon_i\varepsilon_j \qquad (5)$$

where X, Y, Z; x_{ij}, y_{ij}, z_{ij}; r_{xi}, r_{yi}, r_{zi} and p_{xj}, p_{yj}, p_{zj} are the three cartesian components of the vectors $\vec{R}$, $\vec{\sigma_{ij}}$ and $\vec{p_j}$. Cutting off the higher term than the sixth, it is found that the terms involving the first, the second, the third and the fifth derivatives vanish on account of the symmetry properties.

The results calculated by equations (2) and (5), multiplied by $N_A/2$, are tabulated in Table 6.

Table 6

Electrostatic Energies of First and Second Neighbors

Sort of molecule	Number of molecule	Energies per one pair A	B	C
I	4	−3.28	−3.79	−4.35
II	8	−0.72	−0.79	−0.87
III	4	+1.84	+2.08	+2.33
IV	2	+0.25	+0.24	+0.23

Electrostatic Energy Contributions of Different Parts

	A	B	C	
First neighbors (molecules I and II)	−18.88	−21.48	−24.36	*
Second neighbors (molecules III and IV)	+ 7.86	+ 8.80	+ 9.78	*
Outer part	+ 0.05	+ 0.07	+ 0.08	**
Total	−10.79	−12.61	−14.50	

Case A, B and C correspond to the 36%, 39% and 42% ionic character of OH bond. Unit is kcal./mole.

* Calculated by Eq. (2). ** Calc. by Eq. (5).

It is seen that the electrostatic forces of the second neighbors and of the outer part are as a whole contributing repulsively. This is evident from the symmetry and arrangement of the molecules in the crystal.

Discussion of Results

Adding the van der Waals energy to the electrostatic one, we obtain three values for the total energy; 28.59, 30.33, and 32.12 kcal./mole respectively, corresponding to the three degrees of the ionic characters 36%, 39% and 42% of the OH-bond. These values are in general agreement with the experimental value: 31.4 ± 0.2 kcal./mole. By the reason mentioned in the preceding section the latter two of the calculated values may be more reasonable. Evidently, to calculate the interaction energy more exactly, we must take into account the repulsive energy, the energy due to the induction effects, the higher order van der Waals energy and the resonance energy. However, as described at the beginning of the third section, we have seen in many examples that the van der Waals energies calculated by the Slater-Kirkwood formula come out nearly equal to, or somewhat larger than, the experimental values. These facts seem to show empirically that the repulsive energy is nearly cancelled by the higher order van der Waals energies. It may be supposed also that the contribution of the induction effects will be small. In the above calculation, the increment of formal charge of the OH bond may be said to take this effect partly into account in a certain sense. As to the so-called resonance energy of the hydrogen boad, it is estimated from the deuterium and other effects that its contribution for the present bond length of hydrogen bond is very small as compared with the electrostatic contribution. Hence, it may be neglected without introducing any serious error.

For the estimation of the energy of hydrogen bond, it should be remarked that the definition of the energy of hydrogen bond is rather ambiguous and depending on the methods of determination. For example, in the case of dimerization of carboxylic acids, the energy of hydrogen bond is determined from the temperature dependence of equilibrium constant by the application of the van't Hoff isochore. Therefore, the energy obtained in this way involves that of reorganization of the dissociated molecules and does not correspond exactly to the hydrogen bond energy in the state of dimeric association.

Furthermore, it is uncertain whether we should take into consideration the interaction energy only of the atoms directly concerned with hydrogen bonding, or, in addition to it, the energy due to the remaining atoms. It is actually known that the effect of hydrogen bond upon the state of the remaining atoms

will modify the interaction energy.

For the estimation of the magnitude of hydrogen bond energy in this crystal, neglecting the energy of reorganization, there may be considered, for the present, following three cases. Of these the simplest may be such energy defined as interaction energies only between OH groups which are directly linked together by the hydrogen bond. From Tables 5 and 6, this is found to be 5.1 or 5.7 kcal./mole one hydrogen bond, according to whether we adopt the case B or C. The second estimation is as follows. The molecules in this crystal form distinct layers, in each of which they are linked together by the hydrogen bonds (Fig. 1). Thus, the work necessary to separate all the molecules of such a layer may be a second definition of the hydrogen bond energy. Following this definition, it comes out to be about 4.5 or 4.8 kcal./mole. Thirdly, it can be seen in Tables 5 and 6 that, although the intermolecular distances of molecules I and II from the molecule 0 are nearly equal, both the van der Waals and electrostatic energies are considerably different (Table 7). This difference may be looked upon as due to the effect of hydrogen bonding, for the molecule I is hydrogen-bonded with molecule 0, while the molecule II is not. From this point of view, we obtain as the approximated hydrogen bond energy the value of 4.68 or 5.16 kcal./mole.

Table 7

Difference of Interaction Energy between Molecule I and II

Molecule	van der Waals energy	Electrostatic energy		Total	
		B	C	B	C
I	−2.47	−3.79	−4.35	−6.26	−6.82
II	−0.79	−0.79	−0.87	−1.58	−1.66
Difference	−1.68	−3.00	−3.48	−4.68	−5.16

Comparing the energy of hydrogen bond with the total lattice energy, it is found that in any case the contribution of hydrogen bonding amounts to approximately two-thirds of the total energy.[12] It can be seen also in Table 7, as an instance, that, although the electrostatic contribution makes larger part of the whole energy, the van der Waals energy is not at all negligible.

To show such a situation by another example, we calculated in the same way as above, the hydrogen bond energy of formic acid dimer. Moelwyn-Hughes[13] has already calculated the electrostatic part of this energy, adopting the dipole model and neglecting the contribution of the van der Waals energy. His results are 8.6 and 13.1 kcal./mole corresponding to the O—H···O distances of 2.85 and 2.55 Å., respectively. On the other hand, Davies[14] has calculated the electrostatic contribution of this energy using the point charge model, and the induction energy by the use of the dipole model. The sum of these energies amounts to 13.4 kcal./mole for the hydrogen bond distance of 2.67 Å. These results seem, at first sight, to give good agreements with the experimental value of 14.13 kcal./mole.[1b] However, they are both not satisfactory in such regards that the former used the dipole model and hydrogen bonds distance which do not correspond to the actual case, and both authors do not take into account the contribution of the van der Waals energy. Thus, we recalculated the electrostatic energy due to the point charge model, and the van der Waals energy, using the numerical values of the polarisabilities of atomic groups and the ionic character of each bond shown in Table 8. In this case, the revised molecular configuration recently determined by Brockway and others[2a] is used. The obtained results are summerized in Table 9.

Table 8

Atom or atomic group	$\alpha \times 10^{24}$	Bond	Bond moment	Ionic character		
				A	B	C
O	0.630	C=O	2.50D	42%	44%	46%
OH	0.981	C—O	0.8 D	12%	14%	16%
CH	1.350	O—H	1.66D	36%	39%	42%
		C—H	0.4 D	7%	7%	7%

Case A is corresponding to the observed dipole moment.

Table 9

van der Waals energy (O—H··O)	1.36		
ibid. (excluding O—H···O)	1.37		
Electrostatic energy	A, 12.15;	B, 13.77;	C, 15.17
Total	14.88	16.50	17.89 kcal./mole

It is shown that in this molecule the contribution of van der Waals energy is not so

(12) At 187.7°, the tetragonal pentaerythritol transforms into the cubic modification. This phase transition is intimately related to the breaking of the hydrogen bond. I. Nitta, S. Seki, M. Momotani, Proc. Japan Acad., **26** (1950) (9) 25; I. Nitta, S. Seki, H. Momotani, K. Suzuki S. Nakagawa, Ibid. **26** (1950) (10) 11; I. Nitta, T. Watanabé, S. Seki, M. Momotani, Ibid. **26** (1950) (10) 19.

(13) Moelwyn-Hughes, *J. Chem. Soc.*, **1938**, 1243.

(14) Davies, *Trans. Faraday Soc.*, **36**, 333 (1940).

much as in the case of pentaerythritol, and still it amounts to about 15% of the whole.

Comparing this result with the experimental value, the model A is apparently in best agreement. However, as already pointed out, it should be taken into account that the experimental value must contain the energy of reorganization of the dissociated monomer molecules. It is recognized that in the monomer state the *cis*-form is more stable by ca. 7 kcal./mole than the *trans*-form.[9] As the shape of a single molecule in the dimer association state is a midform *cis* and *trans*, that it will be less stable by a few kcal./mole than the *cis*-form.[15] If we assume that almost all dissociated monomer molecules take the *cis*-form at the temperature of experiment, we must compare the calculated value with the experimental one with an addition of a few kcal./mole for such energy of reorganization. Thus, it is seen that again the case B or C is rather in better agreement with the observed value.

After all, the energy of hydrogen bond for this substance may be estimated to be about 8 kcal./mole, which is somewhat larger than that of pentaerythritol.

This work was carried out by the help of the research grant of Ministry of Education.

Department of Chemistry, Faculty of Science, Osaka University, Osaka

(15) We cannot estimate this energy difference exactly, because of the change of molecular structure and interatomic distances on dissociation of the dimer into monomer.

A Note on the Schulz's Osmotic Pressure Equation

By Tôru KAWAI

(Received September 19, 1950)

Introduction

It is well known that there exist two types of osmotic pressure expressions, one presented by Wo. Ostwald:

$$\pi/c = RT/M + Bc^{n-1} \qquad (1)$$

and the other presented by Schulz:

$$\pi/c = RT/M(1-cs). \qquad (2)$$

The notation of these equations is similar to what is usually employed. Recently, many theoretical treatments for high polymer solutions have been accomplished by Flory,[1],[2] Huggins[3],[4] and others, and osmotic pressure was represented by power series expansion in concentrations in all their reports as follows:

$$\pi/c = RT/M + A_2c + A_3c^2 + \ldots \qquad (3)$$

These are regarded as an interpretation of Ostwald type. Concerning the Schulz's equation (SE), however, there has not been any theoretical explanation in spite of its empirical use.

This paper presents an explanation of the SE, which may offer some empirical knowledge for the following points.

(1) For the purpose of computing molecular weight of polymer more accurately, it is necessary to obtain the precise form of the π/c *vs.* c curve. Although recent theories demand upward curve, straight lines were obtained from many experimental data, showing that the accuracy of osmotic measurements cannot predict the higher terms in Eq. (3) at low concentrations. On the other hand, the SE leads to opposite curvature at very low concentrations. Thus it is required to examine the degree of approximation of the SE and to obtain the condition for its application.

(2) In order to investigate the state of polymer molecules in solution, it may be useful to inquire the source of parameters in osmotic pressure equations. The parameters in the equations derived by Flory, Huggins, and others have no clear physical meaning. Although s in the SE is also merely a simple parameter, he gave a physical meaning on it, that is, the "specific

(1) P. J. Flory, *J. Chem. Phys.*, **10**, 51 (1942).
(2) P. J. Flory, *Ibid.*, **13**, 453 (1945).
(3) M. L. Huggins, *Ibid.*, **9**, 440 (1941).
(4) M. L. Huggins, *J. Phys. Chem.*, **46**, 151 (1942).

covolume" of solute. It is necessary to examine whether s calculated by Eq. (2) represents the true value for the above physical meaning.

Formal Transformation of the Schulz's Equation

First of all, on the view-point discussed above, we try to equate the right-hand side of the SE with that of the Huggins, which is expressed as

$$\pi/c = RT/M + RT\left(\frac{1}{2}-\mu\right)c/V_1\rho_2^2, \quad (4)$$

where V_1 is the molal volume of solvent, ρ_2, the density of polymer, and μ a constant for any given system.

Obeying the Flory's expression $c = \rho_2 v_2$ (v_2 is the volume fraction of polymer), and $M/V_1\rho_2 = x$, Eq. (4) is reduced to

$$A = 1+x\left(\frac{1}{2}-\mu\right)v_2, \quad (5)$$

where A is the so-called "osmotic pressure coefficient" ($A = \pi/RTc/M$). Substituting $cs = s'v_2$, the SE is reduced to

$$A = 1/(1-s'v_2). \quad (6)$$

From Eqs. (5) and (6)

$$1/s' = 1/x(\frac{1}{2}-\mu) + v_2 \quad (7)$$

is obtained. It must be noted that s' corresponds to the Flory's "swelling factor," which is defined as the ratio of the volume effectively occupied by a polymer molecule in solvent to that in its unswollen state.[2] While the SE was presented as an approximation, Eq. (5) was derived theoretically, showing that x and μ are predominant factors for osmotic pressure. So if Eq. (7) is derived in any other way, it may be said that the SE is interpreted theoretically, s in the SE being provided with a certain physical meaning.

Before discussing this subject, it is necessary to confirm the agreement of Eq. (7) with experimental results. We quote the Brown and Ferry's data,[5] one of the most reliable results. And $1/s'$ values are plotted against v_2 in Figs. 1 and 2. These plots are on a line with gradient 1/1 within probable experimental error, satisfying Eq. (7). This fact is merely a reiteration of the previously noted agreement

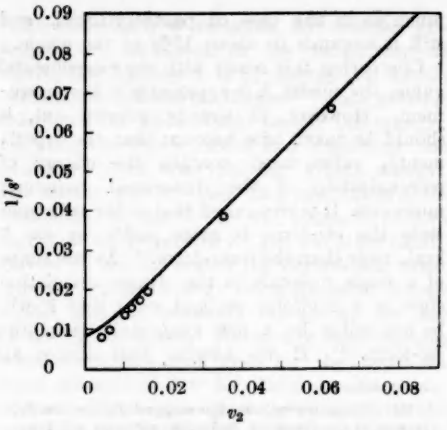

Fig. 1.—Comparison between the theoretical $1/s'$ *vs.* v_2 curve and the experimental plots (PVAc—methyl-ethyl ketone at 25°C.)

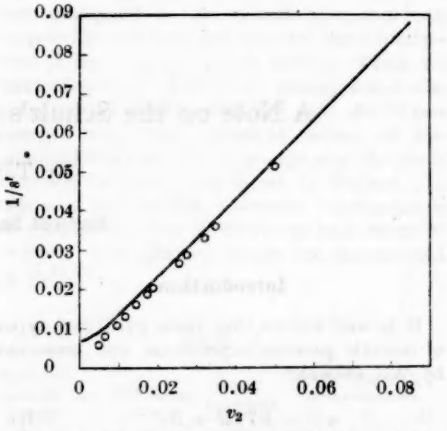

Fig. 2.—Comparison between the theoretical $1/s'$ *vs.* v_2 curve and the experimental plots (PVAc—1, 2, 3—trichloropropane at 15°C.)

of Eqs. (2) and (4) with experimental results, but we can confirm that Eq. (7) is to be allowed in this case.

Theoretical Treatment

As discussed above, since Eq. (7) has been introduced by combining the SE with the theoretical Eq. (4), the independent derivation of Eq. (7) will bring in the theoretical basis of the SE and the condition under which its approximation may be permitted.

It seems an appropriate assumption that very dilute solution consists of two regions, one completely unoccupied by solute, and the other possessing an average "concentration"

(5) G. Bown and J. D. Ferry, *J. Chem. Phys.*, **17**, 1107 (1949).

of solute determined by the statistical configurations of the polymer chain. It must be noted, however, that the state of affairs in the commonly used "dilute solution" differs from that in very dilute solution. In the former case, the intermolecular interaction cannot be neglected but in the latter case it may be neglected. Here, we are concerned with the former case.

We are going to turn our attention to one polymer molecule and consider the influence of its environment on it. The actual domain pervaded by a polymer chain cannot be defined sharply. It may be assumed that each molecule is distributed within an effective volume of sphere of radius R_e. Thus the swelling factor s' employed previously is considered to be the value for this effective volume. The s' *vs.* v_2 relation will be introduced from the condition of the equilibrium between inside and outside of this sphere.

The Flory's treatment[6] of configurations of polymer chain may be acceptable by some modification for the region occupied by a polymer molecule, although his intramolecular statistic treatment as a swelling phenomenon does not indicate the total interferences within the random coiled molecule as the result of neglecting "short range interference." The free energy in the region occupied by a polymer molecule is given by

$$\Delta F/kT = n \ln v_1 + \mu x v_1 + 3(\alpha^2-1)/2 - 3\ln\alpha \qquad (8)$$

(from Eq. (22) in the Flory's report[6]), where n is the number of solvent molecules, v_1, the volume fraction of solvent in this region, x, the number of the "lattice segments," that is, the ratio of the volume of a polymer molecule to the volume of the assumed cell, α, the factor by which linear dimension of the distribution of segments becomes larger than that of the "random flight" configurations owing to long range interference, and μ is a parameter introduced from the van Laar's expression; $\Delta H/kT = \mu x v_1$. This definition of μ is related to μ_1 employed usually in the thermodynamic treatment of polymer solutions as $\mu = \mu_1/x_s$ (where x_s is the number of the lattice cells in a solvent molecule).

Adopting the above equivalent sphere of radius R_e,

$$n = (4\pi R_e^3/3 - xV)/x_s V, \qquad (9)$$

where V is the volume of the lattice cell, and R_e is calculated from Eq. (13) in the Flory's report[6] ($R_e = 0.52\,\alpha l x^{1/2}$, where l is the length of each segment for the "equivalent chain" and x is the number of the segments in a molecule.)

Applying the relations $lx = l'x$, $l' = V^{1/3}$, and $c = l/l'$, to the above expression for R_e, Eq. (9) gives

$$\alpha = \{2c^{3/2}x_s(n + x/x_s)/x^{5/2}\}^{1/3}. \qquad (10)$$

Substituting this expression for α and $nx_s/(nx_s + x)$ for v_1 in Eq. (8) and differentiating with respect to n, there is obtained for the partial molal free energy

$$\ln a_s = \Delta\bar{F}_{1s}/kT = \ln(1-v_{2s}) + v_{2s} + \mu_s v_{2s} + A v_{2s}^{1/3} - B v_{2s},^{(7)} \qquad (11)$$

where a_s is the activity of solvent, and v_{2s} the volume fraction of polymer, subscript s showing the equivalent sphere ($A = 2^{3/3}cx_s/x^{4/3}$, and $B = x_s/x$).

Next, the activity of solvent in the environment region must be investigated. For the range of 0.01 to 0.10 volume fraction, we assume that the Huggins' expression for the activity of solvent in high polymer solutions is applicable to that in the environment region.[8] Therefore,

$$\ln a_e = \Delta\bar{F}_{1e}/kT = \ln(1-v_{2e}) + (1-1/x)v_{2e} + \mu_e v_{2e}^2, \qquad (12)$$

where subscript e illustrates the environment region.

Thus the activity of solvent in the environment region is replaced to the mean value in the whole region of the system. This approximation may be permitted as far as we deal with the equilibrium between one solute molecule and its environment in the vast region involving other polymer molecules. Namely, the activity of solvent in the environment can be put approximately equal to that in the whole region on a statistic average, considering the intermolecular interaction.

For the condition of the equilibrium between the above two regions, $\ln a_s = \ln a_e$ is obtained. Hence from Eqs. (11) and (12),

$$\ln(1-v_{2s}) + v_{2s} + \mu_s v_{2s}^2 + A v_{2s}^{1/3} - B v_{2s} = \ln(1-v_{2e}) + (1-1/x)v_{2e} + \mu_e v_{2e}^2. \qquad (13)$$

(6) P. J. Flory, *J. Chem. Phys.*, **17**, 303 (1949).

(7) This formula is analogous to the Flory's (Eq. (7) in *J. Chem. Phys.*, **18**, 108 (1950)) obtained for the swelling of network structure, except the coefficient B is two times larger than that of the Flory's.

(8) In very dilute solution ($s'v_2 \ll 1$), the activity of the region completely unoccupied by solute can be calculated and the result is $\ln a_e = \ln(1 - 8s'v_2)/8s'x$.

Since v_{2s} obviously equals to $1/s'$, the $1/s'$ *vs.* v_2 relationship has been derived here ($v_{2s} \fallingdotseq v_2$). Because Eq. (13) cannot be solved readily, numerical values of both sides of it are calculated by substituting suitable values for v_{2s} and v_{2s} respectively. Then equating the numerical values of these two sides, $1/s'$ *vs.* v_2 relation is obtained numerically.

In the above calculation constants A, B, μ_s and μ_e, must be estimated:

(1) A. The exact values of c cannot be deduced from theory, but are anticipated in the range from 0.1 to 1.0. We can select the proper dimension of the lattice cell freely and assume that $x_s = 1$, and $x = M/\rho_2 V_1$. Thus A is calculated for the proper values of c such as to illustrate the case that might arise in practice. ($A = 2^{2/3} cx_s/x^{4/3}$)

(2) B is calculated readily. ($B = x_s/x$)

(3) μ_s is obtained by usual manner from the osmotic data.

(4) μ_s may not equal numerically to μ_1 in the Flory's report. While μ_1 is applied to the interaction of an individual polymer molecule with its immediate environments, μ_s is indicative of the total polymer-solvent interaction within the region occupied by a polymer molecule. In order to eliminate the deviation of the Flory's treatment from the true thermodynamical value, it may be appropriate that the Huggins' expression for the partial molal free energy of dilution[9] ($\overline{F}_1 du = kT[\ln(1-v_2) + (1-1/x)v_2 + \mu v_2^2]$) should be applicable to this spherical region, instead of that attained from the Flory's procedure ($\Delta\overline{F}_1 du = kT[\ln(1-v_2) + v_2 + \mu_1 v_2^2]$), resulting that $\mu_1 = \alpha/RT$ is transffered to $\mu = 1/\beta + \alpha/RT$ without any alteration of the expression of the activity of solvent. This procedure is not yet satisfactory because circumstances in the above spherical region differ from those in polymer solutions. μ_s is supposed to be a little larger than the Huggins' μ, owing to the restriction[10] imposed on the possible number of configurations in the above spherical region.

Flory and co-workers used the μ-value determined on a polymer solution for the μ-value of the gel swollen in the same liquid in the treatments[11],[12] of the swelling of gels. In this point, as pointed out by Doty and co-workers,[13] lies an important source of inaccuracy in the Flory's procedure. The difference between μ-values determined by swelling and osmotic pressure is calculated by Doty and co-workers to be about 0.06 unit for a cross-linked polymer (polystylene) in various solvents. Although we can assume the above spherical region as if it were an extremely loose gel, the distinction between the spherical region and its environment is obscure. The difference between μ_s and μ_e, is supposed to be very small in our case. Thus we estimate this difference to be approximately 0.01 unit. Further quantitative discussion may be difficult owing to the complication of the above restriction to configurations and the weakness of the theoretical basis of μ itself.

Now employing these values of A, B, μ_e and μ_s, examples of the numerical calculation and the graphical method for the purpose of solving Eq. (13) are shown in Table 1 and Fig. 3 respectively, and the theoretical curve thus obtained is illustrated in Figs. 1 and 2, compared with the previously inserted experimental plots. A good coincidence between the theoretical curve and the experimental plots is observed.

Table 1

An Example of the Numerical Calculation of Eq. (13)
(methylethyl ketone solution of P. V. Ac.[5])
($M = 300,000$).

(Right-hand side) $x = 2800$, $c = 1$, $A = 4.0 \times 10^{-5}$, $B = 3.57 \times 10^{-4}$, $\mu_s = 0.44$

v_{2s}	$\ln(1-v_{2s}) - v_{2s} \times 10^4$	$Av_{2s}^{1/3} \times 10^4$	$-Bv_{2s} \times 10^4$	$\mu_s v_{2s}^2 \times 10^4$	$\ln a_s \times 10^4$
0.01	− 0.5039	0.0862	−0.0357	0.44	−0.0134
0.03	− 4.5948	0.1243	−0.1072	3.96	−0.6183
0.05	−12.9364	0.1474	−0.1786	11.00	−1.9676
0.07	−25.7127	0.1648	−0.2500	21.56	−4.2379
0.09	−43.1127	0.1792	−0.3214	28.16	−7.6149

(left-hand side) $\mu_e = 0.43$, $x = 2800$

v_{2e}	$\ln(1-v_{2e}) \times 10^4$	$(1-1/x)v_{2e} \times 10^4$	$\mu_e v_{2e}^2 \times 10^4$	$\ln a_e \times 10^4$
0.01	−100.5039	99.9643	0.43	−0.1096
0.03	−304.5948	299.8929	3.87	−0.8367
0.05	−512.9364	499.8214	10.75	−2.3676
0.07	−725.7127	699.7500	21.07	−4.8927
0.09	−943.1127	899.6781	34.83	−8.6042

(9) In our case, v_2/x term in the Huggins' expression vanishes when the entropy of dilution is combined with the entropy of elastic deformation of the molecule.

(10) This restriction is caused by the fact that the spherical region consists of a sequence of segments. Namely in this region the number of configurations is constrained owing to the expectancy for the occurrence of a segment in a cell immediately adjacent to a cell known to be occupied, while in the treatments of polymer solutions the effect of this expectancy is averaged as a whole in some manners considering the discontinuous nature of the solutions.

(11) P. J. Flory and J. J. Rehner, *J. Chem. Phys.*, **11**, 521 (1943).

(12) H. F. Boyer, *J. Chem. Phys.*, **13**, 363 (1945).

(13) P. Doty, M. Brownstein and W. Schlener, *J. Phys. Coll. Chem.*, **53**, 213 (1949).

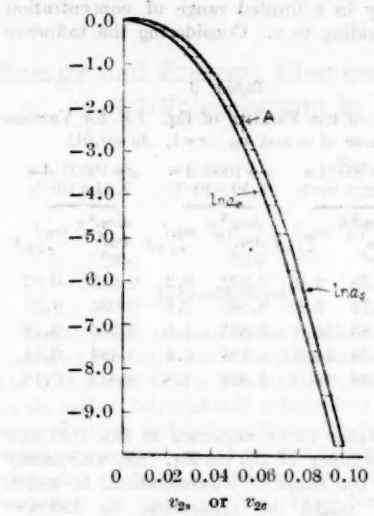

Fig. 3.—An example of the graphical method of Eq. (13). A: Volume fraction of polymer in the spherical region which is in equilibrium with a 0.05 by volume solution of polymer.

Now, expanding the logarithmic terms in Eq. (13) in series and neglecting terms beyond the first two,

$$-(1/2-\mu_s)v_{2s}^2+v_{2s}/x+Av_{2s}^{1/3} = -(1/2-\mu_e)v_{2e}^2-v_{2e}/x \qquad (14)$$

is obtained. If the relation

$$Av_{2s}^{1/3}+\Delta\mu v_{2s}^2 = 2v_{2s}/x, \qquad (15)$$

where $\Delta\mu=\mu_s-\mu_e$, is satisfied, then follows

$$v_{2s} = v_{2e}+1/x(1/2-\mu_e). \qquad (16)$$

Eq. (16) coincides entirely with Eq. (7). Therefore, Eq. (15) is the necessary condition to satisfy Eq. (7) and for the SE to afford a theoretical basis.

The trial substitution of the above numerical values for A, x, $\Delta\mu$ and v_{2s} in Eq. (15) shows that Eq. (15) affords a legitimate approximation as illustrated in Table 2. In spite of the considerable large deviation from Eq. (15) in the range of moderately concentrated solutions, *i.e.*, over 0.07 volume fraction, a good agreement with experimental results is obtained as illustrated in Figs. 1 and 2, probably owing to the fact that the higher terms neglected in the derivation of Eq. (14) is more effective to cover the above deviation as concentration increases. In the above calculation we assume that $c = 1$, from the viewpoint that each segment for the "equivalent chain" is supposed to correspond to one monomer unit of polyvinyl acetate, whose volume roughly equals to the molecular volume of the solvents. However, it must be noted that the deviation from Eq. (15) due to the c-values is rather small as illustrated in Table 2.

Table 2

The Test of the Validity of Eq. (15) for Various Values of c
(Methylethyl ketone and 1,2,3-trichloropropane solutions of P. V. Ac.)[5]

x	v_{2s}	$\Delta\mu v_{2s}^2+Av_{2s}^{1/3}\times 10^4$			$2v_{2s}/x \times 10^4$
		$c=0.25$	$c=0.5$	$c=1.0$	
2,800	0.01	0.033	0.056	0.096	0.071
	0.03	0.121	0.152	0.214	0.213
	0.05	0.286	0.322	0.397	0.355
	0.07	0.532	0.573	0.655	0.497
	0.09	0.855	0.900	0.989	0.639
2,400	0.01	0.030	0.051	0.091	0.083
	0.03	0.119	0.149	0.207	0.250
	0.05	0.285	0.319	0.388	0.417
	0.07	0.529	0.568	0.645	0.583
	0.09	0.852	0.894	0.978	0.750

Meanwhile, Schulz found the following relation form experiments

$$\pi = ks^{-\nu}, \qquad (17)$$

where k and ν are constants characteristic to the polymer-solvent system. The theoretical basis of Eq. (17) may be interpreted as follows: it is obvious from the above assumption that the activity of solvent in the whole region may be approximated to that within the spherical region. Thus it results that the activity of solvent in polymer solutions is the function of $v_{2s}(=1/s\rho_2)$ only (see Eq. (11)). Hence

$$\pi = -\Delta\bar{F}_1/V_1 = -RT\ln a_s/V_1 = -RT\{\ln(1-v_{2s})+v_{2s}+\mu_s v_{2s}^2 +Av_{2s}^{1/3}-Bv_{2s}\}/V_1. \qquad (18)$$

Substituting the numerical values calculated from the Staudinger's experimental data[14] on polyvinyl acetate-acetone system for A, B and μ_s in Eq. (18), the numerical calculation is carried out. The $\log\pi$ *vs.* $\log s$ relations thus obtained are illustrated in Fig. 4, compared with the experimental plots. The calculated

(14) H. Staudinger and H. Warth, *J. prak. Chem.*, **155**, 261 (1940).

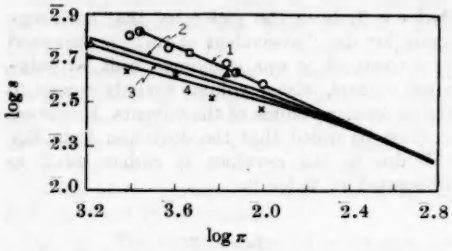

Fig. 4.—Comparison between the theoretical $\log \pi$ *vs.* $\log s$ curves and the experimental plots. Curve 1, Pro. No. 2($x=3350$); curve 2, Pro. No. 3R ($x=2250$); curve 3, Pro. No. 4R ($x=1600$); curve 4, Pro. No. 3 ($x=1870$); □, Pro. No. 2; ○, Pro. No. 3; ◑, Pro. No. 3R; △, Pro. No. 4R; ×, Pro. No. 5.

plots are approximately on straight lines and the experimental plots are also not so far from them.[15] Thus it is proved not only that Eq. (18) can be approximated to Eq. (17), but also that the theoretical values of k and ν agree with those values determined by the experiments. Because swelling pressure is assumed to be an expression of the activity of solvent within the spherical region, it is appropriate that k and ν are applicable to the swelling pressure of the same system.

Conditions for the Establishment of the Schulz's Equation

As discussed above, the influence of both c and $\Delta\mu$ on Eq. (15) are not predominant enough to the considered significant. Now the test of the validity of Eq. (15) for various values of x and v_{2s} is illustrated in Table 3. Eq. (15) holds its validity over the considerable wide range of x. However, it must be noted that Eq. (15) affords a satisfactory approximation only in a limited range of concentration corresponding to x. Considering the influence

Table 3

The Test of the Validity of Eq. (15) for Various Value of x and v_{2s} ($c=1$, $\Delta\mu=0.01$)

v_{2s}	$x=100$ ($A=3.42\times10^{-3}$) $\frac{\Delta\mu v_{2s}^2+}{Av_{2s}^{1/3}}\times10^4$	$2v_{2s}/x\times10^4$	$x=1000$ ($A=1.59\times10^{-4}$) $\frac{\Delta\mu v_{2s}^2+}{Av_{2s}^{1/3}}\times10^4$	$2v_{2s}/x\times10^4$	$x=10000$ ($A=1.34\times10^{-7}$) $\frac{\Delta\mu v_{2s}^2+}{Av_{2s}^{1/3}}\times10^4$	$2v_{2s}/x\times10^4$
0.01	7.38	2.0	0.352	0.2	0.012	0.02
0.03	10.72	6.0	0.583	0.6	0.092	0.06
0.05	12.85	10.0	0.835	1.0	0.253	0.10
0.07	14.58	14.0	1.144	1.4	0.493	0.14
0.09	16.14	18.0	1.521	1.8	0.813	0.18

of the higher terms neglected in Eq. (14) and the uncertainty of $\Delta\mu$ on Eq. (15), we roughly estimate the range of concentration, to which the SE might be applicable, as follows; $v_2=0.04\sim0.08$ for $x=100$, $v_2=0.01\sim0.07$ for $x=1{,}000$ and $v_2=0.01\sim0.05$ for $x=10{,}000$.

Conclusion

(1) We have given a theoretical basis to s in the Schulz's equation (2).

(2) Since the deficiency of this approximate treatment lies in the uncertainty of $\Delta\mu$, a comprehensive investigation including both the experimental and theoretical study of the above "restriction imposed on possible configurations" is necessary for the refinement of our theory.

(3) The above treatment does not concern with extremely dilute solution ($sv_2 \ll 1$).

I should like to express my appreciation to the diretcor K. Makishima for his encouragement and support to this work.

Laboratory of Textile Chemistry,
Tokyo Institute of Technology, Tokyo

(15) When x is extremely small, Eq. (17) fails its validity.

Energy and Entropy Changes Accompanying the Molecular Association of δ-Valerolactam in Its Carbon Tetrachloride Solution

By Masamichi TSUBOI

(Received December 4, 1950)

Introduction

Recently the present writer made measurements of the infra-red absorption intensities of the 3.11 μ and 3.24 μ bands of δ-valerolactam in its carbon tetrachloride solutions at various concentrations and temperatures. The results of these experiments are of interest in connection with the problem concerning the molecular association of cyclic amides, since they show decidedly that δ-valerolactam molecules form on association exclusively ring dimers, the two bands being due to one and the same ring dimer structure. Furthermore, from the data obtained, calculations were made of the changes of energy and entropy accompanying the ring dimer formation. Some details of these experiments and their results are presented in this paper.

Experimental

The samples examined are carbon tetrachloride solutions of δ-valerolactam

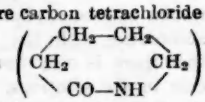

purified by vacuum distillation.

As containers of the solutions, specially-made silica glass cells of different lengths (from 0.1 to 10 cm.) were used. (See Fig. 1.) Each cell has windows of plane-parallel silica glass plates (W), set by welding at both ends of its horizontal tube (H), parallel to each other, and an electric heating device is attached to the cell so that its content can be kept at desired temperatures.

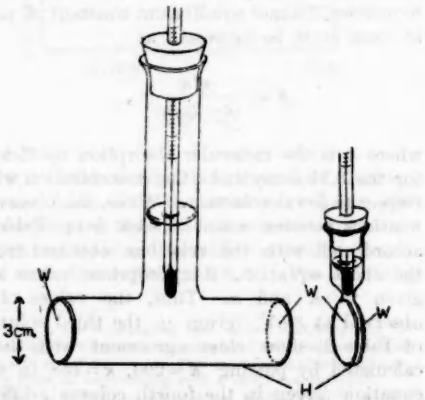

Fig. 1.

The spectrometer with quartz prism here used is the same one which the writer used in his previous work.[1]

δ-Valerolactam in carbon tetrachloride solutions exhibits, as reported in a previous paper,[1] three N-H bands, at 2.92 μ (due to free molecule), 3.11 μ (due to associated molecule) and 3.24 μ (also due to associated molecule). In the present experiments, measurements of the absorption intensities of these N-H bands were made with the object of determining the concentrations with respect to the free and associated molecules in the solutions of various concentrations (with respect to δ-valerolactam) at different temperatures.

Unfortunately, accurate absorption intensity measurements of the 2.92 μ band were not possible, owing to the interference of the absorptions in the neighborhood of 2.9 μ by the quartz prism used. Accordingly, measurements were made only of the other two bands at 3.11 μ and 3.24 μ.

Results and Interpretations

(1) From the measurements of transmittance (I/I_0) of the solutions for rays of 3.11 μ and

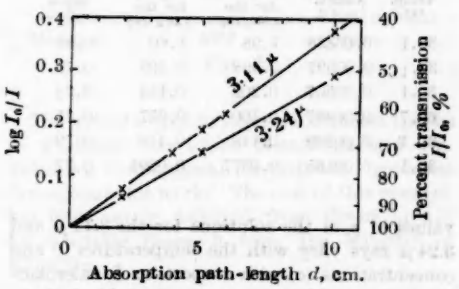

Fig. 2.—Observed relation between $\log I_0/I$ and d; concentration, 0.00165 mol/l.; temperatur, 30.1°C.

(1) M. Tsuboi, This Bulletin, 22, 215 (1949).

3.24 μ of various path-lengths (d), it was found that the observed relations between I/I_0 and d accord with the Lambert's law, deviations from it due to errors in observation being within a few per cent of $\log I_0/I$. Some examples of the relations obtained are shown in Figs. 2 and 3.

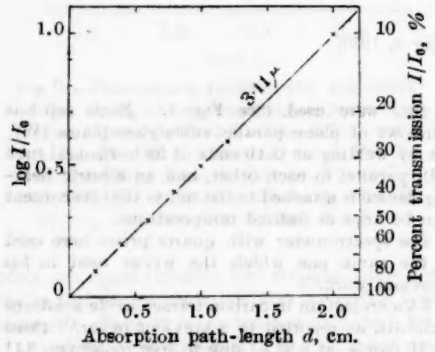

Fig. 3.—Observed relation between $\log I_0/I$ and d: concentration, 0.00997 mol/l; temperature, 30.1°C.

Based on the relations stated above, the value of $\frac{1}{d}\log\frac{I_0}{I}$ (denoted hereafter as x) for each solution is conveniently used in this paper to represent the absorption intensity of each band, for this value is independent of the path-length and is proportional to the concentration of the associated molecules to which the absorption band is assigned.

(2) In Table 1 are given the results of exploratory observations made as to how the

Table 1

Temp. °C.	Concn. mol/l.	x obsd. for the 3.11 μ ray	x obsd. for the 3.24 μ ray	$\frac{x_{3.24\mu}}{x_{3.11\mu}}$
30.1	0.03338	1.98	1.60	0.81
30.1	0.00997	0.498	0.395	0.79
30.1	0.00507	0.202	0.154	0.76
60.7	0.00487	0.100	0.077	0.77
30.1	0.00399	0.148	0.116	0.79
30.1	0.00165	0.0377	0.0291	0.77

values of x of the solutions for the 3.11 μ and 3.24 μ rays vary with the temperatures (t) and concentrations (c) with respect to δ-valerolactam. A notable fact seen in the table is that, while the values of both x for the 3.11 μ ray ($x_{3.11\mu}$) and x for the 3.24 μ ray ($x_{3.24\mu}$) vary with t and c, the ratios $x_{3.11\mu}/x_{3.24\mu}$ for any given t and c remain constant. This fact indicates that the two bands are due to one and the same kind of associated molecule and that the determination of one of the x's is sufficient for determination of the concentration of that molecule.

(3) In the third column of Table 2 are given

Table 2

Temp. °C.	Concn. mol/l.	x for 3.11 μ ray (obsd.)	x for 3.11 μ ray (calcd.)
30.1	0.03338	1.98	2.01
	0.02158	1.24	1.22
	0.01362	0.700	0.709
	0.01320	0.682	0.681
	0.00997	0.498	0.483
	0.00905	0.441	0.429
	0.00757	0.355	0.343
	0.00555	0.231	0.220
	0.00507	0.202	0.203
	0.00399	0.148	0.147
	0.00296	0.0922	0.0975
	0.00165	0.0377	0.0415
45.3	0.01295	0.528	0.538
	0.00497	0.147	0.143
60.7	0.03204	1.47	1.42
	0.01270	0.381	0.392
	0.00487	0.100	0.097
	0.00159	0.0129	0.0143

the values of x for the 3.11 μ ray, as observed with the solutions of various concentrations (with respect to δ-valerolactam) and temperatures. It is to be shown below that these results can be explained on the assumption, in accordance with the indication given in (2), that there is only one kind of associated molecule in the solutions, *i.e.*, $(C_5H_9NO)_2$, to which the 3.11 μ band is attributable, and that this dimer coexists with monomer C_5H_9NO in equilibrium, $2C_5H_9NO \rightleftarrows (C_5H_9NO)_2$.

On the assumption as stated above, the monomer $\rightleftarrows$ dimer equilibrium constant K now at issue must be expressed as

$$K=\frac{x/\kappa}{(c-2x/\kappa)^2},$$

where κ is the molecular absorption coefficient for the 3.11 μ ray and c the concentration with respect to δ-valerolactam. While, the observed relations between c and x seen from Table 2 accord well with the relations obtained from the above equation, if appropriate values are given to K and κ. Thus, the values of x observed at 30.1° (given in the third column of Table 2) show close agreement with those calculated by putting $K=206$, $\kappa=158$ in the equation (given in the fourth column), differences between them being less than several per

cent of the values of x, with one exception.[2] The values of x observed at 60.7° also agree well with those calculated from the equation by putting $K=45$, $\kappa=159$. Furthermore, it is to be noticed that the values of κ given above for 30.1° and for 60.7° are practically equal to each other. This is just as it should be, since in the temperature range now in concern the molecular absorption coefficient for the ray of 3000 cm.$^{-1}$ or thereabout in frequency must be independent of temperatures.[3]

The value of K at 45.3° is 90, as calculated from the observed values of x and the assumed value of κ (=159).

In Table 3 the values of K for three different

Table 3

Temperature, °C.	K	ΔF, kcal./mol	ΔS, E. U.	ΔE, kcal./mol
30.1	206	−3.21		
45.3	90	−2.84	−23.5	−10.3
60.7	45	−2.52		

temperatures are given, with, in parallel column, the values of free energy change (ΔF) on association, which were calculated from the corresponding values of K (by the formula $\Delta F=-RT\ln K$). When the logarithms of these values of K are plotted against $1/T$, the points obtained fall on a single straight line (as shown in Fig. 4) From the inclination and the in-

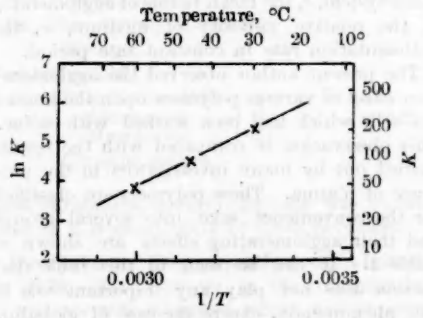

Fig. 4.

tercept of this straight line, the values of energy change (ΔE) and the entropy change (ΔS) accompanying the dimer formation in the solution are obtained as $\Delta E=-10.3\pm1.0$ kcal./mol and $\Delta S=-23.5\pm2.5$ E. U. The ΔE value here obtained is about twice as much as the value known for ordinary single hydrogen bond.

All the facts stated above, in combination, show decisively that δ-valerolactam molecules form on association only one type of dimer—the ring dimer with the inter-monomer double hydrogen bonds of the structure:

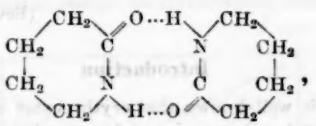

and that both of the two N-H association bands (at 3.11 μ and 3.24 μ) are attributable to this single structure.

The conclusion reached here does not agree with the view advanced by some previous writers, as Darmon and Sutherland,[4] who tend to attribute the two N-H association bands exhibited by cyclic amides to two different types of associated molecules.

Appendix.—In Fig. 5 is shown graphically the relation between association degree of δ-valerolactam molecules and the concentration and temperature of the solution, as obtained from the values of ΔE and ΔS.

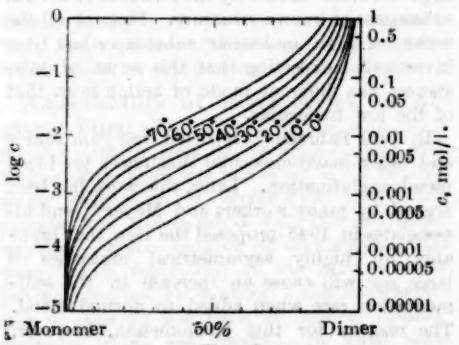

Fig. 5.

The writer wishes to express his sincere thanks to Professor San-ichiro Mizushima and Dr. Takehiko Shimanouchi for their kind guidance throughout this work. The cost of this research has been partly defrayed from Grant in Aid for Scientific Research from the Ministry of Eduction.

Chemical Institute, Faculty of Science, the University of Tokyo, Tokyo

(2) In the exceptional case where $c=0.00163$ mol/l., the difference between the calculated and observed values of x is about 10% of it. This is probably attributable to the error in determining such a small concentration.

(3) R. C. Tolman, "Statistical Mechanics with Applications to Physics and Chemistry", 1927, p. 175.

(4) S. E. Darmon and G. B. B. M. Sutherland, *Nature*, **164**, 440 (1949).

Mechanisms of Agglomeration of Red Cells by High Polymer Compounds[1]

By Kiyoshi INOKUCHI

(Received December 9, 1950)

Introduction

It is well-known that erythrocytes agglomerate each other under various conditions. This erythrocyte agglomeration is devided into two types, *i.e.*, specific and non-specific ones, the former being observed in the immunological reaction while the latter practically in all other cases. The increase in sedimentation rate of erythrocytes, which often becomes the object of clinical examination for various diseases, is considered to be due to the agglomeration of erythrocyte. Recently, the mechanism of immunological (specific) agglomeration has been elucidated by the physicochemical studies carried out by Pauling[2] and his colaborators. The present author's paper deals with the results of experiment performed with the purpose of elucidating the mechanism of the non-specific agglomeration caused by the addition of several substances of known structure. First of all the action of high molecular substances has been investigated expecting that this series of substances has different mode of action from that of the low molecular.

In 1921 Fahraeus[3] reported that gum arabic and other macromolecular substances produced pseudoagglutination. Later, this work has been argued by many workers and Meyer[4] and his associates in 1945 proposed the view that probably all highly asymmetrical molecules of large size will cause an increase in the sedimentation rate when added to normal blood. The reasons for this phenomenon, however, are not definitely known. In order to elucidate the mechanism of this phenomenon, the following experiments were carried out.

Experimental

The quantitative expression of the degree of agglomeration was made by sedimentation experiment. To 0.5 ml. of packed red cells which have been washed with isotonic saline were added 1.5 ml. of colloid saline solution of *p*H about 7, and after sufficient agitation, the sedimentation rate was measured by the Westergren method. As has been reported a period of constant rate of falling was observed to follow an induction period. As the sedimentation rate in the constant rate period can be reproduced with sufficient accuracy and characterizes the sedimentation system under investigation, this value will be employed for further discussion. With the assumption that the sedimentation obeys a modified Stokes' law, the relation between the size of agglomerate and sedimentation rate may be expressed by the following equation

$$r = C\sqrt{\eta v}$$

where C is a constant determined by sedimentation system, r, the mean radius of agglomerate, η, the relative viscosity of medium, v, the sedimentation rate in constant rate period.

The present author observed the agglomeration effect of various polymers upon the human red cells which had been washed with saline. This observation is compared with the results carried out by many investigators in the presence of plasma. These polymers are classified for the convenience sake into several groups and their agglomerating effects are shown in Table 1. It can be seen in this table that plasma does not play any important role in this phenomenon, except the case of globulin. Moreover it may be deduced from this table that among the negative colloids, fibrous ones generally show this effect, while spherical ones exert but little action at best. It has been observed that the agglomeration brought about by negative colloids is reversible and the agglomerate forms rouleaux structure, while the positive polymers which exert far stronger agglomerating action than the negative ones, cause an irreversible agglomeration and the agglomerate forms random clumping, but not rouleaux structure. In order to clarify, first of all, the mechanism of the agglomeration by

(1) This work was reported at the meeting for general discussion of colloid chemistry under the auspices of Chemical Society of Japan, Kyôto, Nov., 1950. The earlier part of this work was carried out at the Faculty of Science of the University of Kyûshû.

(2) L. Pauling, *J. Amer. Med. Assoc.*, **62**, 2643 (1940).

(3) R. Fahraeus, *Acta Med. Scand.*, **3**, 55 (1921).

(4) K. Meyer, E. Hahnel and R. R. Feiner, *Proc. Soc. Exptl. Biol. Med.*, **58**, 36 (1945).

Table 1

Water soluble polymers	Agglomeration effect on red cells: in whole blood	Agglomeration effect on red cells: washed with saline
Negative colloid		
(1) Fibrous colloid		
(a) Electrolytic colloid		
Na-alginate	+[5]	+
Na-glycolcellulose	+	+
Na-desoxyribonucleate	+[4]	+
Pectin	+[6]	+
Gelatin	+[7]	+
Potassium salt of polyvinyl alcohol sulfuric ester	+	+
Gum arabic	+[3]	
Fibrinogen	+[5]	
Na-hyaluronate	+[4]	
Type-III pneumococcus polysaccharide	+[9]	
(b) Non-electrolytic colloid		
Glycolcellulose	+	+
Mannan	+	+
Polyvinyl alcohol	+[10]	+
Dextran[10]	+[11]	+
(2) Spherical colloid		
(a) Electrolytic colloid (Globular protein)		
Ovalbumin	−	−
Serum albumin	−[5]	−
Serum globulin	+[5]	−
Hemoglobin	−	−
(b) Non-electrolytic colloid		
Glycogen	±[6]	±
Positive colloid		
Poly N-trimethyl glucosamine (Macramine)		+++
Clupeine sulfate		+++

these substances, sodium alginate was mainly used as a representative of these polymers.

Decrease in Concentration of Alginate in Bulk.—The decrease in the concentration of alginate was measured, which was expected to occur by the addition of erythrocytes if the adsorption of alginate by erythrocytes would take place. The decrease in concentration, however, was so small that it barely exceeds the limit of experimental error.

Electric Charge of Erythrocytes by the Addition of Alginate.—The change of the electric charge on the erythrocytes by the addition of alginate was also measured using a flat microelectrophoretic cell. As shown in Fig. 1, the electric charge on erythrocytes increases

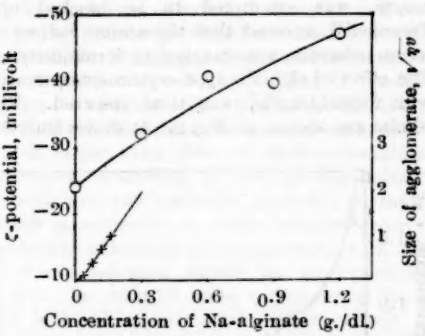

Fig. 1.—Charge of red cell and size of red cell agglomerate *versus* alginate concentration: circles show ζ-potential and crosses, the size of agglomerate, temp., 16°C; *p*H, 7.3.

proportionally with the amount of alginate. This result clearly shows some change have taken place on erythrocyte surface.

Adsorbability of Erythrocytes on Alginate Film.—Thin film of alginic acid made on the glass by treating Na-alginate film with hydrochloric acid, was immersed in an isotonic saline suspension of erythrocyte for a few minutes and then washed with isotonic saline solution. Some number of erythrocytes thus were found remaining on the film without having removed by washing. The adsorbabilities of cells on the films of several metallic alginates which are insoluble in water were observed in the same manner. As shown in Table 2, it was found that the adhering abilities of erythrocyte on alginate films are different according to the kind of metal ion of alginate,

Table 2

Numbers of erythrocytes adhered to the various metallic alginate films (Relative number)

H-alginate	340, 320	Zn-alginate	58, 89, 48
Ca- 〃	10, 5, 12	Ba- 〃	35, 37, 43
Cu- 〃	84, 87, 78	Mn- 〃	43, 32, 36

These metalic alginate films were prepared by treating the Na-alginate films in various metallic solution.

(5) Maynard B. Chenoweth, *Ann. Surg.*, **127**, 1173 (1948).
(6) Ch. Wunderly, *Experimentia*, **1**, 332 (1945).
(7) Koop, *Surgical Clinics of North America*, Philadelphia number, 1313 (1944).
(8) J. Gray and E. B. Mitchell, *Proc. Soc. Exptl. Biol. Med.*, **51**, 403 (1942).
(9) W. J. Nungester and Klein, *Proc. Soc. Exptl Biol. Med.*, **36**, 315 (1937).
(10) cf. F. P. Turner *et al.*, *Surg. Gyn. Obst.*, **8**, 673 (1949).
(11) A. Grönwall and B. Ingelman, *Acta physiol. Scand.*, **9**, 188 (1945).
(16) Ch. Wunderly, Viertel jahrschr, Naturforsch. Ges. Zürich, **89**, 170 (1944).

namely Ca-alginate film almost failed to show the ability to adhere erythrocytes on it, while they adsorb considerably on the film of alginic acid.

The Effect of Some Change Occurred on Erythrocyte Surface.—With the purpose of finding the effect of some change occurred on the erythrocyte surface, the amino radical, considered to be the positive center of erythrocyte, was attempted to be blocked up. Fraenkel[12] reported that the amino radical of serum albumin was attacked by formaldehyde. The effect of alginate upon erythrocytes, treated with formaldehyde, was thus observed. The results are shown in Fig. 2. It shows that the

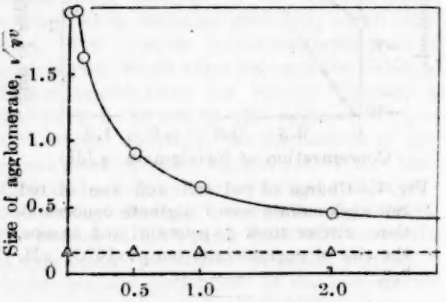

Fig. 2.—Effect of formaldehyde upon the red cell agglomeration by alginate (circles). Triangles show the only effect of formaldehyde on red cells in the absence of alginate, temp., 16.5°C.; Na-alginate, 0.1%; *p*H, 6.6.

agglomerating action of alginate decreases with the concentration of formaldehyde used. Moreover, Klotz[13] has shown that some organic anisons, *i.e.*, methyl orange and dinitrophenol, picric, and cinnamic ions combine with the amino radicals of serum albumin. The effect of these anions upon erythrocyte agglomeration by alginate was observed. It was shown that the coexistence of 0.1 mol/dl. of these four anions prevents completely the agglomeration by alginate. Salicylic, benzoic, and sulfanilic ions, which have been considered to give similar action to the afore-stated substances, also show the inhibiting effect on erythrocyte agglomeration by alginate.

Effect of Degree of Polymerisation of Alginate[14] on the Agglomeration.—As

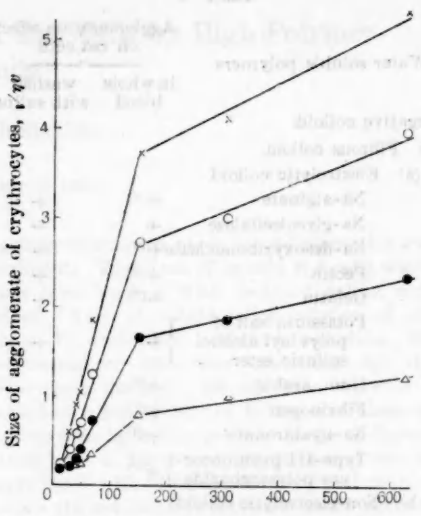

Fig. 3.—Size of agglomerate of red cell *versus* degree of polymerisation of alginate added, × 0.16%, ○ 0.12%, ● 0.08%, △ 0.04%.

shown in Fig. 3, it has been observed that the agglomerating action of alginate increases remarkably with increase in the degree of its polymerisation as well as its concentration. The effect of the former factor is the greatest in certain range of the degree of polymerisation.

Discussion

Possible mechanism of Agglomeration of Erythrocytes by Na-alginate.—From the afore-stated results that the electric charge of cells increases with the increase in concentration of alginate added, and that erythrocytes are capable to adsorb on the alginic acid film, it may be considered that alginate molecule is adsorbed on erythrocyte surface.

It was observed by the author that diacetyl alginate, prepared by the acetylation of OH radicals of Na-alginate, aggregetes to practically the same extent as the original alginate. Furthermore as shown in Table 2, it was found that the adhering abilities of erythrocyte on alginate films are different according to the kind of metal ion of alginate. These facts show that the dissociated radical of alginate, *i.e.*, carboxyl one, is the centre of its adsorption on erythrocytes. On the other hand, the attempts to block up the amino groups on cell surface have brought the preventing effect of agglomeration of cells. This shows that the centre

(12) Fraenkel-Conrat and Olcott, *J. Biol. Chem.*, **174**, 827 (1948).

(13) Klotz and Curme, *J. Amer. Chem. Soc.*, **70**, 937 (1948).

(14) Polymer homologues of alginate was prepared by the method reported by the author in *Memoirs of the Faculty of Science, Kyushu University*, Ser. C, **1**, 115 (1950).

of adsorption on erythrocyte are considered to be the amino groups on its surface, presumably that of lysine, arginine, histidine, etc. From these facts, it may be concluded that alginate molecule is adsorbed on erythrocyte surface by the electrostatic force. Although alginate is a macromolecule having carboxyl radicals on each unit, simulatneous-fitting of all the carboxyl radicals of alginate in the positive centres on the cell probably cannot occur due to the steric hinderance. It is more likely that alginate molecule combines with red cell with a small portion of the radicals and that the remaining portion of them is left unreacted. It is probable that the unreacted radicals then combine with the second cell, thus alginate molecule holding the cells together. Such a view is supported by the experimental fact, as mentioned above, that the agglomerate of erythrocytes increases in size with the increase in the degree of polymerisation of alginate added. The increase in the degree of polymerisation causes the increased molecular extentsion in solution, which in turn facilitates the molecule to act as link joining cells together.

Other substances shown in the group of negative electrolytic fibrous colloid in Table 1 are generally considered to provide the similar properties as alginate with respect to this effect. Besides, it was also reported that with pectin,[6] sodium desoxyribonucleate,[4] and sodium hyaluronate[4] their agglomerating effects increase with the polymerisation degree as seen in sodium alginate. The above indicated mechanism is, therefore, the common one for negative fibrous electrolytes.

Non-electrolytic Fibrous Colloids.—As shown in Table 1, glycolcellulose, mannan, dextran, and polyvinyl alcohol have been known to possess the action to agglutinate red cell. These substances are similar in structure to the fibrous electrolytes, except only that the hydrophilic radicals are OH group which is not dissociated. The dependence of agglomeration upon the polymerisation degree was also reported for this series of substances.[4][6] Moreover, it has been found by the present author that these substances show their agglomerating action neither in the presence of formaldehyde, nor of some organic anions such as cinnamic, salicylic, etc. These facts also support the view that the same mechansim as that of alginate is also available for these substances. However, the force contributing to the adsorption of the colloids upon cells probably is a nature of hydrogen bond, acting between OH groups of colloids and the amino radicals on red cell surface.

Reason for the Lack of Agglomeration Effect of Globular Protein.—As shown in Table 1, the native globular proteins, for instance, ovalbumin, serum albumin, serum globulin, hemoglobin, cause no agglomeration of red cell. The question arises why these proteins lack this action in spite of the presence of dissociated radicals in their molecules. As to this problem, at least two possible reasons may be considered, *i.e.*, the lack of adsorption of these proteins on cell surface or too small molecular extension of these proteins. Pauling[15] reported that erythrocytes previously treated with bisdiazoarsanilic benzidine forms agglomerate and this is due to the formation of -NN-⟨⟩-⟨⟩-NN- bridge between the cells. Obviously, the length of the bridge between the protein molecules is much larger than that of bisdiazobenzidine. Moreover, according to the present author's experiment, the partially degraded alginate, which is estimated to have smaller order of molecular extension in comparision with that of serum albumin, shows the agglomerating action. In view of these experimental facts, the lack of agglutination effect cannot be considered to be due to their too small molecular extension. Thus, we prefer another possibility that this negative result is due to the lack of the adsorption of the protein on cells. Now we face to the problem why globular protein cannot attach to the cell surface, while fibrous colloids can do. Red cells, in this case, possess negative charge as a whole, which causes the repulsive force against negative colloids. Therefore we must consider a necessary condition for the combination of these colloids with cell surface in spite of the repulsion between them. The author proposes the following view concerning this point. In order that negative colloid can couple with the weakly positive radicals situated among strongly charged negative groups on cell surface, it is necessary that the negative group in the polymer molecule has a mobility in solution strong enough to be capable of attaching themselves to the positive centres surrounded by negative ones on the surface of cells. This view is easily understood by the fact that the low molecular organic anions are capable of combining with the amino group of negatively charged protein. A fibrous molecule is considered to have a favorable property to satisfy the necessary condition mentioned above, since each part of the molecule seems to possess a sufficient flexibility in solution. In addition to this property, fibrous molecule easily holds cells together on account of the large molecular extension in solution.

(15) D. Pressman, D. H. Campbell and L. Pauling, *J. Immunol.*, **44**, 101 (1942).

Globular protein, however, does not satisfy this necessary condition, because each part of the protein molecule is closely packed in space by virture of hydrogen bonds. The negative radicals of the protein, which are fixed each other in space and accordingly unfavorable to change their mutual positions in solution, thus cannot appreciably attach to the positive centres on cells surrounded by strongly charged negative ones due to steric hinderance. Owing to such properties of the molecular shape of the polymers, a fibrous molecule exerts agglomeration effect on erythrocytes, while a spherical one does not show it.

It is very interesting to note that a considerable agglomeration occurs when globulin is added to whole blood, which is in accord with the results obtained by Gray and others, while it does not occur in the absence of plasma as shown in Table 1. Many interesting problems concerning globulin remains unexplained, waiting for further research.

Agglomerating action of Glycogen. — Generally speaking, the agglomerating effect of this substance upon cells is very small, but in higher concentration the agglomeration occurs to some extent. The molecular extension of glycogen in solution is considerably small as seen from the knowledge of viscosity. Moreover, the mobility of each part of the molecule in solution is considered to be neither so poor as that of globular protein, nor so rich as of fibrous colloid. In view of these properties of glycogen, the experimental result obtained can be explained.

Some Suggestions to Clinical Problems. —In general, the rate of erythrocytes sedimentation in pathological state has been considered to be dependent on the nature and concentration of the protein components of the plasma. However, some experimental evidences, suggesting that erythrocytes sedimentation rate may likewise be profoundly influenced by non-protein substances, were reported by several workers.[4] If it might be assumed that certain polymers of fibrous shape appear in blood in the course of diseases and they were responsible for the increased sedimentation rate in the pathological state, the mechanism of this clinical phenomenon may also be explained by the same mode proposed above.

Summary

The mechanisms of agglomeration of erythrocytes caused by hydrophilic negative polymers were investigated and the following views were proposed.

(1) Among the negative colloids, fibrous colloids show the erythrocyte agglomeration, while spherical ones do not cause it.

(2) Agglomeration by the negative colloids is caused by two actions, *i.e.*, adsorption of these polymers upon cells and their action to join cells together. Those substances which lack either or both of these actions fail to cause the agglomeration.

(3) Fibrous structure of macromolecule favors these actions on account of the large extension of molecule and adequate flexibility of each part of the molecule in solution.

(4) The dissociated or dipol radicals of the negative polymers and amino groups of the protein of cell surface are considered to be the centres of adsorption respectively.

The author expresses his hearty thanks to Prof. Dr. J. Sameshima and Dr. T. Tachibana of the University of Tokyo and Prof. T. Sasaki of the University of Kyushu for their kind guidance in the course of this study. The author also wishes to express his gratitude to Prof. Dr. T. Tomoda and Prof. Dr. S. Hojo of the University of Kyushu who granted the chance to make this work possible.

Department of Chemistry, Faculty of Science, Kyushu University, Fukuoka

Department of Chemistry, Faculty of Science, the University of Tokyo, Tokyo

A New Synthesis of Progesterone[1]

By Yoshiyuki URUSHIBARA, Misao CHUMAN and Shunyo WADA

(Received December 9, 1950)

The principle used in this synthesis originates in the reduction of cholesterol oxides[2] and is the same as used in the new synthesis of testosterone,[3] consisting essentially of catalytic reduction of a 3β-hydroxy-5,6α-epoxy-steroid to a 3β,5α-dihydroxy-compound followed by oxidation to a 5α-hydroxy-3-ketone and dehydration to a Δ^4-3-ketone. The 5,6α-oxido steroid gives always a 5α-hydroxy-compound on catalytic reduction, and this change can be taken as an evidence for an α-oxido structure. With an oxide possessing a carbonyl group a little complication may possibly arise, because at the same time the carbonyl group may be reduced ot either epimeric alcoholic group. In the case of the synthesis of testosterone, α-dehydroisoandrosterone oxide acetate gave fortunately the

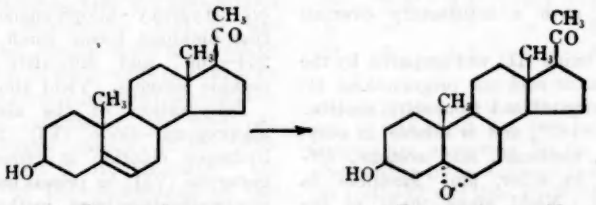

(I) Pregnenolone (II) Pregnenolone oxide

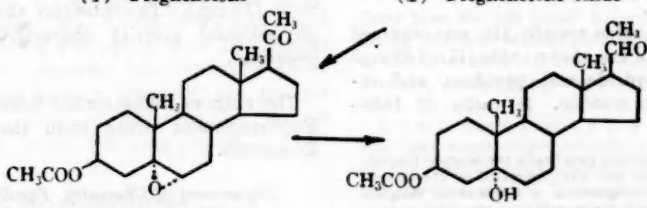

(III) Pregnenone oxide acetate (IV) Allopregnane-triol-(3β, 5α, 20) 3-acetate

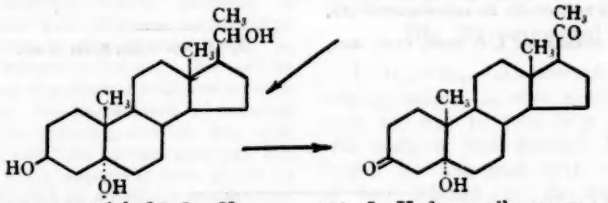

(V) Allopregnane-triol-(3β, 2α, 20) (VI) 5α-Hydroxy-allopregnanane-dione-(3, 20)

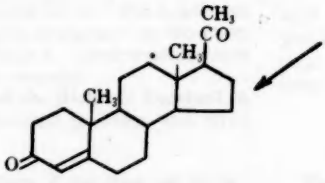

(VII) Progesterone

(1) Japanese Patent applied for on July 1st, 1948, and entered as No. 184914 on October 20th, 1950.

(2) Y. Urushibara and M. Chuman, This Bulletin, **22**, 70 (1949).

(3) Y. Urushibara and M. Chuman, This Bulletin, **22**, 1 (1949).

desired androstane-triol-(3β, 5α, 17β)[4] 3-acetate on catalytic reduction, as reported. Later experiments, however, yielded sometimes mixtures of epimeric triols.[5] The synthesis of progesterone starts from pregnenolone (I), and reduction of the carbonyl group at carbon atom 20 might cause a similar problem. But, such a complication, if any, can be eliminated in this case, because the carbon atom in question is oxidized again to a carbonyl group in the final product, progesterone.

The present synthesis cannot claim a method swifter or simpler than any of the known starting from pregnenolone, if the number of the steps of reactions involved be considered, but it proved notwithstanding a new method worth studying, because it afforded a proof for the α-oxido configuration of the pregnenolone oxide (II) and gave a satisfactory over-all yield.

Pregnenolone oxide (II) was prepared by the action of perbenzoic acid on pregnenolone (I) (65 mg.), and recrystallized from ethyl acetate. It melts at 185—187°, and is soluble in ethyl acetate, ethanol, methanol, and acetone, difficultly soluble in ether, and insoluble in petroleum ether. Yield about 90% of the theory (60 mg.).

Pregnenolone oxide acetate (III) was obtained by acetylation of the above oxide (II) (140 mg.) with acetic anhydride and pyridine, and recrystallized from acetone. It melts at 165—166°. Yield about 90% (130 mg.). M. Ehrenstein and M. T. Decker[6] treated pregnenolone acetate with potassium permanganate and obtained an oxide melting at 163—165°. Although a direct identification is lacking, the present authors believe that they obtained the same substance.

The above acetate (III) (50 mg.) was dissolved in glacial acetic acid and shaken with hydrogen and platinum oxide. About two mols of hydrogen were absorbed. The reduction product (IV) was then hydrolyzed with methanolic potassium hydroxide, and the hydrolyzate, perhaps an epimeric mixture of allopregnane-triols-(3β, 5α, 20) (V), was oxidized without purification with chromic acid in glacial acetic acid. The oxidation product was recrystallized from a mixture of ethanol and ethyl acetate. 5α-Hydroxy-allopregnane-dione-(3,20) (VI) thus obtained forms small plates melting at 264—266° and difficultly soluble in most organic solvents. Yield about 80% (35 mg.).

Dehydration of the above 5α-hydroxy-allopregnane-dione (VI) (20 mg.) with dry hydrogen chloride in chloroform gave progesterone (VII) in prisms melting at 125° after recrystallization from methanol. Yield about 80% (15 mg.). The substance showed a perfect physiological activity characteristic of progesterone.

The authors thank for the Scientific Research Encouragement Grant from the Ministry of Education.

Department of Chemistry, Faculty of Science, The University of Tokyo, Tokyo

(4) The triol 3-acetate gave finally testosterone through succeeding processes and was designated as 17α in conformity with the configuration of testosterone assigned at that time. Later it has been known that the configuration of testosterone was corrected to 17β, and in consequence the triol is undoubtedly the androstanetriol-(3β, 5α, 17β).

(5) Compare L. Ruzicka and A. C. Muhr, *Chem. Abst.*, **38**, 6294 (1944).

(6) *J. Org. Chem.*, **5**, 544 (1940).

Plastic Deformation of the Regenerated Cellulose Fibers. I. Dichroic Study of the Deformation of Freshly Prepared Fibers

By Saburo OKAJIMA and Yasuji KOBAYASHI

(Received December 14, 1950)

I. Introduction

The authors studied quantitatively the dichroic behaviors of the natural and artificial fibers and found that dichroism can reasonably show their inner structures.[1] The deformation process of the regenerated fiber was also studied by using this phenomenon and it was concluded that the results confirm Kratky's second theory[2] in the early stage of stretching in the case of the freshly prepared and swollen state. But this conclusion was made by neglecting the volume change of the fiber during stretching, and P. H. Hermans[3] has recently pointed out the importance of this volume effect. So we also repeated the study taking this effect into consideration and found that the previous conclusion must be changed a little, so it is reported here especially about the case of the freshly prepared and not yet dried fibers. That of the reswollen sample will be given in the following papers.

II. Experiment

(1) **Sample.**—Isotropic model filaments of regenerated cellulose were prepared by the cuprammonium process as already described[4] in the study of the refractive indices. One or two days were necessary to prepare a sufficient amount of the sample, but the degradation of cellulose did not occur if the spinning solution was kept from air (oxygen) and light during spinning. For this purpose the whole apparatus were placed in a closed box controlled at a definite temperature and the surface of the spinning solution was covered with a thin layer of oil. The conditions of preparation and some properties of the fibers are summarized in Table 1. Their cross sections are almost completely circular.

(2) **Measurement of the Dichroic Constant *D*.**—The samples are stretched in water and dyed without drying, in a methanol solution of congo red (0.10-0.05%) for half an hour at room temperature, excepting No. 6a, which was dyed after drying in an aqueous dye solution after the old method[1] and then $D = K_{\parallel}/K_{\perp}$ was measured; $K_{\parallel}$ and $K_{\perp}$ are the absorption coefficients of the dyed fiber for the plane polarized D-line oscillating in the directions parallel and perpendicular to the fiber axis. D is the dichroic constant of Preston,[5] exhibiting the inner structure of the fiber.

Table 1

Sample No.	Spinning solution: Cellulose (%)	Cu (%)	NH_3 (%)	Fiber: DP	Swelling deg.	v_L
14	13.4	4.9	10.1	380	4.5	2.00
6a	11.8	5.5	21.5	380	7.1	1.91
15	9.3	3.1	6.1	370	4.6	1.93
K	4	1.7	4	300	13.6	1.97
20	3	1.5	8	580	14.5	1.95

For this measurement a new microphotometer has been constructed according to the principle of the Leipho-microphotometer (Leitz) used in the previous study. The new photometer has the same accuracy as that of the previous one.

III. Experimental Results

(1) $v_{1w} \sim v_{2w}$.—An isotropic specimen of the original length l_{0w} was stretched to l_{1w} and kept for one to two days at that length, and then it was released and the residual length l_{2w} was read with a calipers after it had relaxed to the equilibrium state. During these operations the specimens were kept always in the water of the room temperature. Then the total (v_{1w}) and the residual (v_{2w}) stretching degrees are calculated as follows:

$$v_{1w} = l_{1w}/l_{0w} \quad \text{and} \quad v_{2w} = l_{2w}/l_{0w}.$$

The relation between v_{1w} and v_{2w} is very characteristic as shown by a typical example in Fig. 1; in the early stage of stretching

(1) S. Okajima and others, *J. Soc. Chem. Ind. Japan*, **49**, 38, 128 (1946); *J. Soc. Textile and cellulose Ind. Japan*, **3**, 89, 94 (1947); **4**, 21 64 (1948).
(2) O. Kratky, *Kolloid- Z.*, **84** (1938).
(3) P. H. Hermans, J. J. Hermans, D. Vermaas and A. Weidinger, *J. Polymer Science*, **3**, 1 (1948).
(4) S. Okajima and others, *J. Soc. Chem. Ind. Japan*, **43**, 355 (1940); etc.
(5) J. M. Preston, "Modern Textile Microscopy," Emmott and Co., London, 1933.

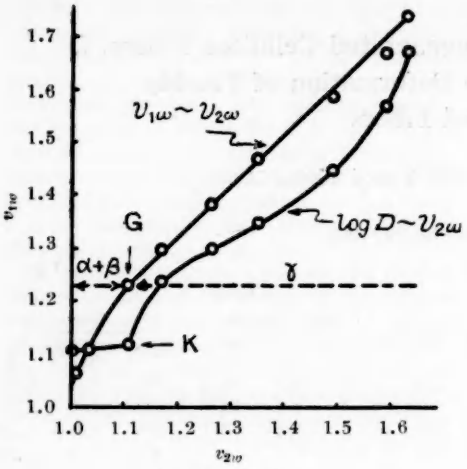

Fig. 1.—No. 15.

($\alpha+\beta$-range) the larger part of v_{1w} is recovered but when v_{1w} goes beyond this range v_{2w} grows in the linear proportion to v_{1w} (γ-range). This transition point from $\alpha+\beta$-range, G, can be recognized clearly.

$\alpha+\beta$-range is generally about 10% as shown by the above example although there exist some fluctuations.

(2) Volume Change during Stretching.— The diameters of the specimen, b_{0w}, b_{1w} and b_{2w}, corresponding to the lengths l_{0w}, l_{1w} and l_{2w} respectively, were measured microscopically and the corresponding volume ratios were calculated as below:

$$R_{1w} = b^2_{1w} \cdot l_{1w} / b^2_{0w} \cdot l_{0w} = V_{1w}/V_{0w}$$

and

$$R_{2w} = b^2_{2w} \cdot l_{2w} / b^2_{0w} \cdot l_{0w} = V_{2w}/V_{0w},$$

and similarly the ratio R_{2d} from the corresponding dry volume V_{2d} and V_{0w}

$$R_{2d} = b^2_{2d} \cdot l_{2d} / V_{0w} = V_{2d}/V_{0w}.$$

The swelling degrees before and after stretching q_0 and q_2 were given by

$$q_0 = V_{0w}/V_{0d} \quad \text{and} \quad q_2 = V_{2w}/V_{0d},$$

where V_{0d} is the air-dried volume of the isotropic fiber.

In the above notation the suffixes 0 and 1 mean the states before and after stretching respectively and 2 especially the equilibrium state after relaxing. The suffixes w and d denote the wet and air-dried states respectively.

The volume change also corresponds to its $v_{1w} \sim v_{2w}$ curve as shown in Fig. 2. R_{1w} increases slightly (4~10%) till $v_{1w} = 1.1$ (α-range) and decreases slowly to the original

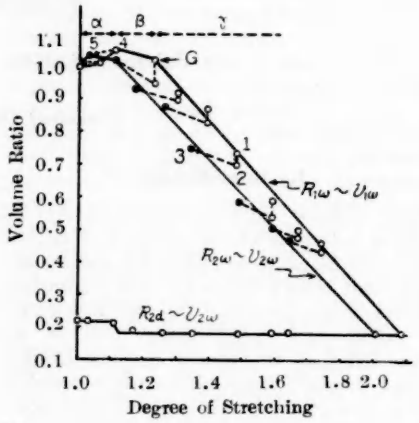

Fig. 2.—No. 15.

value (β-range) and then suddenly and linearly decreases with the increase of v_{1w} till breaking (γ-range). When the fiber is kept at a certain length (l_{1w}) in the γ-range for two days at room temperature, its diameter and the volume decrease slowly, though they increase again when the fiber is released and allowed to shrink freely. In the α- and β-ranges the volume does not change while being kept at l_{1w} but decreases slightly after releasing. These changes are shown in the figure by the two representatives 1→2→3 and 4→5.

Such multiphase deformation is also seen in the change of $R_{2d} \sim v_{2w}$ *i. e.*, it remains unchanged in the $\alpha+\beta$-range ($v_{2w} = 1.0 \sim 1.1$ or $v_{1w} = 1.0 \sim 1.23$) but decreases at G and again is kept constant thereafter (γ-range). Therefore q_2/q_0 is not always equal to R_{2w}.

In Fig. 2 the points R_{1w} or R_{2w} are not always on the smooth lines but small fluctuations can be seen, which are thought to be due principally to the slight fluctuations among the specimens of the same sample. If we trace R_{1w} of the same specimen every time we stretch it a little same remarkable phenomena can be seen as Fig. 3 shows:

(i) The β-range extends to 1.2~1.3 of v_{1w}.

(ii) The curves of No. 15 of lower swelling degree is zig-zag and it is clearly beyond the scope of the experimental error, and it may be supposed that the deformation did not happen uniformly in the exact sense, while this tendency is slight in the case of the highly swollen fiber as No. K.

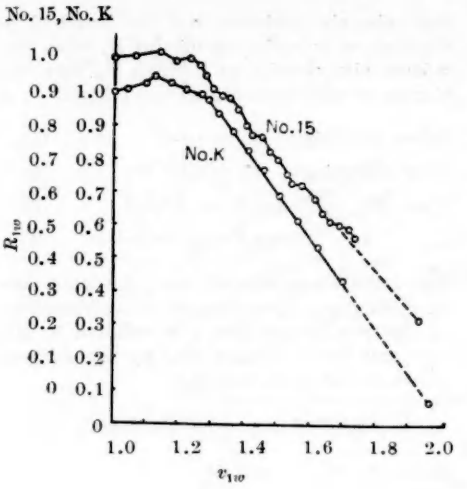

Fig. 3.

(iii) Extrapolating the lines further, beyond the breaking points and reading the values of v_{1w} at $R_{2d}=V_{2d}/V_{0w}$ they are 1.9~2.0 and nearly constant, and correspondingly v_{2w} obtained by extrapolating R_{2w}-line are 1.8~1.9. This means that the stretching follows the expelling of the intermicellar free water and if the stretching can be continued without breaking, the complete dehydration of the free water occurs when the fiber is stretched by nearly 100%. As this is very suggestive the values of these v_{1w} are specially denoted by v_L and shown in the last column of Table 1. We shall return to this point later.

(3) $D\sim v_{2w}$.—As $\log D/\Gamma$ is equal to 20 according to our calculation[1] $\log D$ is plotted against v_{2w} in the present study. Then it is convenient to know also the relation $\Gamma\sim v_{2w}$ directly from the same curve; Γ is the intrinsic double refraction of the fiber and measured as reported previously.[5]

As an example, No. 15 is shown in Fig. 1; there appears a kinck point K on the $\log D$-curve, which corresponds completely to the point G on the $v_{1w}\sim v_{2w}$ curve already described and in the $\alpha+\beta$-range the increase of D is very slight. Fig. 4 shows other examples, which have similar discontinuities and their curves are slightly sigmoid. In the case of No. 6a the values of Γ determined by the retardation method are also given in the figure by the mark +. They were determined by mounting the air-dried specimens into tricresylphosphate, so the values gained are the total double refractions, and the curve of Γ does not coincide completely with that of $\log D$, but runs parallel.

IV. Comparison of the Data with the Theoretically Calculated Curves

In the previous study the above discontinuity was missed due to too small points of observation in the first stage of deformation, and $n_\parallel$ and $n_\perp$[6] are plotted against v_{2w} which was corrected only in the slight intrinsic anisotropy of the original samples. The same treatment applied to the present data leads to the same conclusion as before (Fig. 5), where the curves 1 and 2 are calculated ones on the

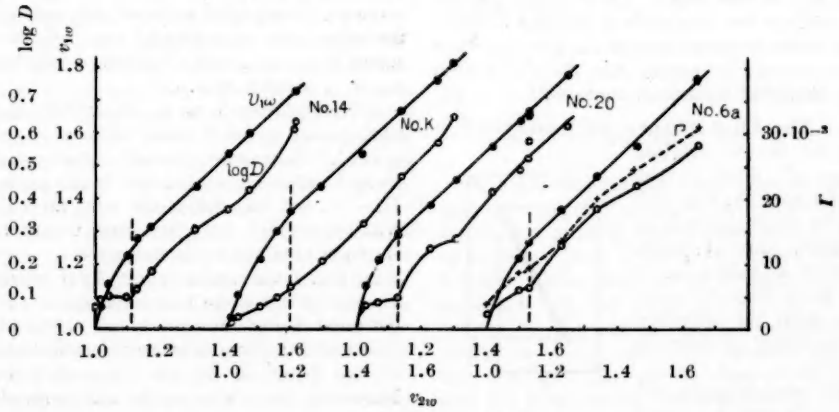

Fig. 4.

(5) S. Okajima and Y. Kobayashi, *J. Soc. Chem. Ind. Japan*, **46**, 941 (1941).

(6) The refractive indices of fiber for the plane-polarized D-line, oscillating parallel and perpendicular to the fiber axis.

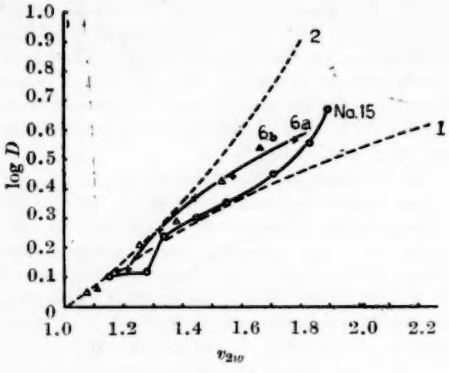

Fig. 5.

assumptions of the first and second theories of Kratky respectively. The point corresponding to the knick point also deviates clearly in this treatment, which has been overlooked carelessly.

Now such discontinuity showing a multiphase deformation was found out in the present stage of our knowledge the authors must be satisfied with discussing the deformation in the last stage only. And in this case stretching degree must be corrected not only from the smallest intrinsic anisotropy of the original sample but also from the volume decrease due to stretching.

As to the theoretical relation assuming the volume change during the stretching, an affined deformation has been described by J. J. Hermans[7] and discussed experimentally by P. H. Hermans and others;[8] it will be discussed later also in this paper. The Kratky's theories also assume the constancy of the fiber volume, so in order to compare with the observed data it is necessary to extend the theories to the case where the volume is changed.

(1) **The First Theory of Kratky.**—It is assumed in the original paper of Kratky that micells are thin rods and a cube is considered in the fiber, each of which contains a micell in it and whose diagonal coincides with the direction of the micell as shown in Fig. 6.

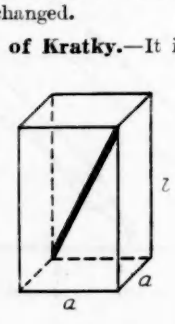

Fig. 6.

Now stretching the isotropic filament by v-fold this cube also deforms and the length l is stretched to lv and a_0 shrinks to a_2, when the volume also shrinks to V_2 from V_0, then the volume of each cube changes as follows:

Before stretching: $V_0 = a_0^2 \cdot l$ (1)

After stretching: $V_2 = a_2^2 \cdot l \cdot v$ (2)

From Fig. 6, $\tan\theta_0 = \sqrt{2}\, a_0/l$ (3)

$\tan\theta = \sqrt{2}\, a_2/vl$ (4)

The initial intensity of the micells in the isotropic fiber, J_0, is constant and indepemdent of the micellar inclination θ_0 relative to the fiber axis but it changes to J by stretching as shown in the next relation.

$$J \sin\theta\, d\theta = J_0 \cdot q_0/q_2 \cdot \sin\theta_0\, d\theta_0 \qquad (5)$$

From (1), (2), (3) and (4)

$$\tan\theta = \{(V_0/V_2)^{1/3} \cdot v\}^{-3/2} \tan\theta_0 \qquad (6)$$

Now from (5) and (6) the desired relation is obtained.

$$J = q_0/q\, J_0 v_a^3/(v_a^3 \sin^2\theta + \cos^2\theta)^{3/2} \qquad (7)$$

where

$$v_a = v(V_0/V)^{1/3} = v \cdot R_2^{-1/3} \qquad (8)$$

The refractive indices and D can be calculated from (7) and (8) as already carried out using the original relation of Kratky, but from the formula (7) it can be easily seen that the new relations $n_\parallel$, $n_\perp \sim v_a$ or $D \sim v_a$ coincide with the relations $n_\parallel$, $n_\perp \sim v$ or $D \sim v$ respectively, so even when the volume changes during stretching, the experimental data can be compared with the already calculated relations by using v_a instead of v.

For calculation of v_a, $v_{2w} \cdot R_{2w}^{-1/3}$ is generally used excepting a few cases, where $v_{2w} \cdot (q_0/q_2)^{1/3}$ is used. These two values are not always equal to each other as pointed out in the paragraph III—(2), but the differences are very slight. $R_{2w}^{-1/3}$ requires only the wet volumes and they are obtained more accurately.

In Fig. 7 the knick point K is placed on the theoretical curve and each value of v_a is corrected being multiplied by $v_k/(v_a$ at the knick point) where v_k is the theoretical abscissa of the point K on the calculated curve. Moreover, the origins of the curves are shifted one by one upward in the order of the decreasing degree of swelling for the sake of avoiding confusion. Then some interesting facts are seen:

(i) The curves nearly correspond to the

(7) J. J. Hermans, *J. Colloid Science*, **1**, 235 (1946); *Trans. Faraday Soc.*, **43**, 591 (1947).

(8) P. H. Hermans and D. Vermaas, *Trans. Faraday Soc.*, **42**, 185 (1946).

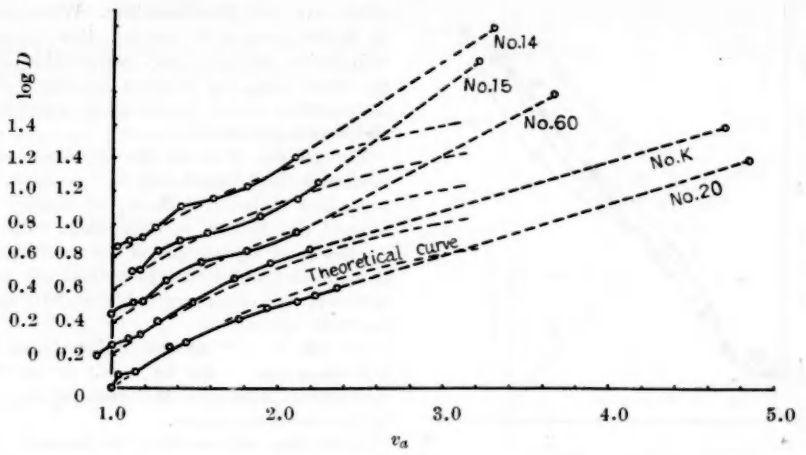

Fig. 7.

theoretical one, but on precise observation the coincidence is not perfect, and the curves are more or less sigmoid. This tendency is more remarkable when the cellulose concentrations of the spinning solutions are larger and the swelling degrees of the filaments are lower (see Table 1). We may consider therefore that the filaments spun from the solutions of the higher concentration have denser structures and their particles (aggregates or parts of molecules) rotate predominantly rather than flow, but in the middle stage of deformation they flow rather easily. This may be due to the change of the relative easiness of the two types of the motion, rotation and flowing, which is caused by the change of the inner structure, depending upon the dehydration, and packing and orientation degrees of the particles. Those three factors, dehydration, orientation and packing, may act dependently to each other. The fibers spun from the dilute solutions are thought to be less dense and flow governs predominantly. Even in this case the curves deviate upward from the theoretical one in the last stage of deformation.

(ii) The authors defined v_L in the paragraph III-(2)-(iii). This is the imaginative degree of stretching, where accompanied with orientation, the free water in the fiber may be expelled completely. So now we suppose that the orientation may also be complete at this point and plot its $\log D = 1.415$ (complete orientation) against the corrected v_L according to the same principle as above. Then those points, marked by ○, can be recognized to be on the extrapolating curve of each sample as shown in Fig. 7. This illustrates that there is an intimate relation between orientation and dehydration due to stretching. But when and how this characteristic of deformation is given during the fiber is regenerated is an interesting problem to be studied further.

(2) **The Affined Deformation Theory of J. J. Hermans.**—A new theory of deformation is proposed for the case of the rubberlike polymers, assuming the constancy of volume. This is given as follows:

$$\beta_{\parallel} - \beta_{\perp} = k(v^2 - v^{-1}),$$

where $\beta_{\parallel} - \beta_{\perp}$ is the orientation of the network, k a constant and v the stretching degree relative to the isotropic state. When the volume changes during stretching this is modified to

$$\beta_{\parallel} - \beta_{\perp} = k(q_2/q_0)^{2/3} \cdot (v_a^2 - v_a^{-1})$$

by J. J. Hermans. So for our present case

$$\log D = k'(V_{2w}/V_{0w})^{2/3}(v_a^2 - v_a^{-1})$$

If this theory is right, $\log D$ must be linearly proportional to $(V_{2w}/V_{0w})^{2/3}(v_a^2 - v_a^{-1})$ and its inclination must be independent of the degree of swelling. And actually plotting our data a linear relationship can be considered nearly applicable on the whole as in Fig. 8. Of course this happens in the γ-range and all the points in the $\alpha+\beta$-range deviate upwards from the line. But precise observation shows that the relations of the samples No. 14, 15 and 6a are slightly sigmoid and there is the same trend as pointed out in Fig. 7, while in the cases of the highly swollen fibers, No. 20 and K, they are exactly linear also in this case.

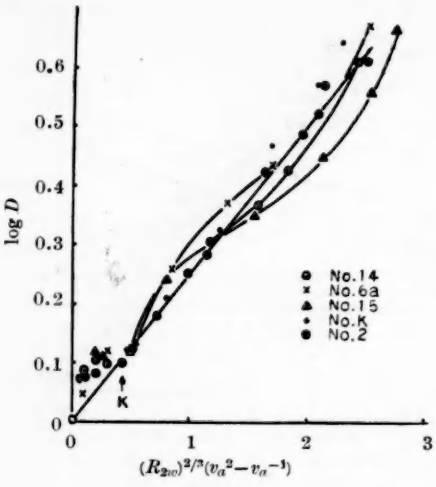

Fig. 8.

V. Conclusion

The results can be concluded as follows:

(1) When a freshly spun fiber is stretched its volume increases slightly at first together with a very slight orientation. When the fiber is further stretched beyond this range, the orientation becomes very remarkable and, at the same time, the volume decreases due to dehydration which proceeds in proportion to the stretching degree.

(2) In the γ-range the deformation may generally be considered to proceed nearly according to the first theory of Kratky in the case of the highly swollen fiber. The curve $\log D \sim v_a$ of the sample of low swelling degree is sigmoid around the theoretical one and this tendency is more remarkable as the swelling becomes lower.

(3) As to the affined deformation theory the same trend can be seen. It holds good nearly completely in the case of the fiber of higher swelling degree.

Thus the deformation mechanism of the cellulose seems to be very complicated to be expressed by a single mechanism on the whole range. It requires more abundant and more direct experimental data as well as the precise theory.

Faculty of Engineering,
Yamagata University, Yonezawa

Plastic Deformation of the Regenerated Cellulose Fibers. II. Deformation of Freshly Prepared Fibers from the Standpoint of Refractive Indices

By Saburo OKAJIMA and Shigeru HAYAMA

(Received December 14, 1950)

I. Introduction

In the report already presented by one of the authors[1] about the same problem, the refractive indices $n_{\parallel}$ and $n_{\perp}$ were plotted against the stretching degree v_{2w}, in the swollen state, for the author believed that the orientation degree of the regenerated fiber remained unchanged even when it was air-dried or reswollen, as its dichroic constant had been found unchanged by these treatments.[2] It was concluded from the result that the deformation conformed to the second theory of Kratky[3] till $v_{2w}=1.4$, but to the first theory[4] thereafter. In this conclusion the volume change during stretching was neglected, so taking this factor into consideration, the authors studied the problem from the standpoint of dichroism and some different conclusions were obtained in the previous paper.

Now to ascertain this result from other points of view the same study was repeated again by tracing the change of the refractive indices during stretching.

(1) S. Okajima, *J. Soc. Chem. Ind. Japan*, **49**, 167 (1946).
(2) S. Okajima, T. Nakayama and F. Adachi, *J. Soc. Chem. Ind. Japan*, **49**, 128 (1946).
(3) O. Kratky, *Kolloid-Z.*, **84**, 149 (1938).
(4) O. Kratky, *Kolloid-Z.*, **64**, 213 (1933).

II. Experiment

(1) Sample.—Two samples were used. They were prepared by the cuprammonium method already described in a previous report,[5] but in the present study the more viscous solution of cellulose was used. The conditions of preparation were summarized in Table 1; the sample No. 20 was the same as that used in the previous paper.

Table 1

Sample No.		S-1	S-20
Spinning solution	Cellulose (%)	13.6	3
	Cu (%)	5.9	1.5
	NH_3 (%)	18.7	8
Spinning temp. (°C.)		25	20
DP		270	580
Swelling degree, q_0[6]		6.56	13.9

(2) Stretching.—The swollen isotropic fiber of 30~95 cm. (l_{0w}) was stretched slowly in water to l_{1w} and the length was kept unchanged overnight. After that tension was released for one day, the residual length, l_{2w} was measured. During the operation the fiber was kept always in water; the temperature were 22.5° and 14° in the cases of S-1 and S-20 respectively. The stretched fibers were air-dried and their refractive indices were measured.

(3) Intrinsic Double Refraction.—The specimens were dried under vacuum at 60° and $n_\parallel$ and $n_\perp$ were measured by the Becke's method. The immersion liquids were prepared by mixing appropriate amounts of two or three among monochlorbenzol, *o*-dichlorbenzol, iodbenzol and tricresylphosphate. Observed data were corrected on the standard base of $n_{iso}=1.5358$, as it has already been precisely reported.[7] The intrinsic double refraction Γ is given by $n_\parallel - n_\perp$.

In the above notations $n_\parallel$ and $n_\perp$ are the refractive indices of fiber for the plane-polarized D-line, oscillating parallel and perpendicular to the fiber axis, while n_{iso} is that of the isotropic one.

(4) Swelling Degree.—The volumes of the fiber swollen in water during streching, V_{0w}, V_{1w}, V_{2w} and the volumes after drying V_{1d}, V_{2d}, were measured microscopically as described previously. From these results the swelling degrees, q_0 and q_2 were calculated. The detail of the method has been given in the preceding paper. The suffixes w and d mean the wet and dry states. 0 and 1 the states before and immediately after stretching and 2 the residual one.

III. Experimental Results

(1) S-1.—Fig. 1 shows the relation R_{2w}~v_{2w} and v_{1w}~v_{2w}. The knick point G can not be observed clearly in this case. Correcting the effect of the small intrinsic double refraction of the original sample and plotting Γ against v_{2w}, a similar curve (1) is obtained to that shown in the previous paper (Fig. 2).

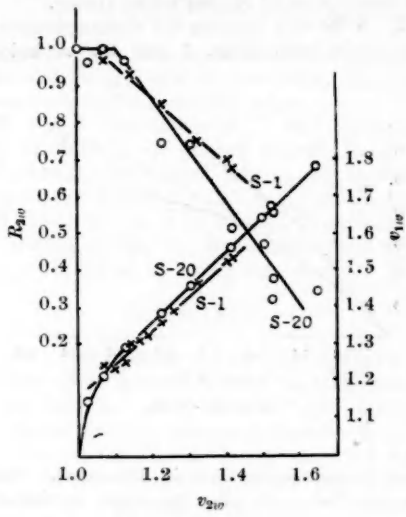

Fig. 1.

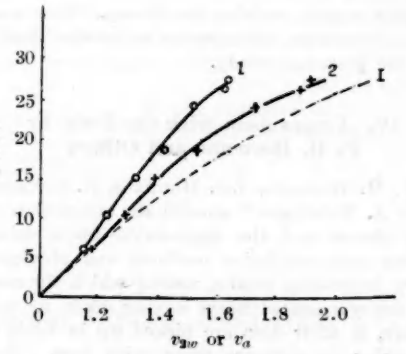

Fig. 2.—S-1.

But when the correction of the volume decrease is added further to the above v_{2w} and it is denoted as v_a the curve (2) is obtained. Both curves are qualitatively similar and it may be concluded that comparing with the theoretical curve (I), they deviate upward at the beginning but afterwards go parallel to the theoretical curve, which has already been calculated[8] on

(5) S. Okajima and other. *J. Soc. Chem. Ind. Japan*, **43**, 355 (1940); etc.

(6) About the notations used in this report, see the preceding paper.

(7) S. Okajima and Y. Kobayashi, *J. Soc. Chem. Ind. Japan*, **46**, 941 (1943).

(8) S. Okajima, *J. Soc. Chem. Ind. Japan*, **40**, 793, 795 (1937).

the assumption of Kratky's first theory.

(2) **S-20.**—In this case too similar phenomena can be seen. (Figs. 1 and 3). A knick

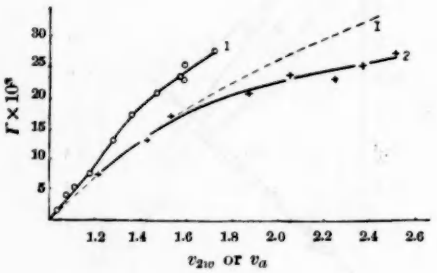

Fig. 3.—S-20.

point G is clearly seen in this case. The relation $\Gamma \sim v_{2w}$ is also the same as that of S-1 but corrected curve against v_a satisfies the theory from the first and deviates for $v_a > 1.6$.

The swelling degrees of S-1 and S-20 are 6.56 and 13.9 respectively. The deformation curve of the former, which is prepared from the solution of the higher cellulose concentration and has a smaller swelling degree, deviates remarkably upward from the theoretical curve, while the latter prepared from the solution of the more dilute cellulose concentration and highly swollen satisfies the theory. This tendency coincides with that gained dichroitically in the preceding study.

IV. Comparison with the Data by P. H. Hermans and Others

P. H. Hermans, J. J. Hermans, D. Vermaas and A. Weidinger[9] studied the orientation of the viscose and the regenerated fibers using x-ray and retardation methods and obtained very interesting results, among which the case of the regenerated fibers is very akin to our study, so their data are picked up in Table 2 in order to compare them with ours. The notations are changed according to the present authors' rule.

In Table 2 Γ is calculated as $f_0 \cdot \Gamma_\infty$, where f_0 is the orientation factor and Γ_∞ is the intrinsic double refraction at the complete orientation and 0.043 according to Hermans. v_a is also corrected in such a way that the first point of each curve comes on the theoretical one.

(9) P. H. Hermans, J. J. Hermans, D. Vermaas and A. Weidinger, *J. polymer Science*, **3**, 1 (1948).

Table 2

Cellulose conc., %		q_0	q_{2w}	v	v_a	q_2/q_0	$\Gamma \times 10^5$
(i) Freshly regenerated fiber.							
F_3	4.0	8.1	7.85	1.04	1.04	0.97	1.5
		7.7	7.35	1.19	1.20	0.96	5.6
		7.6	6.3	1.45	1.545	0.83	15.3
F_5	6.0	5.95	5.8	1.03	1.04	0.98	1.5
		5.95	5.4	1.20	1.24	0.91	8.0
		5.95	4.7	1.49	1.60	0.79	18.9
		5.95	3.5	1.79	2.09	0.59	29.5
F_9	10.5	4.7	4.7	1.05	1.04	1.00	1.7
		4.7	4.3	1.24	1.26	0.92	10.5
		4.5	3.16	1.56	1.73	0.70	23.4
		4.75	3.16	1.65	1.86	0.665	25.8
(ii) Reswollen fiber							
R_3	4.0	2.34	2.45	1.25	1.06	1.05	2.4
		2.09	2.26	1.39	1.17	1.08	7.1
		2.10	2.18	1.62	1.38	1.04	12.0
		2.15	2.02	1.99	1.76	0.94	17.6
R_5	6.0	2.34	2.73	1.22	1.03	1.15	1.2
		2.30	2.84	1.41	1.17	1.23	4.1
		2.36	2.95	1.64	1.35	1.25	10.1
		2.20	2.52	1.92	1.65	1.14	18.1
R_9	15.5	2.31	2.60	1.23	1.05	1.13	1.9
		2.29	2.75	1.48	1.19	1.20	6.45
		2.33	2.35	1.73	1.585	1.00	18.9
		2.31	2.26	1.96	1.83	0.98	24.1

According to these data the volume of the fiber decreases from the first in the freshly regenerated one, but a remarkable increase can be seen in the case of the reswollen fiber. Our data also confirm this, and even the freshly prepared sample also showed a slight increase of the volume as described in Part I.

The relation between Γ and v_a is shown in Fig. 4; all the samples have the similar behaviors and they satisfy the first theory on

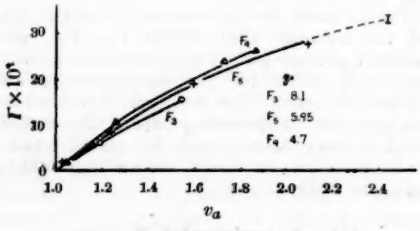

Fig. 4.

the whole. But on precise observation, the curves of F_9 and F_3 deviate up and down respectively from the theoretical curve (1), although F_5 coincides with it completely. At the swelling degrees of F_3, F_5 and F_9 are 8.1,

5.95 and 4.7 respectively, it may be said that the higher the swelling degree of the fiber is, the more effective the orientation is. This tendency is the same as already pointed out repeatedly by the authors.

As to the case of the reswollen fiber it will be treated fully in the following papers.

V. Comparison with the Affined Deformation Theory

Affined deformation formula proposed for the rubber-like polymers has been extended by J. J. Hermans[10] as below for the case where the volume is changed during the deformation

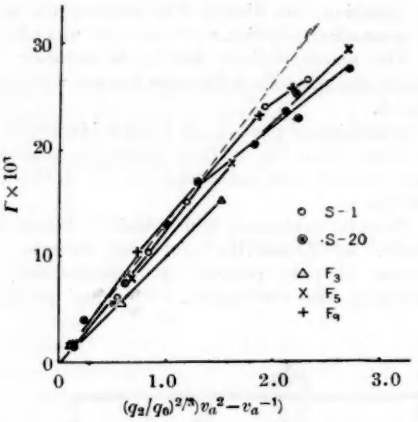

Fig. 5.

$$\Gamma = k(q_2/q_0)^{2/3}(v_a^2 - v_a^{-1}).$$

This has also been discussed by our dichroic data and its approximate conformity has been recognized in the preceding paper.

In Fig. 5 our values of Γ and Hermans' data in Table 2 are plotted against $(q_2/q_0)^{2/3}(v_a^2 - v_a^{-1})$. The broken line in the figure is a theoretical relation which is required by the line shown in Fig. 8 in Part I. Of course the inclination of this line is calculated from that of the $\log D$-line by using the relation.

$$\log D = 20\,\Gamma.$$

Now all the points are on each line for the smaller degree of stretching and the inclinations of the lines are nearly coincide with that of the theoretical one, excepting the cases F_3 and F_5. But for the abscissa larger than 1.3 the points deviate downward. So the conformity between the experiment and theory is limited within a narrow range and can not be said to be perfect.

VI. Conclusion

The results obtained by using the double refraction are similar to that already described in the first report.

The cost of this research has been defrayed from the Grant in Aid for Fundamental Scientific Research from the Ministry of Education, to which the authors' thanks are due.

Faculty of Engineering,
Yamagata University, Yonezawa

(10) J. J. Hermans, *Trans. Faraday Soc.*, **43**, 591 (1947).

Synthesis of Some Organic Compounds by Electric Discharge. I-V.

By Kiichiro SUGINO and Eiichi INOUE

(Received December 26, 1950)

Introduction

Most of the studies on the organic reactions in the electric discharge have been very qualitative in nature. For example, even the synthesis of simple organic compounds by non-disruptive electric discharge has not yet been succeeded from both the practical and the theoretical point of view. The reason for this is that the variables to obtain a desired compound are not systematically examined and also that the identification of the reaction product is not made accurately.

During these five years, the authors have found some interesting reactions occurring in silent discharge, which had not yet been reported

in the literature. These reactions are summarized as follows.

(1) Formation of phenol from benzene and air.

(2) Formation of benzyl alcohol, benzaldehyde, benzoic acid and cresols from toluene and air.

(3) Formation of cyclohexanol and cyclohexanone from cyclohexane and air.

(4) Formation of aniline and other basic compounds from benzene and ammonia.

The authors have then undertaken the present study in order to establish a new practical method of the synthesis of these compounds. The study also seeks to establish the fundamental chemistry of these synthetic reactions in the discharge and at the same time to present some mechanisms and theory of these reactions.

Synthesis of Phenol from Benzene.[1] (II, III)

When a mixture of benzene and air was discharged in an ozonizer under suitable conditions, phenol was obtained in yields as high as 30% of the total reaction product. The apparatus was a simple one as is shown in Fig. 1.

Air was bubbled into benzene reservoir at a definite temperature in order to obtain a mixture of benzene and air of constant composition. The content of benzene gas in air could be varied by changing the temperature of the reservoir and the rate of flow of air. The mixed gas was then flowed into the operated ozonizer at constant velocity. The exit gas was passed through 2 *N* sodium hydroxide solution and then cooled through a trap to 5° to condense almost of the unconverted benzene together with the reaction product which was not absorbed in the alkali solution. A part of the unconverted benzene and gaseous reaction products, if existed, were allowed to exhaust. During the reaction, solid brown deposit was formed on the glass wall of the ozonizer. This deposit, after the reaction, was dissolved by washing the wall with an alkali solution and the latter was added to the above sodium hydroxide solution in which the phenolic substances formed was contained.

Separation of phenol and other acidic reaction products from the sodium hydroxide solution was carried out according to the following scheme.

Phenolic substances thus obtained boiled at 76-78° at 11 mm.Hg and was thought to consist of pure phenol. It was purified by repeating the distillation. The final product

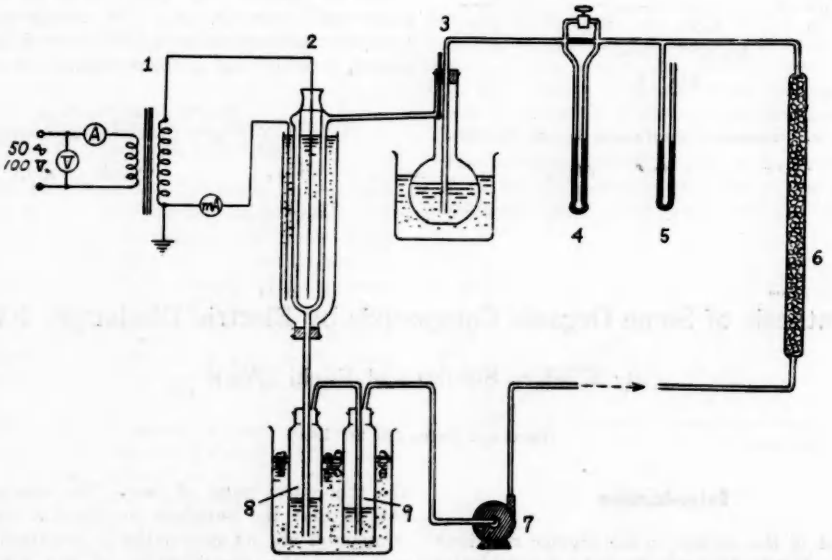

Fig. 1.—1, Transformer; 2, discharge tube; 3, benzene reservoir; 4, flowmeter; 5, manometer; 6, $CaCl_2$ tube; 7, blower; 8, NaOH solution; 9, trap.

(1) A part of the research was already published in Japanese in *Jour. Chem. Soc. Japan*, **71**, 518 (1950).

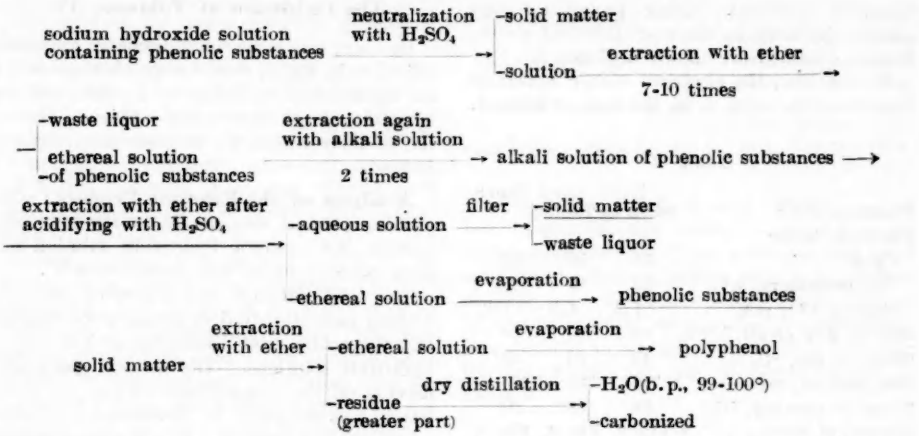

boiled at 177-178° at atmospheric pressure and crystallized at room temperature.

Conditions of experiments and results obtained are shown in Table 1.

Table 1

	Run 1	Run 2	Run 3
Electrical factor			
Cycle	50	50	50
Volt (secondary), kV.	15	15	15
Current (I'), mA.	1.25	1.25	1.25
Temp. of ozonizer, °C.	50	50	50
Composition of gas used, Vol.%			
C_6H_6	5.0	6.5	7.5
Air	95.0	93.5	92.5
Temp. of gas, °C,	30	20	20
Gas pressure, mm.	750	750	750
Rate of flow, l./hr.	120	120	30
Time, hr.	56	17	15.5
C_6H_6 used, kg.	1.0	0.5	0.13
Reaction products			
Phenol, g.	2.5	1.3	1.2
Other products, g.	6.0	3.0	3.7
Conversion efficiency, % (grams of liquid and solid reaction products/grams of C_6H_6 used) × 100	0.85	0.86	3.8
% of phenol in total reaction product	30	30	25

Magnitude of the tube: all glass (pyrex) ozonizer. Effective length, 22 cm.; space gap, 0.25 cm.; diameter, 4 cm.

Formation of gaseous decomposition products of benzene has not been able to recognize exactly.

As is clear from the table, under the conditions described above, 0.85-3.8% of benzene used could be converted to phenol and other reaction products by running it with air one time in the ozonizer (effective length, 22 cm.). The quantity of phenol in the reaction product was reached to about 30% and the electrical energy consumed was about 150-250 kwhr./1 kg. phenol.

In these experiments, solid brown deposit was always formed on the glass wall and it is the main reason for the decrease of the conversion of benzene to phenol. Later, it was found that when the glass wall of the discharge tube was covered with liquid layer of benzene, the formation of solid deposit was reduced to to a very small quantity and the reaction product consisted mainly of phenol. In this case, the mixed gas of benzene and air, before flowing into the ozonizer, was cooled by the methods shown in Fig. 2, so a part of benzene was condensed and it was run down on the glass wall of the ozonizer, where the silent

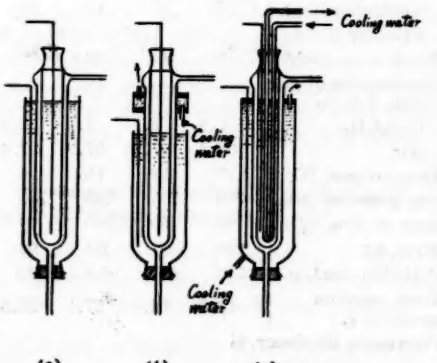

Fig. 2.—(a), air cooling; (b) and (c), water cooling.

discharge occurred. Other procedures were almost the same as the case described above. Results obtained are shown in Table 2.

In this case, the electrical energy consumed was about the same as in the case of Table 1.

Table 2

Discharge tube	Run 1 (same as Table 1)	Run 2	Run 3
Electrical factor			
Cycle	50	50	50
Volt (secondary), kV.	15	15	15
Current (ϕ), mA.	1.3	1.3	1.3
Rate of flow of air, l./hr.	25	50	50
Temp. of gas, °C.	45	64	60
Gas pressure, mm.	755	765	755
Temp. of ozonizer, °C.	58	58	20
Method of cooling of the mixed gas	Fig. 2, (a)	Fig. 2, (b)	Fig. 3, (c)
Rate of ruuning of liquid C_6H_6, cc./hr.	120	550	550
Time, hr.	60	30	32
C_6H_6 used, kg.	6.3	14.5	15.5
Reaction product			
Phenol, g.	3.8	1.7	1.6
Other products, g.	2.0	0.7	0.4
Conversion efficiency (same as Table 1), %	0.1	0.017	0.013
% of phenol in total reaction product	66	71	80

Table 3

	Run 1	Run 2	Run 3	Run 4
Magnitude of the tube (all glass (pyrex) ozonizer)				
Effective length, cm.	24	25	50	70
Space gas, cm.	0.25	0.25	0.25	0.25
Diameter (outer), cm.	4.0	3.5	3.5	3.5
Electrical factor				
Cycle	50	50	50	50
Volt (secondary), kV.	15	15	15	15
Primary kwhr.	1.32	1.36	2.24	2.85
Temp. of ozonizer, °C.	40	40	40	40
Composition of gas used, Vol. %				
$C_6H_5CH_3$	1.8	2.1	2.1	2.2
Air	98.2	97.9	97.9	97.8
Temp. of gas, °C.	17	18	18	18
Gas pressure, mm.	765	725	725	725
Rate of flow, l./hr.	60	60	60	60
Time, hr.	110	80	80	62
$C_6H_5CH_3$ used, g.	510	420	418	332
Total reaction product, g.	17.9	14.1	27.1	28.5
Conversion efficiency, % (grams of total reaction product/grams of $C_6H_5CH_3$ used) × 100	3.5	3.4	6.5	8.6

The Oxidation of Toluene. (IV)

By using the same silent discharge apparatus described in Fig. 1, results were obtained which are summarized in Table 3. In this case, the variation of the conversion efficiency due to the effective length of the ozonizer was examined.

Analysis of the Reaction Product :—The reaction product was caught in the trap containing 5 *N* sodium hydroxide solution and some toluene which was cooled to 4-5°.

The total product was separated into the neutral part (dissolved in unconverted toluene) and the acidic prat (dissolved in 5 *N* sodium hydroxide solution). The neutral part, after driving off the unconverted toluene by distillation, was subjected to fractional distillation under reduced pressure. It was thus separated into four fractions which had the properties shown in Table 4 and were identified as benzaldehyde (Fraction 1) and benzylalcohol (Fraction 2) respectively. Recovery of acidic compounds from the alkali solution was carried out as usual and the crude product thus obtained was also subjected to fractional distillation under reduced pressure into four fractions. Fraction 2 and 3 had the properties noted in Table 4 and were identified as *o*-cresol and benzoic acid respectively.

Table 4

Neutral Part: Fraction (B. p., °C.)	Properties	Acidic Part: Fraction (B. p., °C.)	Properties
1. $(50\text{-}55)_5$	B.p., 179-181°C. $n_D^{20}=1.545$ benzalphenylhydrazone M. p., 156°C.	1. $(20\text{-}35)_{35}$	odor like to CH_3COOH
2. $(70\text{-}75)_5$	B.p., 200-205°C. $n_D^{20}=1.540$	2. $(60\text{-}65)_5$	B. p., 187-191°C. $n_D^{20}=1.543$ color reaction with $FeCl_3$, +
3. $(100\text{-}120)_5$	$n_D^{20}=1.567$	3. $(100\text{-}110)_5$	M.p., 121°C. sublime
4. Residue		4. Residue	

Table 5

	Run 1	Run 2	Run 3	Run 4
(1) Benzyl alcohol, g.	5.2	3.7	7.2	8.7
(2) Benzaldehyde, g.	3.3	1.8	3.7	6.7
(3) Benzoic acid, g.	0.3	0.5	0.7	0.8
(4) *o*-Cresol, g.	4.8	4.0	6.8	4.0
(1)+(2)+(3)+(4)/Total reaction product × 100, %	76	71	68	71
(1)+(2)+(3)+(4)/kwhr. g.	10.3	7.4	8.2	7.1

The yield of the main reaction product is shown in Table 5.

Mean percentage of each compounds in the reaction product was as follows: (1) Identitified products: benzylalcohol 26-30%, benzaldehyde 13-20, benzoic acid 2-4%, *o*-cresol 25-28%; (2) unidentified products: solid deposit on the wall 9-10%, fraction 3 of the neutral part 4-5%, fraction 1 of the acidic part 1-4%, distillation residue 11-17%.

In the ozonizer, toluene was found to be oxidized more easily than benzene. It was converted to the extent of 3.5-8.6% to give benzylalcohol, benzaldehyde, benzoic acid and cresols as main products, by running it only one time in the ozonizer. (Effective length, 25-75 cm.). Solid brown deposit formation on the glass wall was very small in this case.

Oxidation of side chain (1) and nucleus (2) of toluene are the main reactions. The ratio of the two reactions (1)/(2) was about 1.6-1.9 in the above experiment. But it may somewhat vary according to the voltage applied, the effective length of the tube and the rate of the flow of gas.

Oxidation of Cyclohexane. (V)

By the oxidation in an ozonizer, cyclohexane gave a mixture of cyclohexanol and cyclohexanone with a fair conversion efficiency. Methods of experiments were almost the same as the above two cases. The results are summarized in Table 6.

Table 6

	Run 1	Run 2	Run 3
Magnitude of the tube (all glass (pyrex) ozonizer)			
Effective length, cm.	75	75	75
Space gap, cm.	0.25	0.25	0.25
Diameter (outer), cm.	3.5	3.5	3.5
Electrical factor			
Cycle	50	50	50
Volt (secondary), kV.	20	25	20
Primary kwhr.	1.7	2.4	1.35
Temp. of ozonizer, °C.	45-55	55-60	45-50
Composition of gas used, Vol. %			
Cyclohexane	7.7	6.9	6.0
Air	92.3	31.1	94.0
Temp. of gas, °C.	20-22	17-19	15-19
Gas pressure. mm.	740	740	740
Rate of flow, l./hr.	21.7	21.5	50.5
Time, hr.	50	50	40
Cyclohexane used, g.	314	282	456
Total product, g.	80.2	122	80.5
Cyclohexanol, g.	44.1 (55%)	54.1 (44%)	50.3 (63%)
Cyclohexanone, g.	14.7 (18%)	30.4 (25%)	17.7 (22%)
Adipic acid, g.	5.0 (6%)	6.1 (26%)	2.3 (13%)
Distillation residue, g.	16.4 (20%)	31.4 (25%)	10.2 (13%)
Conversion efficiency, %	25.5	43.3	17·7

In this case, the gas flowing out the ozonizer was cooled through a trap containing some cyclohexane to 5-10° to condense the total reaction product together with unconverted cyclohexane. The crude product, after driving off the unconvertd cyclohexane by distillation, was subjectd to fractional distillation into four fractions which had the properties shown in Table 7.

Table 7

Fraction (B.p., °C.)	Properties		Note
1. $(42\text{-}50)_{3-4}$	B.p., 155-158°C., $n_D^{20}=1.4507$,	Cyclohexanone semicarbazone M. p., 166-167°C.	Chclohexanone
2. $(50\text{-}60)_2$	B. p., 158-163°C.,	Cyclohexanol phenylurethane M. p., 80°C.	Cyclohexanol
3. $(153\text{-}180)_2$	M. p., 148-150°C.		Adipic acid
4. Residue			

The oxidation of cyclohexane in the ozonizer was found to proceed very fast as compared with the case of aromatic hydrocarbons. The conversion efficiency reached to about 18-43% by running it one time in the ozonizer (effective length, 75 cm.). The reaction product consisted mainly of cyclohexanol and cyclohexanone and their content in the product were 44-63% and 18-25% respectively.

The results of these three researches offer a possibillity of the use of silent discharge for the industrial preparation of (1) phenol from benzene, (2) benzylalcohol, benzaldehyde and cresols from toluene, and (3) cyclohexanol and cyclohexanone from cyclohexane respectively.

Synthesis of Aniline from Benzene and Ammonia.[2] (I)

Benzene has also been studied in an ozonizer in the presence of ammonia in order to obtain aniline according to the following reaction.

$$C_6H_6+NH_3=C_6H_5NH_2+H_2 \quad \Delta F=+9900 \text{ cal.}$$

(2) Already publised in Japanese in *Jour. Chem. Soc. Japan*, **71**, 343 (1950). So this description is an abstract of the result.

An example of the experimental conditions and results obtained are summarized in Table 8.

Table 8

Magnitude of the tube: all glass ozonizer; effective length, 30 cm.; space gap, 0.26 cm. Conditions: cycle, 50; volt (secondary), 13 kV.; current (secondary), 2.5 mA.; temp. of ozonizer, 30°C.; temp. of trap, −5°C.; gas pressure, 730 mm.; rate of flow, C_6H_6 8.2 l./hr. NH_3 34 l./hr.; composition of mixed gas, C_6H_6/(total gas) × 100 = 20; time, 63 hr. Results; C_6H_6 used, 1.8 kg.; NH_3 used, 1.6 kg.; liquid products subjected to fractional distillation, 14.08 g.

Fraction (B. p.,°C.)	Yield, g.	n_D^{20}	Properties	Note
81-85	7.46			Unconverted benzene (mainly)
85-100	0.23		Crystallized by absorbing CO_2 in air. Picrate and chloroplatinate were formed.	Aliphatic amine or diamine
100-115	0.12			
$(67\text{-}76)_{15}$	1.08	1.5410 (d_4^{20} = 1.000)	B.p.,175-182°C. M. p., of acetanillide, 113°C.	Aniline
$(91\text{-}92)_{15}$	0.14	1.5420	A crystal (M.p. 63°C.) was isolated	*m*-phenylenediamine
$(111\text{-}114)_{15}$	0.28	1.5440		
$(121\text{-}134)_{13}$	0.19	1.5390		
Residue	0.75			
Loss	3.83			Unconverted benzene

Summary

(1) By running a gas mixture of aromatic and hydroaromatic hydrocarbons and air in an ozonizer, following reactions were found to occur mainly.

(a) C_6H_6 $\quad C_6H_6 + O \rightarrow C_6H_5OH$

(b) $C_6H_5CH_3$

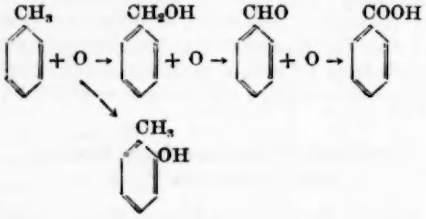

(c) C_6H_{12}

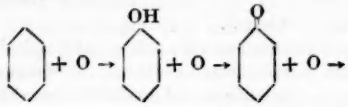

$HOOC(CH_2)_4COOH$

(2) Conversion efficiency at one run under suitable conditions was found to be (a) 0.86-3.8% (effective length of ozonizer, 22 cm.), (b) 3.5-8.6% (effective length of ozonizer, 25-75 cm.), and (c) 18-43% (effective length of ozonizer, 75 cm.), respectively. The yield of each compound produced (grams of each compound produced/grams of total reaction product × 100) was as follows: (a), phenol 25-30%; (b), benzylalcohol 26-30%, benzaldehyde 13-20%, benzoic acid 2-4%, *o*-cresol 25-28%; and (c), cyclohexanol 44-63%, cyclohexanone 18-25%.

(3) In the case of the oxidation of benzene, the yield of phenol could be increased to above 60% of the total reaction product by the special method.

(4) Aniline and other basic compounds were obtained by the reaction of benzene and ammonia in an ozonizer.

In conclusion, one of the authors (K. Sugino) wishes to express his hearty thanks to Prof. M. Suzuki of Tokyo Municipal University for his sincere friendship which facilitated this research. The authors also extend their thanks to Dr. K. Odo, Lecturer of Tokyo Institute of Technology and Mr. K. Shirai, Assistant of the same Institute, for their valuable collaboration on the analytical work. Thanks are also due to their collaborators, H. Yamada, M. Hattori and H. Yamakawa, who gave earnest assistance in the investigations. The cost of this research has been defrayed from the Grant in Aid for Fundamental Scientific Research of the Ministry of Education and from the funds of the Nippon Carbide Industries Inc. to which thanks are due.

Research Laboratory of Electrical Science
and
Laboratory of Organic Electrochemistry and Biochemistry,
Tokyo Institute of Technology, Tokyo

Dipole Moments of Halogen-Derivatives of Hinokitiol

By Yukio KURITA, Tetsuo NOZOE and Masaji KUBO

(Received January 26, 1951)

Introduction

In the previous paper,[1] we reported the results of measurements on the dipole moments of tropolone,[2] hinokitiol(4-isopropylcycloheptatriene-2, 4, 6-ol-2-one-1)[3] and their derivatives. We arrived at the conclusion that these molecules resonate among various electronic structures contributing to the normal states of these molecules and that the cycloheptatrienolone ring is planar. We found that the dipole moment of hinokitiol is nearly pointing along the line from the center of the ring to the C-atom at 2-position with a positive end at the ring, as shown in the Figure 2 in the next paper.[4]

We have prepared another halogen-derivatives of hinokitiol and carried out, besides investigations in the field of organic chemistry, measurements on the dipole moments of these compounds to determine the position of substituents in these compounds.

Experimental Method and Materials

The dipole moments were measured in benzene solution at 25°. The apparatus and the method of measurements were the same as described in the previous report.[1] The materials used were prepared by one of us and his collaborator. They are: β-monobromohinokitiol, m. p. 42°, α-monochlorohinokitiol, m. p. 117.5-8.5°, β-monochlorohinokitiol, m. p. 47.6-8.5°, γ-monochlorohinokitiol,[5] m. p. 44-46°, and α-dichlorohinokitiol,[6] m. p. 126-7°.

Experimental Results

For the extrapolation of molecular polarization to infinite dilution, Hedestrand's method[7] was used, *i.e.*,

$$\varepsilon_{12} = \varepsilon_1 + \alpha w_2,$$

$$d_{12} = d_1 + \beta w_2,$$

$$p_{2\infty} = p_1\left(1-\frac{\beta}{d_1}\right)+\alpha C,$$

$$C = \frac{3}{d_1(\varepsilon_1+2)^2},$$

where p and w denote specific polarization and weight fraction respectively. Other notations have their usual significances. For benzene at 25°, we have

$$p_1 = 0.3414 \text{ cc./g.},$$

$$d_1 = 0.8727 \text{ g./cc.},$$

$$C = 0.1883 \text{ cc./g.},$$

which can be used throughout the whole calculation. The results are shown in Table 1, in which P and R_D denote molecular polarization and molecular refraction for D-line respectively.

Table 1

Dipole Moments of Halogen-Derivatives of Hinokitiol, 25°

w_2, %	ε_{12}	d_{12}
β-monobromohinokitiol		
0	2.273	0.8727
0.629	2.329	0.8749
1.118	2.374	0.8767
1.382	2.393	0.8777

$\alpha = 8.87$, $\beta = 0.35$, $P_{2\infty} = 455.6$ cc., $R_D = 54.1$ cc., $\mu = 4.40$ D

α-monochlorohinokitiol		
0	2.273	0.8727
0.697	2.301	0.8744
1.116	2.319	0.8756
1.957	2.356	0.8778

$\alpha = 4.13$, $\beta = 0.26$, $P_{2\infty} = 202.0$ cc., $R_D = 51.2$ cc., $\mu = 2.70$ D

β-monochlorohinokitiol		
0	2.273	0.8727
0.546	2.330	0.8741
1.075	2.389	0.8755
1.855	2.473	0.8776

$\alpha = 10.7$, $\beta = 0.26$, $P_{2\infty} = 447.8$ cc., $R_D = 51.2$ cc., $\mu = 4.38$ D

(1) Y. Kurita, T. Nozoe and M. Kubo, This Bulletin, **24**, 10 (1951).
(2) T. Nozoe, S. Seto, Y. Kitahara, M. Kunori and Y. Nakayama, *Proc. Japan Acad.*, **26** (No. 7), 38 (1950).
(3) T. Nozoe, *Yakugaku (Science of Drugs)*, **3**, 172 (1949); *Proc. Japan Acad.*, **26** (No. 9), 30 (1950).
(4) Y. Kurita and M. Kubo, This Bulletin, **24**, 13 (1951).
(5) T. Nozoe, T. Mukai and K. Takase, *Proc. Japan Acad.*, **26** (No. 8), 19 (1950).
(6) T. Nozoe, K. Kikuchi and T. Ando, *Proc. Japan Acad.*, **26** (No. 10), 32 (1950).
(7) G. Hedestrand, *Z. physik. Chem.*, **B 2**, 428 (1929).

γ-monochlorohinokitiol

0	2.273	0.8727
0.465	2.332	0.8739
0.919	2.386	0.8750
1.467	2.457	0.8764

$\alpha=12.5$, $\beta=0.25$, $P_{2\infty}=515.9$ cc.,
$R_D=51.2$ cc., $\mu=4.74$ D

α-dichlorohinokitiol

0	2.273	0.8727
0.610	2.331	0.8745
1.196	2.388	0.8765
1.675	2.430	0.8779

$\alpha=9.50$, $\beta=0.31$, $P_{2\infty}=468.3$ cc.,
$R_D=56.1$ cc., $\mu=4.46$ D

Discussion

We have already measured the dipole moment of hinokitiol and determined the direction of the moment in the molecule. The conceivable position of substituent in bromohinokitiol are 3 (ortho), 5 (para) or 7 (ortho') as justified by molecular orbital treatment,[4] which have shown that π-electron distribution is concentrated at C-atoms 3, 5 and 7. The cycloheptatrienolone ring is planar. We may, as a first approximation, assume that the ring has a regular heptagon form. Assuming the bond moment $\mu(C-Br)=1.48$ D as before, we can calculate the theoretical moments for 3-bromo-, 5-bromo- and 7-bromohinokitiol to be 4.8 D, 2.6 D and 4.32 D[8] respectively. Comparing these values with the observed one, it is concluded that the position of substituent in β-monobromohinokitiol is 3 (ortho).

The bond moment $\mu(C-Cl)$ is 2.0 D in aliphatic compounds and 1.5~1.7 D in benzene derivatives. Assuming $\mu(C-Cl)=1.7$ D, we can calculate the theoretical moments for monochloro- and dichlorohinokitiols. The results are: 3-monochlorohinokitiol, 4.95 D; 5-monochlorohinokitiol, 2.4 D; 7-monochlorohinokitiol, 4.4 D; 3,5-dichlorohinokitiol, 3.6 D; 3,7-dichlorohinokitiol, 4.8 D; and 5,7-dichlorohinokitiol, 2.8 D. Comparing these values with the observed ones, it is concluded that the position of substituents in α-monochlorohinokitiol is 5 (para), in β-monochlorohinokitiol 7 (ortho'), in γ-monochlorohinokitiol 3 (ortho) and α-dichlorohinokitiol is 3, 7-dichloroderivative. The results are summarized in Table 2.

Table 2

The Position of Substituents in Halogenated Hinokitiols

Hinokitiol derivatives	$\mu_{obs.}$	$\mu_{calc.}$	Position of substituents
α-monobromo-	4.32 D	(4.32 D)	7 or *o'*
β-monobromo-	4.40 D	4.8 D	3 or *o*
γ-monobromo-	—	2.6 D	5 or *p*
α-dibromo-	4.27 D	4.7 D	3, 7 or *oo'*
β-dibromo-	3.14 D	2.9 D	5, 7 or *o'p*
dibromo-	—	3.7 D	3, 5 or *op*
α-monochloro-	2.70 D	2.4 D	5 or *p*
β-monochloro-	4.38 D	4.4 D	7 or *o'*
γ-monochloro-	4.74 D	4.95 D	3 or *o*
α-dichloro-	4.46 D	4.8 D	3, 7 or *oo'*
β-dichloro-	—	2.8 D	5, 7 or *o'p*
dichloro-	—	3.6 D	3, 5 or *op*

These conclusions are in conformity with and supported by the results of structural determinations in organic chemistry carried out by one of us (Nozoe) and his collaborators.[5],[6],[9]

Summary

The dipole moments of halogen-derivatives of hinokitiol (4-isopropylcycloheptatriene-2, 4, 6-ol-2-one-1) were measured in benzene solution at 25°. The values obtained are: β-monobromohinokitiol (3-bromo-), 4.40 D; α-monochlorohinokitiol (5-chloro-), 2.70 D; β-monochlorohinokitiol (7-chloro-), 4.38 D; γ-monochlorohinokitiol (3-chloro-), 4.74 D; α-dichlorohinokitiol (3,7-dichloro-), 4.46 D. By analysing the results obtained, the position of substituents in the halogenated hinokitiols were determined and are given immediately after each name of these compounds in parentheses.

We wish to express our cordial thanks to Mr. T. Mukai, Mr. K. Kikuchi and Mr. T. Ando of the Tohoku University for collaborating with us in the syntheses of these new compounds. Our thanks are also due to the Ministry of Education in aid of this research.

Chemical Institute, Faculty of Science, Nagoya University, Nagoya

Chemical Institute, Faculty of Science, Tohoku University, Sendai

(8) α-Monobromohinokitiol (μ=4.32 D) was assigned to 7-mono-bromohinokitiol from considerations in organic chemistry.[3],[5]

(9) T. Nozoe, Y. Kitahara and K. Doi, *Proc. Japan Acad.*, **26** (No. 10), 25 (1950).

A Note on the Theory of Solution of Hydrated systems

By Toshio IKEDA

(Received July 12, 1950)

The Solution of Electrolytes

It is well-known that the Debye-Hückel's theory of solution of strong electrolytes does not hold good any longer for the solutions of the concentration greater than 0.01 mols per litre. But taking the hydration of solute into account we can interpret the experimental results almost up to the concentration of saturation for any sort of solution.

Fundamental Equations.—Now, this theory is based on the following three assumptions:

1. The complete dissociation of electrolyte is assumed for simplicity.

2. The second, the most essential of this theory, is that the hydration water attached to an ion in a co-ordinated position by its strong field can not play the rôle of solvent in an ordinary sense; hence the number of molecules of free solvent in an aqueous solution of the concentration m represented in molality, namely mols of solute per 1000 g. of solvent, may be reduced to

$$55.51-(\nu_+\alpha_+ +\nu_-\alpha_-)m,$$

where ν_+ and ν_- are the number of positive and negative ions created by the dissociation of one molecule of salt, while α_+ and α_- being the hydration number of positive and negative ions respectively and assumed to be constants at a given temperature characteristic of the sorts of ion and solvent throughout the whole range of concentration.

3. The third is that the water outside of hydration shell, within which the dielectric saturation takes place, behaves normal. Furthermore, for simplicity it is assumed that the interactions between hydrated ion and molecules around it are independent of concentration. In this model, therefore, the solution is composed of the hydrated ions and of the free water molecules bearing themselves quasi-ideal, if the electrostatic interactions were ignored.

Upon taking the hydration into consideration the partial molal free energy of solute, $\overline{F}_1$, can be expressed in the following form:

$$F_1=\overline{F}_1^\circ+RT\ln f_\pm^{\nu_+ +\nu_-}\times \frac{(\nu_+ m)^{\nu_+}(\nu_- m)^{\nu_-}}{[55.51-(\nu_+\alpha_+ +\nu_-\alpha_-)m+(\nu_+ +\nu_-)m]^{\nu_+ +\nu_-}} =\overline{F}_1^{\circ\prime}+RT\ln \nu_+^{\nu_+}\nu_-^{\nu_-}(\gamma_\pm m)^{\nu_+ +\nu_-}, \quad (1)$$

where $\overline{F}_1^\circ$ and $\overline{F}_1^{\circ\prime}$ are the standard free energies, which differ from the ordinary ones owing to hydration, R, gas constant, T, absolute temperature, $f_\pm$, Debye-Hückel's mean activity coefficient of salt (in which only the interionic attractions are taken into account), and $\gamma_\pm$, stoichiometrical mean activity coefficient of salt (in which both effects of interionic attractions and of hydration are taken into consideration).

Upon introducing into Eq. (1) the usual convention of $f_\pm=\gamma_\pm=1$ at infinite dilution *i.e.*, $m\to 0$, the relations

$$\overline{F}_1^{\circ\prime}=\overline{F}_1^\circ-(V_+ +V_-)RT\ln 55.51$$

$$\ln\gamma_\pm=\ln f_\pm -\ln\left[1-\frac{1}{55.51}\{(\nu_+\alpha_+ +\nu_-\alpha_-)m -(\nu_+ +\nu_-)m\}\right] \quad (2)$$

may be obtained. According to Debye and Hückel,

$$\ln f_\pm=-\frac{z_+z_-e^2}{2DkT}\cdot\frac{\kappa}{1+a\kappa},$$

$$\kappa^2=\frac{8\pi e^2 N\omega}{1000DkT}, \quad (3)$$

where z_+ and z_- are the ionic valencies of positive and negative ions respectively, e, the electronic charge, D, the dielectric constant of solvent in solution, k, Boltzmann's constant, a, the mean distance of approach of two hydrated ions, N, Avogadro's number, and ω, the ionic strength.

In a similar way we can define the partial molal free energy $\overline{F}_0$ of free solvent in aqueous solution of a single sort of salt as,

$$\overline{F}_0-\overline{F}_0^\circ=RT\ln f_0 \times\frac{55.51-(\nu_+\alpha_+ +\nu_-\alpha_-)m}{55.51-(\nu_+\alpha_+ +\nu_-\alpha_-)m+(\nu_+ +\nu_-)m} \equiv RT\ln a_0, \quad (4)$$

where F_0° is the standard free energy of solvent, and a_0 is the activity of free solvent. And f_0 is the electrostatic activity coefficient of the free solvent of the following formula

$$\ln f_0 = +\frac{V_0\kappa^3}{24\pi}\cdot\frac{3}{x^3}\left[1+x-\frac{1}{1+x}-2\ln(1+x)\right], \quad (x=\kappa a) \qquad (5)$$

where V_0 is the molecular volume of solvent. It may easily be shown that the hydration has strictly no effect upon F_0°.

Now the practical osmotic coefficient, ϕ, may be defined as follows:

$$\phi = -\frac{55.51(\bar{F}_0-\bar{F}_0^\circ)}{(\nu_++\nu_-)mRT} = -\frac{55.51}{(\nu_++\nu_-)m}\ln a_0$$
$$= -\frac{55.51}{(\nu_++\nu_-)m}\ln f_0 \times\left[\frac{55.51-(\nu_+\alpha_++\nu_-\alpha_-)m}{55.51-(\nu_+\alpha_++\nu_-\alpha_-)m+(\nu_++\nu_-)m}\right]. \qquad (6)$$

Table 1

The Activity Coefficients of Sodium Chloride and the Logarithms of Activity of Water at 25°C.[1],[2],[3]

m	$\gamma_\pm$	$\gamma_\pm$ obs.		$1+\log a_0$	$1+\log a_0$ obs.	
	calc.*	(1)	(2)	calc.**	(2)	(3)
0.1	0.780	0.786	0.781	0.9985	0.9985	0.9985
0.2	0.736	0.741	0.737	0.9971	0.9971	0.9971
0.3	0.712	0.717	0.713	0.9956	0.9957	—
0.5	0.686	0.688	0.685	0.9927	0.9928	0.9928
0.7	0.673	0.674	0.671	0.9898	0.9898	—
1.0	0.664	0.664	0.661	0.9853	0.9853	0.9854
1.2	0.663	—	0.651	0.9822	0.9823	—
1.4	0.664	—	0.658	0.9790	0.9792	—
1.6	0.667	—	0.659	0.9758	0.9760	—
1.8	0.670	—	0.662	0.9725	0.9727	—
2.0	0.675	0.672	0.667	0.9691	0.9694	0.9695
2.5	0.691	—	0.686	0.9606	0.9605	—
3.0	0.712	0.713	0.713	0.9515	0.9511	0.9514
3.5	0.737	—	0.746	0.9419	0.9409	—
4.0	0.767	0.772	0.785	0.9319	0.9301	0.9314
4.5	0.801	—	0.832	0.9215	0.9184	—
5.0	0.839	—	0.884	0.9104	0.9061	—
5.2	0.857	0.859	—	—	—	0.9044
6.0	0.935	—	1.007	0.8868	0.8793	—

* $a=4.32$ Å., $\alpha_+ + \alpha^- = 6.0$

** $a=4.32$ Å., $\alpha_+ + \alpha_- = 3$.

(1) Landolt, Börnstein, "Physic. Chem. Tabellen," Erg. Bd. III, Berlin, 1936, p. 2153.

(2) G. Scatchard, W. Hamer and S. E. Wood, *ibid.*, **60**, 3061 (1938).

(3) Landolt, Börnstein, "Physik. Chem. Tabellen," Erg. Bd. II, 1931, p. 1126.

If the hydration does not exist, *i.e.*, in the case of $\alpha_+ = \alpha_- = 0$, all the equations cited above may be reduced to the ordinarily known formulae.

However, these equations contain two constants, a and $\nu_+\alpha_+ + \nu_-\alpha_-$, of which exact values are not obtainable at present by purely theoretical bases. Therefore, they must be determined at present as parameters so as to give agreements between the observed and calculated values. It is evident, however, that they are in the closest relation with each other and must be reduced ultimately to one.

The Comparison between the Calculated and Observed Values of $\gamma_\pm$ and ϕ at 25°. —The calculations for about 31 electrolytic aqueous solutions at 25° were made by the writer. Some of these results are compared in Table 1, Fig. 1 and Fig. 2.

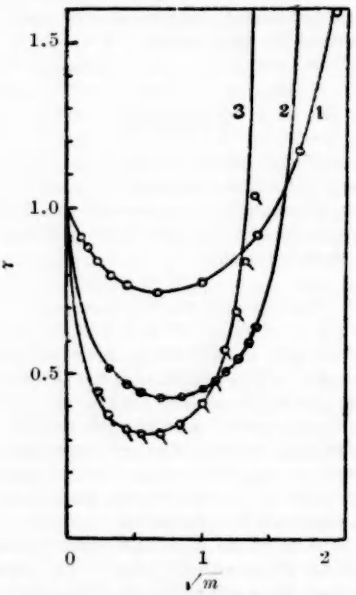

Fig. 1.—The activity coefficients of 1-1, 2-1 and 3-1 electrolytes at 25°C. Observed values: ○, LiCl; ⊖, $SrCl_2$; ◻, $PrCl_3$. Full line is calculated by Eqs. (2) and (3): curve 1 (LiCl), $a=5.26$ Å., $\alpha_+ + \alpha_- = 11$; curve 2 ($SrCl_2$), $a=4.68$ Å., $\alpha_+ + 2\alpha_- = 18$; curve 3 ($PrCl_3$), $a=6.14$ Å., $\alpha_+ + 3\alpha_- = 28$.

The agreements between calculated and observed values are satisfactorily excellent over the wide range of concentration: the deviations being within 1 % for most uni-uni valent salts of the concentration up to 4 M (but to 3 M in case of HCl and LiCl) and for $CaCl_2$ type

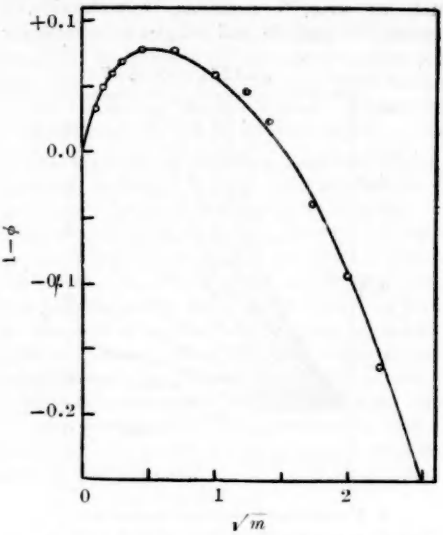

Fig. 2.—The osmotic coefficient of NaCl at 25°C.: ○, observation. Full line is calculated by Eqs. (5) and (6): $a=4.32$ Å., $\alpha_+ + \alpha_- = 3$.

salts of the concentration up to 2 *M* (but to 0.5 *M* in case of $ZnCl_2$), and the deviations being within 2% for $LaCl_3$ type salts of the concentration up to 1.6 *M*. The best fit values of a and $\nu_+\alpha_+ + \nu_-\alpha_-$ for activity coefficients are tabulated in Table 2, in which the fourth row refers to the literatures with which the values are compared.

For all nitrates, sulphates and for a few of chlorides such as $ZnCl_2$ and $CdCl_2$, both the a values and $\nu_+\alpha_+ + \nu_-\alpha_-$ values are either exceedingly small or not satisfactorily obtainable. This probably might be due to the fact the ions of these salts, as compared with the other salts, are so liable to associate or to form the complexes even in the dilute solution that the apparent concentration of these ions becomes small enough to cancel the effects of hydration on the activity coefficients. If these contributions are taken into consideration the values in Table 2 might slightly be altered. And in addition to them the effects of the change of the dielectric constants of solution by varying the concentration[6] must be taken into consideration in order to make the theory more complete.

Considering the sizes of molecules and ions the hydration number of an ion would probably be less than 12 for most monovalent simple ions. According to Bernal and Fowler[7], it must be 4 for all the monovalent simple ions, and 6 or 8 for divalent ions. But from the lowering of the dielectric constant of aqueous salt solutions, Hasted, Ritson and Collie[8] have estimated the minimum hydration number of positive ions at 10 for H^+, 6 for Li^+, 4 for Na^+, K^+ and Rb^+; 14 for Mg^{++} and Ba^{++}, and 22 La^{+++}.

Finally, however, it is not yet understood why the most favorable values of a and $\nu_+\alpha_+ + \nu_-\alpha_-$ for $\gamma_\pm$ and for ϕ do not agree with each other.

Table 2

The Values of the Mean Distance of Approach of Ions, and of the Molecular Hydration Number.[4][5]

$z_+=1$	HCl	KOH	LiCl	LiBr	LiI	NaCl	KCl	RbCl	CsCl	NH_4Cl	K_2SO_4
a, Å.	5.26	3.51	5.26	5.80	6.86	4.32	3.72	3.14	2.30	3.07	3.00
$\nu_+\alpha_+ + \nu_-\alpha_-$	12	10	11	12	14	6	4	4	4	5	(10)
Lit. No.	(5)	(3)	(3)	(4)	(4)(5)	(1)(2)	(2)(4)	(4)	(4)	(3)	(5)

$z_+=2$	$MgCl_2$	$NiCl_2$	$CoCl_2$	$CaCl_2$	$MnCl_2$	$BaBr_2$	$SrCl_2$	$CuCl_2$	$BaCl_2$	$ZnCl_2$	$MgSO_4$
a, Å.	6.14	5.16	5.00	5.10	5.10	4.93	4.68	4.65	4.42	5.28	2.93
$\nu_+\alpha_+ + \nu_-\alpha_-$	22	22	22	20	18	18	18	14	14	(2)	11
Lit. No.	(4)(5)	(5)	(5)	(5)	(5)	(5)	(5)	(5)	(5)	(5)	(5)

$z_+=3$	$AlCl_3$	$ScCl_3$	YCl_3	$LaCl_3$	$CeCl_3$	$PrCl_3$	$NdCl_3$	$SmCl_3$	$EuCl_3$
a, Å.	6.60	6.50	6.39	6.22	6.20	6.14	6.14	6.48	6.58
$\nu_+\alpha_+ + \nu_-\alpha_-$	34	32	30	28	28	28	28	28	28
Lit. No.	(5)	(5)	(5)	(5)	(5)	(5)	(5)	(5)	(5)

(4) Landolt, Börnstein, "Physik. Chem. Tabellen," Erg. Bd. III, 1936, p. 2138.
(5) R. A. Robinson and H. S. Harned, *Chem. Rev.*, **28**, 419 (1941).
(6) E. Hückel, *Physik. Zeits.*, **26**, 93 (1925).
(7) J. D. Bernal and R. H. Fowler, *J. Chem. Phys.*, **1**, 515 (1933).
(8) J. B. Hasted, D. M. Ritson and C. H. Collie, *J. Chem. Phys.*, **16**, 1 (1948).

The Solution of Non-Electrolytes

The van't Hoff's theory of dilute solution does not hold good any longer for the concentration higher than 0.1 mol per liter, while the hydration theory is applicable also for the interpretation of the properties of the solutions of non-electrolytes. The mechanism of hydration of non-electrolytes, different from that of electrolytes, is due chiefly to the hydrogen bond formation between solute and water molecules. As the strength of the hydrogen bond between water and hydroxyl radicals of organic compounds is assumed, in many cases, to be somewhat stronger than that of water[9], the function of water as solvent might be somewhat diminished when the hydration occurs. Thus the activity coefficient γ and the osmotic coefficient ϕ of the aqueous solution on the molality (mols of solute per 1000 g. of solvent) scale can be calculated by the following equations (*cf.* Eqs. (2) and (6)),

$$\ln \gamma = -\ln[1-(\alpha-1)m/55.51] \qquad (7)$$

$$\phi = -\frac{55.51}{m} \ln \frac{55.51-\alpha m}{55.51-\alpha m+m} \qquad (8)$$

by adjusting only one parameter α, the number of hydrated water molecules per one molecule of solute.

Some of the results are shown in Fig. 3 and Table 3. The agreements between calculated and observed values are excellent up to 2 *M* with each characteristic α value, but unsatisfactory in the region of high concentration, as is seen in Fig. 3. It seems here that α value decreases with increasing concentration, suggesting that the association of the solute begins to play some rôles. The behaviors of solutes such as urea,[10] urethane,[10] acetamide,[10] acetone,[11] methyl- and ethyl-alcohols[11] are

Table 3

The Osmotic Coefficients of Aqueous Solution of Sucrose at 25°C.[12]

m	ϕ calc. $\alpha=5$	ϕ obs.	m	ϕ calc. $\alpha=5$	ϕ obs.
0.1	1.008	1.007	1.2	1.108	1.108
0.2	1.016	1.015	1.4	1.128	1.128
0.3	1.024	1.023	1.6	1.149	1.149
0.4	1.033	1.032	1.8	1.170	1.169
0.5	1.042	1.041	2.0	1.195	1.189
0.6	1.051	1.050	2.5	1.255	1.236
0.7	1.059	1.059	3.0	1.322	1.282
0.8	1.069	1.069	3.5	1.397	1.326
0.9	1.078	1.078	4.0	1.482	1.369
1.0	1.088	1.088	5.0	1.686	1.448

(9) L. Pauling, "The Nature of the Chemical Bond," Cornell University Press, New York, 1940, pp. 284-334.

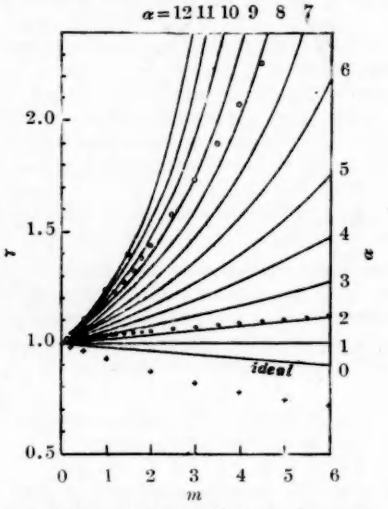

Fig. 3.—The activity coefficients of non-electrolytes at 25°C. ○, Sucrose; ●, Glycerol; +, Urea. Full line is calculated by Eq. (7).

Table 4

The Hydration Numbers of Some Organic Compounds.

Name of solute	No. of free OH radicals	α	Temp., °C.	Obtained from	References
Glycerol	2	3	0	γ(Fr)	(11)
		3	25	γ(p)	(2)
		1	25	ϕ(p)	(2)
Erythrit	4	4	0	γ(Fr)	(11)
Methyl Glucoside	4	3	0	p	(12)
		5	0	P	(13)
Glucose	5	4	0	γ(Fr), P	(11), (13)
Mannit	6	2	20	ϵ(p)	(11)
Sucrose	8	12	0	γ(Fr)	(11)
		5	0	p, P	(12), (13)
		9~10	25	γ(p)	(2)
		5	25	ϕ(p)	(2)
		4~5	25	p	(12), (14)
		5	30	P	(13), (15)
		4	55.7	P	(13), (15)
		4	100	p	(12)

(Fr...Freezing point depression; p...Vapor pressure; P...Osmotic pressure.)

(10) H. M. Chadwell and F. W. Politi, *J. Am. Chem. Soc.*, **60**, 1292 (1938).
(11) Landolt, Börnstein, "Physik. Chem. Tabellen," Erg. Bd. II, Berlin, 1931, p. 1130.
(12) "International Critical Table," Bd. III, p. 293.
(13) *ibid.*, Bd. IV, p. 429.
(14) Landolt, Börnstein, "Physik. Chem. Tabellen" Erg. Bd. III, 1936, p. 2493.
(15) *ibid.*, Erg. Bd. III, 1936, p. 2664.

exceptional in that their activity coefficients are, even in dilute solution, always below the ideal line. Therefore, such solutes must always be in associated states, because the activity coefficient is diminished by association.

The Hydration Number and the Structure of Solute.—In order to get the most probable value of the hydration number, we must determine it from the activity observed in the solution as dilute as possible, in which the association of the solute can be neglected. The best fit values of α are tabulated in Table 4. Here, it is possible to imagine a certain relation between α and the structural configuration of the solute molecule: a rough correspondence exists between α and the number of hydrogen-bond-forming radicals in the molecule of solute, although some exceptions such as mannit exist.

It is inexplicable in this case too, the reason why some of the values of α estimated from γ are approximately two times of those estimated from ϕ.

Summary

(1) Upon taking the hydration into consideration the thermodynamical properties of solutions of electrolytes and non-electrolytes can be well represented over the wide range of concentration.

(2) The values of hydration number of non-electrolytes seem to be related to the configuration of solute molecules. The hydration number was determined for 37 solutes.

Laboratory of Chemistry, Liberal Arts Faculty, Shizuoka University, Shizuoka,

Fungus and Enzyme. Preparation of Aspergillus Oryzae Amylase and its Use in Bread Making

By Taichi HARADA

(Received July 28, 1950)

Introduction

The degree of panary ferment which is caused by yeast depends largely upon the presence of fermentable sugar produced by the action of diastatic enzyme in flour. The amount of diastase in the flour is, therefore, one of the important factors in bread making. Flour deficient in diastatic activity can not be baked into a desired large loaf of bread unless a sufficient amount of sugar is added to the dough. It is known that to supplement the deficiency, wheat is mixed with a little sprouting one[1] and is milled in the usual manner or the flour is mixed with corn flour[2] having a high diastatic activity or with malt preparation.

In the experiment, it is observed that the use of fungal amylase preparation, taka-diastase, in bread making gives an undesirable effect, caused not by the true amylase of such preparation but by the proteolytic enzyme accompaning the amylase. That is to say the proteolytic enzyme is not only responsible for a reduction of gas retaining power of the dough but also for the characteristic bread disease "Ropiness".[3]

Therefore, it is desirable to prepare the diastatic enzyme preparation as free as possible from the proteolytic enzyme.

Discussion

The present author[4] has shown that the diastatic enzyme solution passes through a colloidal membrance, indicating that it possesses a relatively small molecule. The enzyme preparation prepared by this method was tried in bread making but this was abandoned since it was not economical. There are many methods for the separation or purification of amylase but they are not applicable to the industry from the same stand point.

Although it was thought that alkaline or acidic of the culture medium, bran, might

(1) Sherwood and Bailey, *Cereal Chem.* **3**, 163 (1926).
(2) Sapozhnikova, *C. A.* **43**, 7569 (1949).
(3) Unpublished observation by the author at Takamine Laboratory, Inc., Clifton, N. J., U. S. A. (1930).
(4) T. Harada, *Ind. Eng. Chem.* **23**, 1424 (1931).

influence the production of proteolytic enzyme, a few experiments has proved otherwise. The best method is to find the special strain of the fungus which does not produce any of the enzyme in question in its growth, but such is almost impossible at present.

In the previous paper[5] the present author reported that in precipitating the enzyme with 70 volume percent alcohol when the precipitate becomes gum-like it may be adjusted to a desired precipitate by cutting down the amount of alcohol. However, in this case this will cause a loss of diastatic enzyme preparation. When the precipitating diastase preparation of this dilute alcohol was determined for diastatic and proteolytic (casein-digesting) enzymes, a relatively large amount, in other words, a strong proteolytic enzyme (Fuld-Gross' method) was present in comparison to that of diastatic enzyme in the control.

Therefore, it is interesting to note here that the proteolytic enzyme could be removed by this simple fractional precipitating process, and that the diastase preparation, free or almost free from the enzyme in question is possible to be used in the bread making industry instead of malt preparation not only more economically but in producing fine loaves of bread. It is seen that the amount of diastase and protease in the flour or the dough in bread making becomes a real problem.

Fraction

It was shown that a fractional precipitation by alcohol serves to a certain degree as separation or purification of the amylase; that is, in the first fraction, with around 57 volume

Table 1

The Influence of Fractional Alcoholic Precipitation upon Diastase and Proteolytic Enzyme

Origin of fungus strain*		Yield, g.	L. V.	% L. V.**	Total L. V., %	T. V.	Total T. V.	T. V. in 100% L. V.
A	1. Koji extract 100 +alc. 150 (61%)	1.40	1100	73.3	102.6	111.1	155.5	151.6
	2. The filtrate of No. 1 225+alc. 215 (77.6%)	2.99	5651	376.7	1126.3	3.2	9.6	0.9
	3. Koji extract 100 +alc. 375 (75%)	4.12	4100	273.3	1126.0	41.7	171.8	15.3
B	1. Koji extract 100 +alc. 115 (51%)	0.9	125	8.3	7.5	47.6	42.8	573.5
	2. The filtrate of No. 1 205+alc. 230 (74%)	1.2	1967	131.1	157.3	37.0	44.4	28.2
	3. Koji extract 100 +alc. 350 (74%)	2.0	1283	85.5	171.0	47.6	95.2	55.7
	1. Koji extract 125 +alc. 188 (57%)	1.2	125	8.4	10.1	25.7	30.8	306.0
	2. The filtrate of No. 1 290+alc. 270 (75%)	1.1	2117	141.1	155.2	8.9	9.8	6.3
	3. Koji extract 125 +alc. 438 (74%)	2.2	1034	68.9	155.1	22.2	48.8	32.2
C	1. Koji extract 110 +alc. 190 (60%)	1.4	190	12.7	17.8	111.1	155.4	874.8
	2. The filtrate of No. 1 275+alc. 230 (72%)	2.0	535	35.7	71.4	15.4	30.8	43.1
	3. Koji extract 110 +alc. 350 (72%)	3.0	480	320	96.0	66.7	200.1	208.4
	1. Koji extract 100 +alc. 137 (55%)	0.6	230	8.7	5.2	8	4.8	92.0
	2. Whole filtrate of No. 1+alc. 270 (79%)	0.7	4600	306.7	214.7	6	4.2	2.0
	3. Koji extract 100 +alc. 375 (75%)	1.1	3240	216.0	237.6	8	8.8	3.7

* Orgin of fungus strain A, Asp. oryzae strain of Takamine Laboratory; B, Asp. oryzae, a mixed strain; C, Asp. oryzae B. strain of the Sakaguchi Laboratory of this institute.

** 100% = 1500 L. V.

(5) T. Harada, This Bulletin, **22**, 197 (1949).

percent alcohol of Koji water extract, it gives a relatively strong tryptic but weak diastatic enzyme preparation, and in the second fraction, with 72 percent alcohol or over, it gives a preparation, fairly free from the proteolytic enzyme with a strong diastatic power, in comparison to the first fraction and the control.

It is seen that as total L. V. (Table 1), the diastase preparation may greatly be lost in the first fraction but this loss may be collected in the second fraction to make it up to about 70 volume percent or over. Further purification might be carried out by dissolving the precipitate and by repeating the process of the fraction but it is industrially not economical. The degree of purity, of course, depends largely upon the strength of the extract and the origin of the fungus strain as shown in the experiment.

Selective Use of the Fraction

The rich proteolytic but poor diastatic enzyme content preparation in the first fraction may be superior than that of an ordinarily prepared taka-diastase or the control when used internally such as for stomach disturbance but the proteolytic freed rich diastatic enzyme preparation is superior than malt preparation in the bread making industry.

Experiment

(a) One hundred cc. (Table 1, A) of the water extract of Asp. oryzae fungus Koji (free from spore) No. 1 and 3 were treated with 150 and 375 cc. of about 95 percent alcohol to give about 61 and 75 volume percent respectively in a 500 cc. capacity Erlenmayer flask, mixed well, left standing one hour or so, then supernatant liquid decantated to another flask. The bottom liquid mixture with precipitate was transferred a to precipitation tube, centrifugalized and separated. The precipitate was washed with 95 percent alcohol and filtered rapidly by suction, washed with ether and finally it was dried in a calcium desiccator. On the other hand (No. 2), the whole (225 cc.) alcoholic liquid part, the filtrate of No. 1, was treated with further addition of alcohol (215 cc.), mixed, precipitated again, and this second precipitation was washed with 95 percent alcohol, finally dried in a calcium desiccator. Table 1, B and C are the results of the similar treatment for the samples of different origins.

(b) When the amylase, fairly free from proteolytic enzyme, was tried number of times in bread making (flour, 350: diastase, 50 L. V. in total) by the method[6] of Bailey, the result was quite a satisfactory bread in every respect. The characteristic fermentation (bread-disease) does not easily set in comparison with that prepared by the Takamine's method. This publication will soon follow.

Summary

1. The fungal amylase preparation containing rich proteolytic but poor diastatic enzyme has been prepared by precipitating Koji water extract with the amount of alcohol which gives around fifty to sixty volume percent solution.

2. A strong fungal amylase but very weak proteolytic enzyme preparation has been prepared by fractional precipitation of the filtrate of 1 by adding further alcohol up to seventy percent or over.

3. The possibility of utilizing fungal diastase preparation in the bread making industry has been pointed out.

The author thanks the Sakaguchi Laboratory for the Asp. oryzae B. strain which was kindly given for this investigation.

Scientific Research Institute, Ltd., Tokyo

(6) Bailey, *J. Ind. Eng. Chem.*, **8**, 53 (1916).

Amperometric Titration of Potassium with Sodium Dipicrylaminate

By Yoshikazu YASUMORI

(Received September 15, 1950)

Amperometric titration of potassium with sodium dipicrylaminate has been studied by B. Sandberg[1] and A. Langer *et al.*,[2] but the details are not given. In the present paper

(1) B. Sandberg, *Svensk. Kem. Tid.*, **58**, 197 (1946); *C. A.*, **41**, 349 (1947).

(2) A. Langer and D. P. Stevenson, *Ind. Eng. Chem., Anal. Ed.*, **14**, 770 (1942).

the analytical procedure is shown and the results are discussed.

Experimental

Chemicals and Apparatus Used.—Sodium Dipicrylaminate was Hexyl Natrium made by Nippon Kasei Chemical Industries Limited. The polarograph used by the author was a Heyrovsky-Shikata type made by Yanagimoto Co., Kyoto. For amperometric titration both the portable electronic instrument of Delahay's type[3] and the arrangement as shown in Fig. 1 were used.

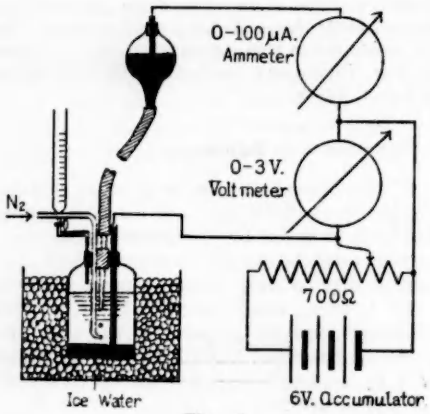

Fig. 1.

Polarographic Behavior of Sodium Dipicrylaminate.—A polarogram of sodium dipicrylaminate in Palitzsch's borate buffer solution (*p*H 8.98) is shown in Fig. 2. Three waves were obtained, the first small, the second obscure and the third was a large wave with maximum. The wave-height of the first was not proportional to the concentration of dipicrylaminate. The maximum in the third wave was not suppressed by gelatin, but the diffusion currents of dipicrylaminate in the above mentioned buffer solution at −1.60 V. applied *vs.* mercury pool were proportional to its concentration smaller than 3×10^{-3}.

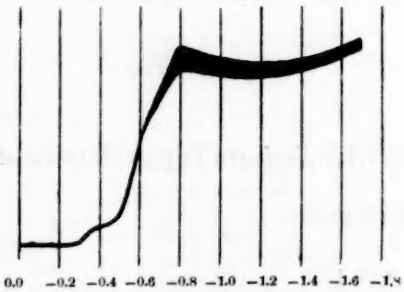

Fig. 2.—A polarogram of sodium dipicrylaminate in Palitzsch's borax buffer solution (*p*H 8.98): Sensitivity, 1/100; concentration, 16.4×10^{-5}; anode, Hg-pool.

(3) P. Delahay, *Anal. Chem.*, **21**, 1425 (1949).

Procedure.—A measured volume of the sample was introduced into the cell, neutralized with sodium hydroxide and 50 ml. of the buffer solution were added. After passing nitrogen gas for ten minutes and cooling in an icewater-bath, the −1.60 V. *vs.* mercury pool was applied to the cell and the current was measured. *N*/10 sodium dipicrylaminate solution was added successively with a microburette. After each addition the content in the cell was mixed by passing nitrogen gas for ten minutes and the current was recorded. During the titration, the electrolyte must be cooled in an icewater-bath at 0° −2°. In all cases the values of the current, corrected for the volume change, were plotted against the amount of reagent added.

Results

Results obtained in the titration are given

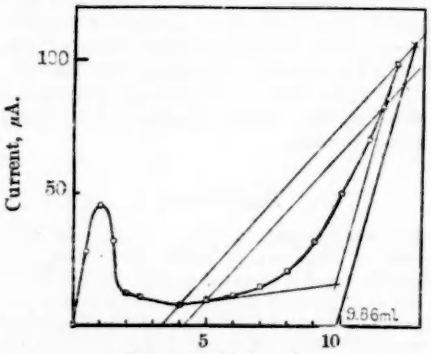

Fig. 3.—Titration curve of sample No. 1.

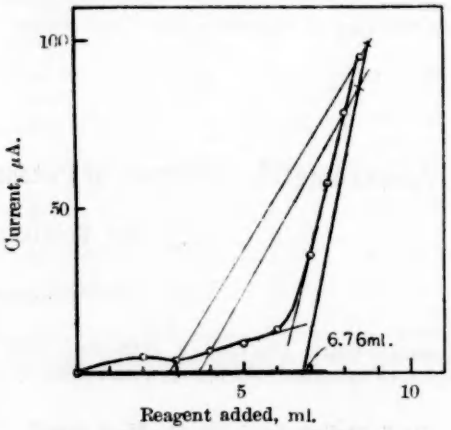

Fig. 4.—Titration curve of sample No. 2.

in Table 1 (Figs. 3, 4, 5, 6, 7, 8 and 9). The point obtained by the intersection of the tangents became different from the point obtained by the intersection of the asymptotes

Table 1

Sample No.	Used, mg.	End-point obtained, ml.	K found, mg.
1	K 39.1 Na 17.3	9.86 (9.80)	39.1 (38.9)
2	K 27.6 Na 17.3	6.76 (6.49)	26.8 (25.8)
3	K 72.7 Na 17.3	18.36 (16.97)	72.9 (67.4)
4	K 52.2 Na 412.6	13.18 (12.67)	52.3 (50.3)
5	K 26.4 Na 412.6	6.31	25.0
6	K 34.7 Na 336.4	8.68	34.5
7	K 51.4 Na 17.3 Fe 43.2 Al 22.3	12.97 (12.28)	51.5 (48.8)

The values obtained by the intersection of tangents were given in brackets. No. 7 was titrated, using a microammeter of 100 microamperes in full scale.

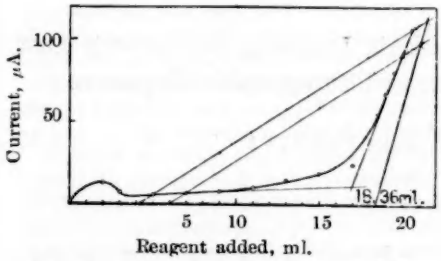

Fig. 5.—Titration curve of sample No. 3.

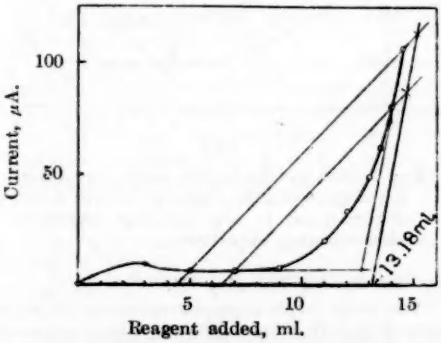

Fig. 6.—Titration curve of sample No. 4.

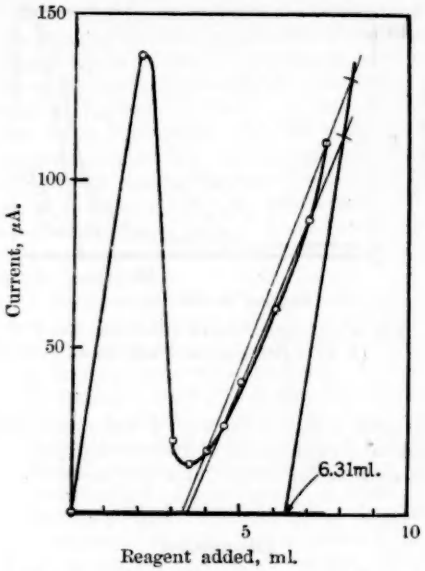

Fig. 7.—Titration curve of sample No. 5.

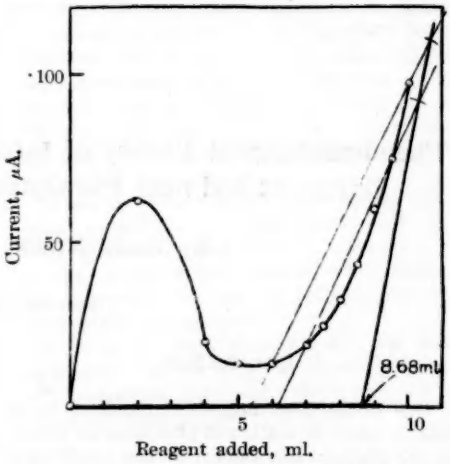

Fig. 8.—Titration curve of sample No. 6.

of titration curve according to Langer *et al.* When the end-point was located on the point obtained by the intersection of the asymptotes, the results obtained showed coincidence with that calculated. At the beginning of titrations supersaturation was held, so that when there was no more than 30 mg. K, the portion of the titration curve before the end-point was not complete enough to obtain an asymptote. The presence of 350 mg. Na did not interfere and in presence of aluminate and precipitate of ferric hydroxide the titration was not affected.

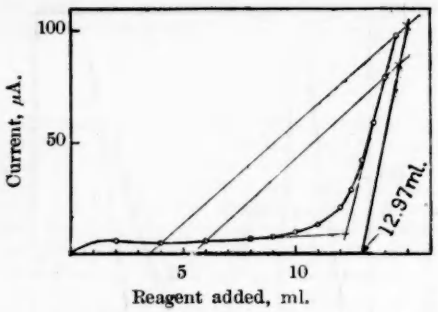

Fig. 9.—Titration curve of sample No. 7 (A 100-microammeter was used).

The great diffusion current of dipicrylaminate made a microammeter of 100 microamperes in full scale useful instead of a galvanometer.

Discussion

Mercury pool was used for the anode, for the reason that if calomel electrode was used, potassium ion might stray into the cell and that the diffusion current of dipicrylaminate was so great that the potential drop through the connecting bridge would not be negligible. Applied potential should be changed with the composition of sample. When the sample was chloride, −1.60 V. was applicable. Although dipicrylaminate seemed to be not completely dissociated, in the present work the end point was located negleting the undissociated dipicrylaminate.

Summary

In the amperometric titration of potassium with dipicrylaminate, the end-point located by the theory of Langer *et al.* showed satisfactory results. The accuracy was within 1 mg. with more than 30 mg. K. In presence of 350 mg. Na, or aluminate and precipitate of ferric hydroxide the titration was not affected.

In conclusion the author wishes to express his sincere thanks to Mr. S. Sato in this laboratory for his kind advice.

The Laboratory of Nippon Kasei Chemical Industries Limited, Kawasaki

---

Phenomenological Theory of Intermediate Intensity Reciprocity-Law Failure at and near the Optimum in Photographic Exposure

By Eiichi Mizuki and Shin Fujisawa

(Received March 3, 1951)

Introduction

One of the most important problems in the latent image formation in photographic process is the phenomenon known as the reciprocity-law failure corresponding to the breakdown of Bunsen-Roscoe's law for a photo-chemical reaction. As is well known, the developed density of a photographic emulsion does not depend only upon the exposure of light, namely the product of the intensity and time factors. In most cases, there exists an optimal intensity at which the photographic process proceeds most efficiently.

This phenomenon is in general represented graphically by a reciprocity-failure curve. The curve A in Fig. 1 shows a typical case of it, in which the log exposure (It) required to produce a constant developed density is plotted against the log intensity (I).

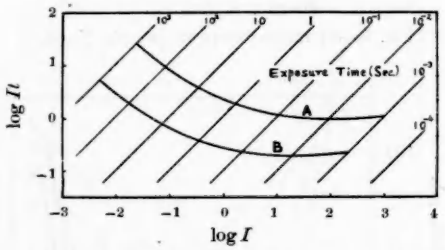

Fig. 1.—Reciprocity-failure curves for different degrees of after-ripening: curves A and B correspond to low and high degrees of after-ripening respectively.

The drop in photographic efficiency at intensities higher than the optimum, which is termed as the high intensity failure, is caused by the

relative sluggishness of the inonic process compared with the high rate of the production of the photo-electrons and the limited electric capacity of the electron traps.[1] On the other hand, the failure of reciprocity-law at intensities lower than the optimum arises from the fact that the thermal agitation impedes the creation of the silver specks in the initial stages of the latent image formation.[1],[2]

These interpretations are qualitatively acceptable, but it is highly desired from both theoretical and practical standpoints to develop this theory, especially so as to interpret quantitatively the shape of the reciprocity-failure curve. This is the reason why the problem in this field has received so much discussion in recent years. Katz[3] and Webb,[4] for instance, have succeeded independently in deriving the theoretical curves in the region of very low intensities. Their methods are based upon the following considerations : (1) the assumed existence of the stable speck in the initial stages of latent image formation and (2) the statistical fluctuation of the number of light quanta absorbed by a grain. Their separate treatments arrived at the same conclusion that the shape of the curve at very low intensities is a straight line, and this is in good agreement with the experimental results.

In the above treatments by Katz and Webb, they attempt to extend their treatments so as to include the region of intermediate intensities below the optimum. However, it seems[5] that in their extensions they do not fully appreciate the interplay of ionic and electronic processes at intermediate intensities below the optimum.

In such a region of exposure intensities special attention must be given to what becomes of the photo-electrons after they have been captured by the electron traps. In some cases, some of such trapped electrons may not be neutralized by ionic process, but, due to thermal motion, escape from the trapping states. Thus these two possibilities may act competitively on the trapped electrons (hereafter referred to as the competitive action).

It is the purpose of this paper, therefore, to point out that there is a more appropriate treatment in the region of intermediate intensities at and near the optimum. The present authors emphasize that in such a region the competitive action should be taken into account.

Moreover, by assuming the accumulation of the trapped electrons in an electron trap throughout exposure, the present authors have phenomenologically formulated a dynamical equation for the rate of increase in the number of the trapped electrons. On the basis of this, analytic expression for the log exposure required to produce the developable image has been derived. Finally, by means of adjustable parameters, comparison has been made to see how this theoretical curve is compatible with the experimental data.

A phenomenon which produces strong evidence for our viewpoint is that the reciprocity-failure curve is shifted as a whole in a definite way in accordance with the changes in various factors such as the degree of the after-ripening, the ionic conductivity, the temperature, etc.

For instance, as the after-ripening is prolonged in its earlier stages, the reciprocity-failure curve at intermediate intensities is in most cases shifted as a whole toward lower intensity along the direction of lines of constant exposure times (hereafter referred to as the diagonal shift).[3] The experimental reciprocity-failure curves at different degrees of after-ripening are shown in Fig. 1, where the curve B refers to the emulsion subjected to a longer after-ripening than that of the curve A. This diagonal shift seen here which is composed of the vertical descent component as well as the traverse shift component would be inexplicable by any idea, unless the competitive action were taken into account.

It seems to be also the case with the similar shift caused by the temperature changes, although Katz[3] and Webb[4] have some remarks on this point without being aware of the importance of the competitive action at intermediate intensities.

It is to be noted, therefore, that the treatment given in this paper is especially suitable for interpreting the bodily shifts of the whole curves at intermediate intensities.

Derivation of the Equation Representing the High Intensity Failure Component

Exposure of silver halide grains of the photographic emulsion releases electrons from the bromide ions or the local absorption centers and raises them up to the conduction levels of the crystal lattice. Such electrons move through the lattice and then may be captured by the electron traps (sensitivity specks) distributed haphazardly on the grains.

Let us consider first the process of electron

(1) R. W. Gurney and N. F. Mott, *Proc. Roy. Soc.*, **A 164**, 151 (1938).
(2) J. H. Webb and C. H. Evans, *J. Opt. Soc. Am.*, **28**, 431 (1938).
(3) E. Katz, *J. Chem. Phys.*, **17**, 1132 (1949).
(4) J. H. Webb, *J. Opt. Soc. Am.*, **40**, 3 (1950).
(5) S. Fujisawa and E. Mizuki, to appear in *J. Opt. Soc. Am.*, (L).
(6) E. Mizuki, *Kagaku Butsuri* (in Japanese), **1**, 49 (1949); E. Mizuki and S. Fujisawa, to be published.

trapping. We assume that the electron trap responsible for the latent image formation may be capable of capturing several electrons simultaneously. In this case, however, owing to their electrostatic repulsion against subsequent electrons, the capture cross section σ of an electron trap diminishes with increasing the number n of the electrons already captured, in accordance with the relation

$$\sigma=\beta n^{-\gamma}, \tag{1}$$

where β and γ are the numerical constants, the former being one of parameters determing the position of the reciprocity-failure curve and the latter one of adjustable parameters which serve to fit the shape of the theoretical curve to the experimental one. It is on this account that the present treatment is to be considered as essentially phenomenological.

Secondly, we now suppose the existence of the competitive action on the trapped electrons. The electrons staying in the electron trap may be either neutralized by the ionic migration (mobile silver ions or vacant anion sites) owing to their negative charge, or ejected on to the conduction band by the thermal motion (leading to inefficiency). These two possibilities should be considered as competing (simultaneously existing) so long as the lifetime of a trapped electron is of the same order as the time of neutralization by ionic migration. Under the existence of such competitive action, the rate of increase in the number of trapped electrons during exposure with intensity I is given by the equation,

$$\mathrm{d}n/\mathrm{d}t = P\beta n^{-\gamma}I-(Q+R)n. \tag{2}$$

Herein P is the constant proportional to the product of the grain area and the light absorption factor of the grain; the factor $\beta n^{-\gamma}$ is given by Eq. (1): Q is the constant proportional to ionic conductivity for the ionic process playing a role in the neutralization of trapped electron; R is the probability of an electron escaping from an electron trap, or the reciprocal of average lifetime of a trapped electron, having the relationship,

$$R = \nu \exp(-\Delta E/kT). \tag{3}$$

In this relation ΔE is the thermal depth of the electron trap, and ν the frequency with which a trapped electron collides with the potential walls of the electron trap, k the Boltzmann constant and T the temperature.

It should be remarked about Eq. (2) that the present authors deal only with the case where the magnitude of the first term $P\beta n^{-\gamma}I$ is larger than that of the second term $(Q+R)n$. If, however, the ionic migration is so rapid that the second term surpasses the first term even when the magnitude of the factor R is very small, the accumulation of trapped electrons in an electron trap will not occur. Accordingly, Eq. (2), therefore the present treatment will be meaningless, but the extensions attempted by Katz and Webb will be found the good approximations in such a case.

Integrating Eq. (2), we have

$$n^{1+\gamma}=\{\beta PI/(Q+R)\}[1-\exp\{(1+\gamma)(Q+R)\}t]. \tag{4}$$

When the factor $(1+\gamma)(Q+R)$ is large enough, Eq. (4) shows that the value of n approaches the saturation value $n_s(I)$ given by,

$$n_s(I) = \{\beta PI/(Q+R)\}^{1/1+\gamma}, \tag{5}$$

as soon as the grain is exposed. Then we can tentatively assume that the number of the trapped electrons in an electron trap remains constant throughout the whole exposure time, but increases slowly with increasing the exposure intensity I in accordance with the relation (5). On this assumption, the number N of the silver atoms produced by the neutralization process during exposure time t can be calculated by the following equation

$$N = \int_0^t Q n_s(I)\mathrm{d}t. \tag{6}$$

Substituting for $n_s(I)$ from Eq. (5) and then integrating, we obtain the following equation after a slight rearrangement,

$$\log It = \frac{\gamma}{1+\gamma}\log I-\log\frac{Q}{N} -\frac{1}{1+\gamma}\log\frac{\beta P}{Q+R}. \tag{7}$$

Eq. (7) expresses the log exposure required to produce the N silver atoms. Eq. (7) plotted on the $\log It$ *versus* $\log I$ type of diagram gives a straight line having a positive slope, and thus represents only the component of the high intensity failure.

Consideration of the Low Intensity Failure Component

It is believed that the cause of the low intensity failure is found in the initial stages of latent image formation. Thermal vibration of the crystal lattice impedes the creation of the silver specks in the initial stages of latent image formation.

We now assume that the silver speck will begin to form only when the number of the trapped electrons in an electron trap at which the silver speck will be formed exceeds a critical value n_c, and that the silver speck so formed is stable to thermal agitation (the stable speck). Such interpretation is very similar to, but slightly different from that proposed by Gurney and Mott.[1]

Since the silver speck can not be formed under the condition that the intensity of exposure is so low that the value of $n_s(I)$ is less than a critical value n_c ($n_s(I)<n_c$), where $n_s(I)$ is the average number of trapped electrons given by Eq. (5), the slope of the reciprocity-failure curve should become suddenly infinite at a critical intensity in the lower intensity side of the curve. Most experimental results, however, do not show such an abrupt upturn in the curve. It seems quite reasonable that the fluctuation of light quanta absorbed by a grain should be taken into account to interpret the non-existence of such an abrupt upturn in the lower intensity failure curve. This step has been already taken by many workers.[7]

Even if the average intensity of light is sufficiently low, its momentary value may be raised up because of the fluctuation phenomenon. Accordingly, it may be assumed[8] that the momentary number of trapped electrons may become larger than n_c, although its average number can not exceed n_c. Therefore, it is expected that even at such low intensities there exists the possibility of formation of a stable speck, and this possibility will decrease as the average intensity of light is lowered.

Let us now calculate the exposure required to produce the stable speck at intermediate intensities with considering the low and high intensity failure component simultaneously. We believe that Eq. (6) can answer our purpose if such modification is made on it as is based on the afore-said considerations. This modification is made in the following way: When the average number of trapped electons existing in an electron trap is $n_s(I)$, the probability $P(n)$ of n electrons existing in an electron trap can be represented by the use of the Poisson equation,

$$P(n)=\exp\{-n_s(I)\}\{n_s(I)^n/n!\}. \qquad (8)$$

By summing this expression for all n values from n_c to infinity, we can obtain a factor $F\{n_s(I)\}$ corresponding to the probability of at least n_c electrons existing in an electron trap

$$F\{n_s(I)\}=\exp\{n_s(I)\}\sum_{n=n_c}^{\infty}\{n_s(I)^n/n!\}. \qquad (9)$$

The above mentioned modification will be made when $n_s(I)$ in Eq. (6) is multiplied by the factor F so obtained. Thus we can calculate approximately the exposure required to produce the stable speck (the number of silver atoms in it is N_s) by means of the equation

$$N_s=\int_0^{t_s} QF\{n_s(I)\}n_s(I)\mathrm{d}t. \qquad (10)$$

Substituting for $n_s(I)$ from Eq. (5) and then integrating, we obtain the following equation after a slight rearrangement,

$$\log It_s=\frac{\gamma}{1+\gamma}\log I-\log\frac{QF\{n_s(I)\}}{n_s}-\frac{1}{1+\gamma}\log\frac{\beta P}{Q+R}. \qquad (11)$$

This equation expresses the log exposure (It_s) required to produce the stable speck in the initial stages of latent image formation. The value of $F\{n_s(I)\}$ for a given value n_c (say two), which can be calculated by the graphical method, begins to decrease less than unity as $n_s(I)$ is lowered. In addition, $n_s(I)$ varies with the intensity I in accordance with Eq. (5), and thus following relation will be given,

$$\Delta\log n_s(I)=\left(\frac{1}{1+\gamma}\right)\Delta\log I. \qquad (5')$$

Using this relation we can easily get an idea of how the factor $F\{n_s(I)\}$ varies with the intensity I. It follows that the curve of Eq.

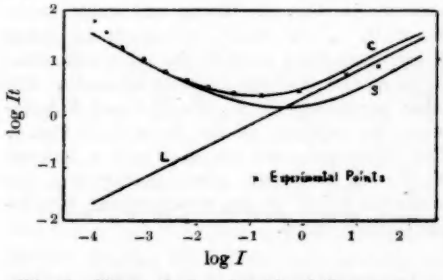

Fig. 2.—Theoretical reciprocity-failure curves for: (S), initial stages; (L), later stages; (C) total stages. Comparison of theoretical composite curve C with experimental curve.

(7) L. Silberstein, *J. Opt. Soc. Am.*, **29**, 432 (1939); P. C. Burton and W. F. Berg, *Phot. J.*, **86B**, 2 (1946); references (3) and (4)

(8) As has been stated, it is assumed that the saturation of the electron concentration in an electron trap is achieved as soon as the grain is exposed.

(11) plotted on $\log It$ *versus* $\log I$ type of diagram has its optimum point (the optimal intensity). Its schematic curve is shown by the curve S in Fig. 2. It has been derived, therefore, that the reciprocity-failure curve for the initial stages of formation of the latent image (the stable speck formation) has the optimal intensity.

Composite Reciprocity Failure Curve

In order that the stable speck may be brought up to the developable size, there are still repuired some additional silver atoms N_a. Then, we assume that this process takes place in that later stages of the latent image formation in which there is no influence of the low intensity failure component, but of the high intensity failure component. Therefore, in order to calculate the further exposure (It_a) required to produce N_a addtional silver atmos, Eq. (7) can be directly applicable. Thus we obtain the equation,

$$\log It_a = \frac{\gamma}{1+\gamma}\log I - \log\frac{Q}{N_a} - \frac{1}{1+\gamma}\log\frac{\beta P}{Q+R}. \qquad (12)$$

Since Eq. (12) does not contain the factor F, the shape of its reciprocity-failure characteristic is a straight line having a slope $\gamma/(1+\gamma)$ as shown by the line L in Fig. 2.

Finally, the log total exposures (It) required to produce the developable latent image from unexposed state will be

$$\log It = \log(It_s + It_a), \qquad (13)$$

where It_s and It_a are given by Eqs. (11) and and (12) respectively. Summation in Eq. (13) can be easily carried out by the graphical method. A composite reciprocity-failure curve so obtained is schematically shown by the curve C in Fig. 2. Using adjustable parameters γ, n_c, and N_a/N_s, we can fit the shape of the theoretiacl curve to that of experimental curve at and near the optimal intensity. The other parameters β, N_s, N_a, P, Q and R determine the position of the curve C in Fig. 2. The theoretical curve having $\gamma = 1$, $n_c = 2$ and $N_a/N_s = 2$ is shown here together with the measured points of the experimental reciprocity-failure curve.

Discussion of Theoretical Results

Discrepancies at Lower and Higher Intensities.—As is shown in Fig. 2, the theoretical curve C does not perfectly agree with the experimental points in the region of lower and higher intensities. The discrepancy at lower intensities is probably connected with the fact that in such a region the trapped electron in an electron trap can not be accumulated continually during the entire course of exposure, therefore the fundamental Eq. (2) will lose its meaning. On the other hand, the discrepancy in the region of higher intensities presumably arises from the following fact: The present theoretical curve redresenting the log exposure required to produce only one just-developable speck in a grain is worthy of comparing with the experimental results obtained under the special condition that only the grains having a just-developable speck can initiate the development. In the region of higher intensities, however, the grains having the sub-speck whose size is too small to be developable for a short duration of development are likely to be formed together with the grains having the developable one. This tendency will progressively predominate with increasing the intensity. Thus, it is expected that the development conditions exert strong influence upon the shape of the curve in the region of higher intenisities at and beyond the optimum. Accordingly, the experimental curves would be more compatible with the theoretical curves, if the exposed emulsions were developed for a shorter period by means of a weaker developer.

Bodily Shift of the Whole Curve.—It is to be emphasized that the important feature of this theory is the strong dependence of the position of the whole curve in diagram upon the factors such as β, P, Q and R. An interesting conclusion theoretically derived on the basis of this is that the position of the reciprocity-failure curve will make a bodily shift if the value of the above factors is changed.

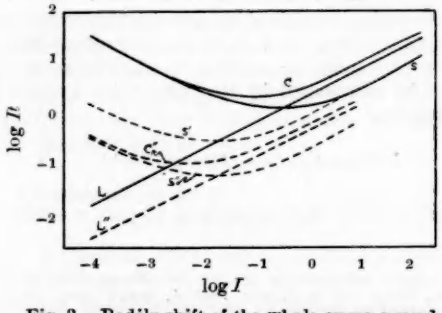

Fig. 3.—Bodily shift of the whole curve caused by the change in the magnitude of the factor R.

This conclusion has been reached in the following way: Let us consider, for instance, the case of the factor R, which is also applicable to the case of the factors β, P and Q with slight modifications. When the thermal depth ΔE of electron trap is increased, the probability R of an electron escaping from the electron trap will be decreased in accordance with the relation (3). This decrease in the R factor exerts an influence upon the factors $n_s(I)$ in accordance with the relation (5). If the value of $\beta P/(Q+R)$ is increased by a factor λ due to a decrease in the R factor, it is easily seen that the value of $n_s(I/\lambda)$ after this change equals to that of $n_s(I)$ before this change, and thus leaving the value of the F factor unchanged. In Eq. (11), because of the existence of the term containing the F factor, the position of the minimum point in the curve S will be shifted toward lower intensities along a straight line having a slope $\gamma/(1+\gamma)$ by an amount whose projection on the abscissa is $\log\lambda$ (as shown by the shift $S \rightarrow S'$ in Fig. 3). It is to be noted here that the curves S and S′ have the same shape. Hence, the magnitude of the vertical descent of the upturn portion of the curve S will be $\{\gamma(1+\gamma)\}\log\lambda$. In addition, the curve S′ will vertically descend as a whole by an amount $\{1/(1+\gamma)\}\log\gamma$ (the shift $S' \rightarrow S''$), since Eq. (11) has the last term containing the R factor. This shift will change the shape of the composite curve. However, the straight line L will only vertically descend by the same amount originating in the last term in Eq. (12) (the shift $L \rightarrow L''$), which does not contain the F factor. Accordingly, the shape of the composite curve does not change. The vertical descend of the upturn portion of the composite curve (the shift $C \rightarrow C''$) will be $\log\lambda$ after all. Thus, the composite curve will be shifted toward lower intensities diagonally (along the direction of 45-degree lines of constant exposure times) as a whole, since the vertical descend equals to the traverse shift in their magnitudes.

The present authors maintain that the above theoretical conclusion is tenable,[5] since it is consistent with the experimental facts concerning the diagonal shifts caused by the prolongation of after-ripening in its earlier stages. The detailed effects of after-ripening upon the position and shape of the reciprocity-failure curves will be discussed in our forthcoming publication.[6] It is to be added here that the measurements[9] of the reciprocity-failure curves of the photographic emulsions having the different ionic conductivities respectively are consistent with the theoretical conclusion derived by means of changing the factor Q in the theory of this paper.

We are indebted to Prof. S. Makishima for helpful discussions concerning several points.

Fuji Research Institute, Fuji Photo Film Company, Minami-ashigara-cho, Kanagawa-ken

(9) S. Fujisawa and E. Mizuki, *Bull. Soc. Sci. Phot. Japan*, (in press).

LETTER

On the New Method for Increasing the Sensitivity in Polarographic Analysis. The Use of Rotating Current Alternator

By Masayoshi ISHIBASHI and Taitiro FUJINAGA

(Received March 1, 1951)

Previously, the authors reported the use of rotating current alternator for the differential polarographic technique.[1]

In this paper, the authors report the method for increasing the sensitivity in the ordinary polarography using the same apparatus. Fig. 1 shows the scheme of the circuit. As seen in this figure, the voltage of E is applied to the cell and the reduction current flows through the galvanometer. The next instant when the alternating switch is half rotated, the circuit is shorted through the galvanometer and the oxidation current due to the dissolution of the

(1) M. Ishibashi and T. Fujinaga, This Bulletin, **23**, 261 (1950).

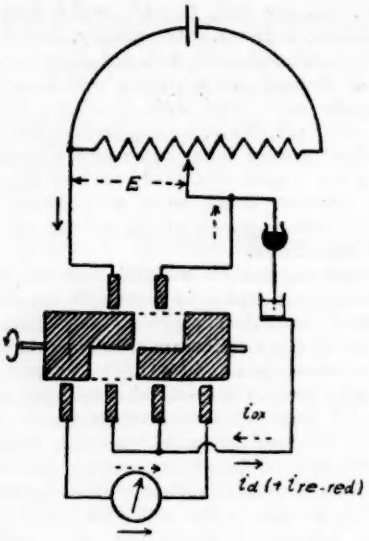

Fig. 1.

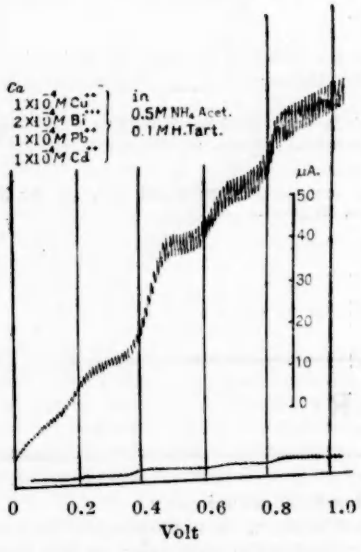

Fig. 2.

depositted metal flows additively through the galvanometer and moreover in the next half rotation, the dissolved ion is reduced again together with the diffused ion. So concentration of the ion occurs on the electrode surface instead of the diffusion layer. The total current is practically *ca.* twenty times greater than the ordinary diffusion current (hundreds microamperes per millimolar ion). By this method, the change of the concentration of the solution before and after the electrolysis is thought to be smaller than that in the ordinary method in spite of the larger current. Fig. 2 shows the polarogram taken with the switch rotated (the new method) and that, taken with the switch stopped (the ordinary polarogram) using the galvanometer of the same sensitivity. Some other intersteing characteristics and the circuits using this rotating switch will be submitted later.

Institute of Chemistry, Faculty of Science, Kyoto University, Kyoto

---

Chemical Analysis by the Measurement of Nuclear Moment. (Nuclear Momentscope Analysis)

By Shizuo FUJIWARA

(Received April 11, 1951)

An apparatus for observing the nuclear magnetic resonance has been constructed as an extention of the researches on the high-frequency titrimetry,[1] and the utility for the qualitative and quantitative analysis has been studied, although this resonance experiment has been already carried out for the precise measurement of the moments[2] or of the magnetic field.[3]

The sample is mounted in a coil of the receiver circuit and the coil is placed in the magnetic field with its axis perpendicular to the field direction. The radio-frequency waves of constant frequency (15.25 MC; with the modulation unit of 280 C. P. S.) are supplied to this circuit and the strength of the magnetic field is varied very slowly. The transitions occur which result in an absorption of energy from the radiofrequency field when the radio-frequency coincides with the Larmor precessional frequency of the atom. As the moment of $_1H^1$ is close to that of $_9F^{19}$, the absorption lines of the two elements have been compared with each other. The intensity of the energy absorption which is measured by the voltage drop of the out-put power from the detector circuit has shown good correspondence to the amount of the each element in the sample, as it is given in Table 1, when the sensitivity of

(1) S. Fujiwara and S. Hayashi, *Report of Univ. of Electro-Communications*, **1**, 112 (1950).
(2) J. E. Mack, *Rev. Modern Phys.*, **22**, 64 (1950).
(3) N. J. Hopkins, *Rev. Sci. Inst.*, **20**, 401 (1949).

Table 1

No.	Sample		Intensity of the energy absorption	
	Paraffin	$+Na_2SiF_6$	$_1H^1$, volt	$_9F^{19}$, volt
1	0.5 g.	0 g.	−0.10	0
2	"	0.1	−0.10	−0.08
3	"	0.3	−0.10	−0.27

the apparatus has been held appropriate. When the sensitivity of the apparatus is sufficiently raised, the energy absorption line has been easily observed with one-tenth milligramme of fluorine.

With the improvements in the apparatus, it will be possible to utilize the method for the chemical analysis, especially, of the solids, or for the determination of isotopes of heavy metals as an only suitable method.

The author expresses his sincere thanks to Mr. S. Hayashi for his devoted cooperation and heartily willing assistance, and also to Dr. K. Terasawa, the president of the Univ. of Electro-Communications, Dr. K. Kimura, the professor of Tokyo Univ. and Mr. K. Kambe, the assistant professor of the Univ. of Electro-Communications, for their interests and encouragements during this work. He wishes to thank also Dr. S. Wada of Tokyo-Shibaura Electric Co., and Mr. H. Yamada for their kindnesses shown in the construction of the magnet.

University of Electro-Communications, Tokyo

The Presence of Bismuth in Fish Bones and Human Teeth as Revealed by Cathodo-luminescence Method of Analysis

By Shin'ichiro HAKOMORI and Shohei TAMURA

(Received April 16, 1951)

The vertebrae of *Cololabis saira* and *Paralichthys olivaceus* are well washed with water, dried and heated at 950° for 2 hrs. The specimens are excited with cathode ray and the colors of luminescence produced are observed. The different phases of luminescence indicate the presence of different trace elements acting as luminescence activators; $Ca_3(PO_4)_2$ of the bones working as the luminophoric base.

The conclusion that the intense bright red luminescence is due to the $Ca_3(PO_4)_2$-Bi phosphor and thus indicates the presence of Bi in the bones mentioned is drawn from the following facts:—

(1) If the specimens are boiled for more than 12 hrs. with 5% NaCl or 1% KOH solution at the beginning, then the color of luminescence is very faint blue even when treated in the same manner as mentioned above. Boiling for more than 12 hrs. with $CHCl_3$ or water does not alter the red luminescence.

(2) Pure $Ca_3(PO_4)_2$ is prepared with elaborate care and heated at 950° for 2 hrs. The luminescence obtained is the same as in (1). But when Bi is chemically added to the $Ca_3(PO_4)_2$ in the ratio 10^{-6}: 1 and the same heat treatment is given, the same bright red luminescence as mentioned above is produced.

(3) Bi was microchemically detected in the above NaCl extract. A solution in which Bi is concentrated was obtained from 320 g. of the boes of *Paralichthys olivaceus*. A drop of the solution when added to the specimen of (1), reproduces the bright red luminescence. This solution also gives CaS, the well known violet blue luminescence of CaS-Bi phosphor.

(4) When Bi is chemically added to the specimen of (1) in the ratio 10^{-6}: 1, the bright red luminescence is also reproduced.

The same bright red luminescence is also observed in the case of human teeth when treated in the same manner as in the case of the vertebrae mentioned above.

A decayed tooth showed no such bright red luminescence.

The writers surmise that Bi may be a "nutritional trace element" which is indispensable in the metabolism of $Ca_3(PO_4)_2$ in the animal body. With respect to this point, further research is still being done. The cathodo-luminescence method will offer a convenient method for studying the manner of the trace of Bi in bones and teeth.

Chemical Institute, Faculty of Science
Tohoku University, Sendai,